

**Comparing the operation of aerobic granular sludge under
different hydrodynamic regimes during the treatment of
textile wastewater containing engineered silver
nanoparticles**

Miguel Alexandre Salvador Coelho

Thesis to obtain the Master of Science Degree in

Biological Engineering

Supervisors: Prof. Helena Maria Rodrigues Vasconcelos Pinheiro
Prof. Nídia Dana Mariano Lourenço de Almeida

Examination Committee

Chairperson: Prof. Arsénio do Carmo Sales Mendes Fialho
Supervisor: Prof. Helena Maria Rodrigues Vasconcelos Pinheiro
Member of the Committee: Prof. Jorge Humberto Gomes Leitão

December 2018

Agradecimentos

Nesta história há quase tantos obrigados como pedidos de desculpa. Que sirvam uns pelos outros:

À Professora Helena e à Professora Nídia, por me terem acolhido quando lhes bati à porta a reclamar um tema de tese que afinal já tinha dona, pelo apoio durante o trabalho experimental, por me ajudarem a organizar as ideias quando queria escrever sobre tudo e sobre nada, por insistirem que havia de sair qualquer coisa quando não saía nada e por não insistirem quando precisei de desanuviar. Metade da ajuda e compreensão que me dispensaram durante estes dois anos teria sido suficiente para fazer chorar Jesus Cristo. Acho que nunca vou saber muito bem o que dizer sobre a totalidade.

Ao Professor Jorge e ao Professor Arsénio, pela paciência e por continuarem disponíveis para discutir o assunto passado este tempo todo.

À chefe Rita, por me dar a conhecer os cantos da casa, pela boa disposição, pela disponibilidade para responder a todos os Rita-diz-me-só-uma-coisinha, por aceitar os meus horários de morcego e por nunca me ter apresentado a fatura de toda a loiça que parti no laboratório.

À Marta, à Sofia, à Renata, ao Pedro, ao João, à Laura e à Lília, pela companhia e pela ajuda durante os dias de laboratório. Sem vocês não teria tido a mesma piada.

À Sofia, ao Diogo, à Freire, à Leonor, à Paiva, à Mélica, à Rita, à Mariana, à Mafalda, ao Jorge e à Filomena, por coisas a mais e por nada em especial.

Ao núcleo-duro da santa terrinha, porque não me lembro de não me lembrar deles.

À minha irmã Teresa, por segurar as pontas de tudo como segura sempre. Só espero que um dia deixes de sentir a necessidade de fazê-lo.

À minha mãe.

Este trabalho foi financiado pela Fundação para a Ciência e a Tecnologia (FCT, Portugal) através do projecto “Impact of engineered nanoparticle and microplastics on textile wastewater treatment with aerobic granular technology – NanoMicroImpact”, PTDC/AAG-TEC/4501/2014

Abstract

Two aerobic granular sludge (AGS) sequencing batch reactors (SBRs) were operated for 192 days in order to investigate the effects of hydrodynamic regime (tested along the dimensions of hydrodynamic shear and anaerobic feeding strategy) and silver nanoparticle (Ag NP) loading over AGS properties and stability. SBRs were fed with a synthetic textile wastewater containing 10 mg Ag NPs L⁻¹ under either a fast, static filling (SBR1) or a plug-flow filling configuration (SBR2); shear differences between the two systems were determined by stirring speeds (70 rpm in SBR1 and 280 rpm in SBR2). Granulation was achieved successfully in both SBRs without any impact from Ag NP addition. Lower shear stresses in SBR1 resulted in increased settleability, granulation and sludge N-acetyl-L-homoserine concentrations over the first 50 days but proved irrelevant in driving sludge properties thereafter. Damaging effects over settleability – possibly caused by prolonged Ag NP dosing – were observed in the long term and caused severe washout episodes in both SBRs on day 85. This event initiated a period of cyclical sludge accumulation and washout which was likely driven by nanoparticle build-up and removal and which could point to a negative, concentration-dependent effect of Ag NPs over AGS stability. Finally, the plug-flow filling arrangement imposed on SBR2 was found to have a positive long-term effect on sludge density that reflected in superior sludge settleability.

Keywords: Aerobic granular sludge; Silver nanoparticles; Textile wastewater; Stability; Hydrodynamics; Feeding strategy

Resumo

Dois reatores sequenciais descontínuos (SBRs) foram operados por 192 dias com lamas granulares aeróbias (AGS) de modo a investigar os efeitos de diferentes regimes hidrodinâmicos (em termos de tensões de corte hidrodinâmicas e de estratégia de alimentação anaeróbia) e da adição de nanopartículas de prata (Ag NPs) sobre a estabilidade das AGS. Os SBRs foram alimentados com um efluente têxtil sintético preparado com 10 mg Ag NPs L⁻¹ usando um regime estático de carga rápida (SBR1) ou um regime de fluxo-pistão (SBR2). Cada sistema foi adicionalmente operado com uma velocidade de agitação própria de forma a gerar diferentes tensões de corte (70 rpm no SBR1 e 280 rpm no SBR2). Ambos os SBRs formaram grânulos sem qualquer impacto associado à presença de nanopartículas. Tensões de corte mais baixas no SBR1 resultaram em melhores propriedades de sedimentação, melhor granulação e maiores concentrações de *N*-acil-L-homosserina lactonas durante os primeiros 50 dias, mas revelaram-se irrelevantes *a posteriori*. No longo prazo foram observados efeitos danosos sobre a sedimentabilidade – possivelmente causados pela adição prolongada de Ag NPs – que resultaram na remoção de grandes quantidades de biomassa no dia 85. Este episódio encetou consecutivos períodos de acumulação de biomassa e *washout* que poderão ter sido desencadeados pela acumulação e remoção de nanopartículas – sugerindo um efeito negativo sobre a estabilidade das AGS dependente da concentração de Ag NPs. Por último, a alimentação em fluxo-pistão aplicada no SBR2 teve efeitos de longo prazo positivos sobre a densidade dos grânulos que se refletiram em propriedades de sedimentação superiores.

Palavras-chave: Lamas granulares aeróbias; Nanopartículas de prata; Efluentes têxteis; Estabilidade; Hidrodinâmica; Estratégia de alimentação

Table of contents

Agradecimientos	i
Abstract	iii
Resumo	iv
List of figures.....	vii
List of tables	viii
List of acronyms and abbreviations	ix
1. Introduction.....	1
1.1. The textile industry: structure and environmental impact	1
1.1.1. Production chain and key industrial processes	1
1.1.2. Water use, wastewater emissions, and discharge standards	2
1.2. Azo dyes: environmental impact and treatment solutions	4
1.2.1. Textile dyes and dyeing: basic principles and environmental strain.....	4
1.2.2. Azo dyes: demand, environmental releases and specific ecotoxic properties	7
1.2.3. Treatment strategies for azo dye-laden wastewaters: the case of anaerobic-aerobic biodegradation.....	9
1.2.4. Bioreactor systems for the application of sequential anaerobic-aerobic treatments: the case of the sequencing batch reactor (SBR)	12
1.3. Aerobic granular sludge (AGS) technology	14
1.3.1. General characterization and application to textile wastewater treatment	14
1.3.2. Physical and biological properties of aerobic granules (AGs)	15
1.3.3. AG formation and maintenance: insights from biochemistry, SBR engineering and microbiology	18
1.4. AGS stability and feeding configuration	23
1.4.1. The link between anaerobic feeding in AGS SBRs and AG stability	23
1.4.2. Bioreactor geometry and anaerobic feeding configurations as determinants of AG stability	24
1.5. Silver nanoparticles (Ag NPs) and AGS: environmental impact and fate during wastewater treatment	26
1.5.1. Antimicrobial finishing of textiles and Ag NPs: basic principles, antimicrobial action and environmental impact	26
1.5.2. Fate and impacts of Ag NPs during biological wastewater treatment: the effects of environmental silver transformations and microbial growth mode	29
2. Materials and methods.....	31
2.1. Synthetic textile wastewater	31
2.1.1. Carbon source and azo dye stock solutions.....	31
2.1.2. Synthetic wastewater composition	31
2.1.3. Silver nanoparticle suspension.....	31
2.2. Sequencing batch reactor (SBR) setup and operation.....	32
2.3. SBR inoculation and aerobic granulation	33
2.4. SBR performance monitoring	34
2.4.1. Sludge properties	34

2.4.2. Treatment performance: pollutant conversion and pH profiles.....	36
2.5. <i>N</i> -acyl-L-homoserine lactone-based quorum sensing analysis.....	37
2.5.1. Biosensor strain and growth conditions.....	37
2.5.2. Model AHL and auxiliary chemicals	38
2.5.3. AHL extraction.....	38
2.5.4. Development of the AHL bioassay	38
2.5.5. Reference calibration curve.....	40
2.6. Statistical analysis	40
3. Results and Discussion	41
3.1. Biomass properties, inventory and morphology	41
3.1.1. Aerobic granular sludge morphology.....	41
3.1.2. Biomass particle size distribution	45
3.1.3. Sludge settleability, biomass inventory and sludge retention time	47
3.1.4. Hydrodynamic shear as a determinant of granulation grade and sludge settleability	51
3.1.5. Contradictory short- and long-term impacts of Ag NP dosing	53
3.1.6. Long-term impacts of anaerobic feeding strategy on sludge properties.....	55
3.2. Treatment performance.....	56
3.2.1. COD removal performance and pH profiles	56
3.2.2. Colour removal and aromatic amine conversion	62
3.3. AHL-based quorum sensing analysis.....	70
3.3.1. Development of the AHL bioassay and reference calibration curve.....	70
3.3.2. Equivalent 3OC12-HSL concentration profiles.....	72
4. Conclusions and future work	78
4.1. The impacts of Ag NPs over AGS properties, stability and treatment performance.....	78
4.2. The effects of hydrodynamic shear and anaerobic feeding strategy over AGS properties and stability	78
4.3. AHL-based QS signalling as a reporter variable for sludge properties	79
References	80
Annex A SVI and MLVSS profiles (from Bento, 2016)	89

List of figures

1	Introduction.....	
Figure 1.1	General overview of the fate of azo dyes and aromatic amines during anaerobic–aerobic treatment processes (from van der Zee & Villaverde, 2005)	10
Figure 1.2	Microbial community structure and metabolic functions inside an aerobic granule (after Nanchaiah & Reddy, 2018)	18
Figure 1.3	The aerobic granulation process (after Sarma <i>et al.</i> , 2017)	19
2	Materials and methods.....	
Figure 2.1	Schematic representation of a full 6-h sequencing batch cycle in SBR1 and SBR2.	33
Figure 2.2	Simplified equipment diagram of the experimental sequencing batch reactor system.....	34
3	Results and Discussion	
Figure 3.1	Morphological development of granular sludge along the experimental run	43
Figure 3.2	Representative morphological and microbiological features of AGS samples collected during the initial granulation and biomass accumulation stage	44
Figure 3.3	Biomass particle size distribution (in terms of mass fraction) along the experimental run.	46
Figure 3.4	Sludge volume index (SVI) profile along the experimental run.....	48
Figure 3.5	Biomass concentration and sludge retention time (SRT) along the experimental run.....	49
Figure 3.6	Reference initial COD levels in the bioreactors	57
Figure 3.7	COD removal performance along the experimental run	59
Figure 3.8	Physicochemical feed characteristics along the operational run and COD conversion and pH variation curves along the reaction phase of selected representative cycles.....	61
Figure 3.9	Colour loading (measured as equivalent AR14 concentrations, AR14 _{eq.}) and colour removal performance along the experimental run	63
Figure 3.10	Colour removal profiles along the reaction phase of a selected representative cycle	65
Figure 3.11	Chemical structures of the azo dye Acid Red 14 and of the two aromatic amines formed during the azo bond reduction reaction	66
Figure 3.12	UV-visible spectra for the analysis of colour removal and aromatic amine conversion.....	67
Figure 3.13	Probing the aerobic degradation of aromatic amines along the experimental run in terms of near UV absorbance.....	69
Figure 3.14	UV-visible absorption spectrum of indigo in spent AT minimal medium.....	71
Figure 3.15	Correction factors α and γ	71
Figure 3.16	Calibration curve for the conversion of normalized β -gal activities into equivalent 3OC12-HSL concentrations	72
Figure 3.17	Equivalent 3OC12-HSL concentrations, 3OC12-HSL _{eq.} , in cell-free AGS extracts collected along the experimental run.....	73
Annex A	SVI and MLVSS profiles (from Bento, 2016).....	
Figure A.1	Sludge volume index profiles along the experimental run (from Bento, 2016).....	89
Figure A.2	Biomass concentration profiles along the experimental run (from Bento, 2016)	89

List of tables

1	Introduction.....	
	Table 1.1 Description of selected textile finishing operations and pollutant composition of the generated effluents (after Correia et al., 1994; Biscchops & Spanjers, 2003; Holkar et al., 2016; Patel & Vashi, 2016) .	3
	Table 1.2 Typical physicochemical properties of textile wastewaters and selected limits for discharges into surface waters, public sewers, and discharge collectors (after Ghaly et al., 2014; ZDHC, 2015)	5
	Table 1.3 Application classes of dyes, their chemical types and degrees of fixation (after O'Neill <i>et al.</i> , 1999)	6
	Table 1.4 Chemical structures of selected azo dyes and their toxic moieties (after Rawat et al., 2016).....	8

List of acronyms and abbreviations

1N2A4S	1-naphthol-2-amino-4-sulfonic acid	GAO	Glycogen-accumulating organisms
3OC12-HSL	<i>N</i> -(3-oxododecanoyl)-L-homoserine lactone	H/D	Height-to-diameter ratio
4A1NS	4-aminonaphthalene-1-sulphonic acid	HPLC	High-performance liquid chromatography
Abs	Absorbance	HRT	Hydraulic retention time
Ag NPs	Silver nanoparticles	LB	Luria broth
AGs	Aerobic granules	MixSBR1	Concentration at the onset of mixing in SBR1
AGS	Aerobic granular sludge	MixSBR2	Concentration at the onset of mixing in SBR2
AHL	<i>N</i> -acyl-L-homoserine lactone	MLTSS	Mixed liquor total suspended solids
AI-2	Autoinducer-2	MLVSS	Mixed liquor volatile suspended solids
ANAMMOX	Anaerobic ammonium oxidation	NP	Nanoparticle
An_{COD}	Anaerobic chemical oxygen demand removal yield	OD	Optical density
ANOVA	Analysis of variance	OLR	Volumetric organic loading rate
AR14	Acid Red 14	PAO	Polyphosphate-accumulating organisms
AR14_{eq.}	Equivalent Acid Red 14 concentration	PHA	Polyhydroxyalkanoate
ASP	Activated sludge process	Q_E	Effluent removal flow rate
BOD	Biochemical oxygen demand	QS	Quorum sensing
BOD₅	5-day biochemical oxygen demand	QQ	Quorum quenching
CAS	Conventional activated sludge	ROS	Reactive oxygen species
CI	Colour Index	RSD	Relative standard deviation
COD	Chemical oxygen demand	SBR	Sequencing batch reactor
DMSO	Dimethyl sulfoxide	SEM	Standard error of the mean
EPS	Extracellular polymeric substances	SRT	Sludge retention time
ETSS	Effluent total suspended solids	SUAV	Superficial upflow air velocity
EVSS	Effluent volatile suspended solids	SVI	Sludge volume index
FAS	Ferrous ammonium sulphate	SVI₃₀	Sludge volume index after a 30-minute settling period
FISH	Fluorescence <i>in situ</i> hybridization	SVI₅	Sludge volume index after a 5-minute settling period
		TDS	Total dissolved solids

ThSBR2	Theoretical initial concentration in SBR2	VSS	Volatile suspended solids
TSS	Total suspended solids	WWTP	Wastewater treatment plant
VER	Volumetric exchange ratio	X-gal	5-bromo-4-chloro-3-indolyl- β -D-galactopyranoside
VFA	Volatile fatty acids	β-gal	β -galactosidase
V_R	Working reactor volume	ϕ	Impeller diameter
V_s	Total volume of mixed liquor collected for sampling purposes		

1 Introduction

1.1 The textile industry: structure and environmental impact

1.1.1 Production chain and key industrial processes

The textile industry covers a broad range of activities from the transformation of natural (e.g., cotton, flax, wool, hemp, jute) or man-made (e.g., viscose, polyester, nylon, glass, carbon) fibres into yarns and fabrics, to the production of a wide variety of products such as hi-tech synthetic yarns, home furnishings, industrial filters, and garments (European Commission, 2017). It is one of the oldest and largest export industries, as well as the most globally prevalent, with most countries partaking in manufacturing activities for the international textile and apparel market (Gereffi & Frederick, 2010). In 2015, the industry generated US\$744,000 million in world exports (with US\$454,000 million coming from the clothing market alone) and accounted for a 4.5 per cent share in global merchandise trade (WTO, 2017). From a structural perspective, the sector is comprised of a diverse and fragmented group of mostly small- and medium-sized enterprises that receive and prepare fibres; transform fibres into yarn, thread, or webbing; convert the yarn into fabric or related products; and dye and finish these materials at various stages of production (EPA, 1997; Volmajer Valh *et al.*, 2011). The process of converting raw fibres into finished products is distinctively complex and usually sees a multi-stage flow of materials from one specialized textile mill to another. Adding to the complexity, little or no overlap occurs between the processing of fabrics derived from man-made and natural fibres, and additional branching points can be found further downstream in the industrial chain as textile materials are moulded into various products for both universal and technical applications (EPA, 1997). General classification systems usually reconcile all possible combinations of textile processing activities in four broad production stages: (i) yarn formation, (ii) fabric formation, (iii) finishing, and (iv) fabrication (Lacasse & Baumann, 2004).

During yarn formation, textile fibres are converted into yarns by using grouping and twisting operations to bind them together. While methods of spinning yarn from man-made fibres are similar to those used for natural fibres, different preparation steps are required in each case. Because of their origin, raw materials used to produce natural fibres, such as raw wool, must be cleaned by wet processes (e.g., wool scouring) before being processed into yarn. For man-made fibres, however, only one step of texturizing is needed before spinning (Lacasse & Baumann, 2004). Yarns produced in spinning mills can be sold directly to final consumers or introduced as inputs in fabric manufacturing. During this stage, yarns are meshed into cloth using one of several different methods, including weaving, a technique of yarn interlacing, and knitting. Together, these two processes account for the largest worldwide consumption of textile fibre and the highest volume of finished textile goods, mainly in the clothing and household furnishing sectors (EPA, 1997). The simpler of these products, such as bags, sheets, towels, and draperies, often involve simple fabrication stages requiring little specialization. Apparel and more complex housewares, on the other hand, are usually produced by dedicated businesses responsible for cutting, sewing, and pressing the fabric into the shape of the final product (EPA, 1997).

Before being processed into apparel and other finished goods, woven and knitted fabrics must, however, pass through several water-intensive operations – collectively referred to as finishing stages – designed to enhance their appearance, durability, and serviceability (EPA, 1997; Lacasse & Baumann, 2004). During these stages, undyed and unfinished textiles, known as grey or greige goods, are imparted with colours and properties such as increased softness, shrink resistance, and flame retardancy using a diverse array of chemicals and other raw materials. Textile finishing can be performed by commission in finishing mills or vertically integrated within the yarn and fabric manufacturing pipeline, in which case it usually comprises a non-linear and non-standard combination of unit processes that can be applied in different stages of production (e.g., yarn finishing, fabric finishing, 'ready-to-wear' article finishing) according to the demands of the final user (EPA, 1996; Lacasse & Baumann, 2004). As a whole, finishing operations (along with a few fibre preparation processes that use water for cleaning purposes) are frequently referred to as wet processing stages on account of their heavy water requirements (Bisschops & Spanjers, 2003; Lacasse & Baumann, 2004; Volmajer Valh *et al.*, 2011). Brief descriptions of the most relevant among these processes can be found in Table 1.1. Conversely, yarn manufacturing and other operations involving mechanical and physical transformations (e.g., carding, combing, spinning, singeing, cutting) are regarded as dry processes with comparatively negligible water inputs (Bisschops & Spanjers, 2003; Lacasse & Baumann, 2004; Volmajer Valh *et al.*, 2011).

1.1.2 Water use, wastewater emissions, and discharge standards

In terms of waste generation and environmental impacts, wet processing is unanimously regarded as the most significant part of textile manufacturing (EPA, 1997). Textile mills engaging in wet processing activities represent one of the most exhaustive industrial sectors in terms of water use, with an estimated average consumption of 200 litres per kilogram of fabric processed per day (Kant, 2012). Process water is frequently withdrawn from ground and surface bodies, contributing to the depletion of freshwater sources with particularly nefarious effects in water-stressed regions where the industry represents a major economic force (including China, India, Pakistan, and Bangladesh) (Maxwell *et al.*, 2015). Along the various wet stages of textile finishing, multiple chemicals – including sizes, dyes, salts, acids, alkalis, metals, and surfactants – are applied to textile substrates from water baths and subsequently discharged or rinsed off, generating heavily polluted wastewaters that require suitable treatments prior to discharge (Volmajer Valh *et al.*, 2011; Ghaly *et al.*, 2014; Holkar *et al.*, 2016). Estimates for wastewater production during textile processing place emissions between 1,000 and 3,000 m³ per 12–20 tonnes of textiles per day (Ghaly *et al.*, 2014) depending on fibre type, fabric type, and several operation-specific parameters such as the type of equipment, the classes of dyes and finishing agents, and even management policies regarding water use and pollution prevention (EIPPCB, 2003; Volmajer Valh *et al.*, 2011; Holkar *et al.*, 2016). Effluent characteristics vary largely between processing operations and materials, resulting in a combined wastewater with wide-ranging concentrations of organic and inorganic chemicals (Bisschops & Spanjers, 2003; Volmajer Valh *et al.*, 2011). The contributions of several important wet processing stages to the pollutant make-up of discharged wastewaters are outlined in Table 1.1.

Table 1.1 | Description of selected textile finishing operations and pollutant composition of the generated effluents (after Correia *et al.*, 1994; Biscchops & Spanjers, 2003; Holkar *et al.*, 2016; Patel & Vashi, 2016)

Operation	Description	Typical wastewater composition
Sizing and desizing	Performed on cotton and synthetic fibres to increase strength and minimize fibre breakage during spinning or weaving; organic sizes are applied to the textile substrate during sizing and removed via solubilization, acid hydrolysis, enzymatic hydrolysis, or oxidation during desizing	Sizing agents (e.g., carboxymethyl cellulose, starch and its derivatives, polyvinyl alcohol, polyacrylates); enzymes; mineral acids/alkalis; fats; oils; hemicelluloses; wetting agents
Scouring	Performed to remove impurities (natural or applied) that can interfere with dyeing using alkaline liquors supplemented with soaps and surfactants	Surfactants; soaps; mineral alkali; fats; pectin; oils; lubricants; sizing agents; suint; wool grease; wool wax; cotton wax
Wool carbonising	Performed to remove leftover traces of vegetable matter on scoured wool fibres or woollen fabrics; stepwise treatment involving immersion in dilute mineral acids, high-temperature charring of cellulosic matter, mechanical cleaning, and neutralization	Neutralization salts; suint; wool grease; surfactants; charred vegetable residues
Wool felting	Performed to increase wool density (fabric mating and contraction); textiles are mechanically circulated in neutral, acid, or alkaline baths containing felting auxiliaries (e.g., soaps)	Soaps; suint; wool grease
Bleaching	Performed to eliminate unwanted coloured matter from textile materials; substrates are treated with oxidizing or reducing agents that solubilize coloured substances or destroy their chromogenic sites	Hydrogen peroxide; mineral alkali (common) or acids (rare); chlorine; sodium bisulphite; sodium silicates; surfactants; chelating agents
Cotton mercerising	Performed to improve the tensile strength, dimensional stability, dye affinity, and lustre of cotton; fabrics are treated under tension in concentrated caustic soda supplemented with organic wetting agents; neutralization prior to wastewater discharge is common	Mineral alkali or neutralization salts; sulfonates; non-ionic surfactants; phosphoric esters
Dyeing	Uniform dye application on textile substrates to obtain an even colour; colourants are applied from aqueous dyebaths containing a wide range of chemical auxiliaries – acids, bases and buffers for pH control, reducing or oxidizing agents to solubilize or insolubilize dyes, salts to reduce electrostatic forces on the surface of the fibre, wetting agents to ensure uniform dyeing	Dyes; salts; surfactants; mineral acids/alkali; metals; dispersing agents; wetting agents
Printing	Localized dye application on textile substrates to obtain specific patterns; dyes or pigments are applied using printing pastes containing thickeners, urea, surfactants, and organic solvents; wastewater generated mostly from paste preparation equipment during cleaning	Dyes/pigments; urea; organic solvents; formaldehyde; metals
Finishing	Performed to improve fabric appearance, texture, and performance using mechanical or chemical methods; chemical finishing involves the application of chemicals from aqueous liquors and is used to impart properties such as water repellence, flame retardancy, mothproofing, and antimicrobial activity	Urea; melamine; formaldehyde; organophosphorus/polybrominated compounds; polysiloxanes; salts; catalysts; fatty acids; metals and other antimicrobial agents (e.g., triclosan, chitosan, peroxyacids)

Untreated textile mill wastewaters are characterized by substantial chemical oxygen demand (COD), biochemical oxygen demand (BOD), total suspended solids (TSS), total dissolved solids (TDS), and colour loads, as well as high pH levels and temperatures (Table 1.2) (Correia *et al.*, 1994; Savin & Butnaru, 2008; Kanu & Achi, 2011; Pang & Abdullah, 2013; Ghaly *et al.*, 2014). The suspended solids and colour contents (along with insoluble oils and grease) combine to produce highly turbid waste streams that can seriously damage the transparency and aesthetic value of receiving water bodies if unsuitably treated before discharge (Kant, 2012). Because they can significantly impact the perception of water quality, coloured substances are often regarded as top priority contaminants and take up a central position in the development and monitoring of textile wastewater remediation strategies (O'Neill *et al.*, 1999; Volmajer Valh *et al.*, 2011). The polluting effects of textile effluents on aquatic ecosystems

are, however, hardly limited to the presence of colour and can be hard to overstate. Suspended solids contents play an important role in affecting the environment, as they combine with oily scum and interfere with the oxygen transfer mechanism in the air-water interface. In addition, organic components are found to undergo chemical and biological changes that result in the removal of oxygen from water and further disturb the ecological balance (Ghaly *et al.*, 2014). The presence of excess concentrations of soluble salts renders receiving waters unsuitable for use and poses a serious threat to aquatic life, along with toxic compounds such as formaldehyde, acetic acid, soaps, heavy metals, and many other pollutants (Kant, 2012; Kamal *et al.*, 2016). Beyond the impacts of the major macropollutant classes, the release of individual chemical species can produce particularly deleterious effects arising from specific ecotoxic properties. Along the following pages, the discussion will shift focus to analyse the properties and ecological behaviour of two priority pollutants released by the textile industry in the context of dyeing and finishing operations: textile dyes (mainly azo dyes) and engineered silver nanoparticles. All subsequent topics will be examined through the lens of their relevance in the removal of these contaminants during textile wastewater treatment in order to provide a suitable theoretical preamble for the investigation at hand.




Because of the strong characteristics of textile wastewaters, several environmental protection agencies worldwide have imposed rules for discharge entrusted with guarding the environment from pollution (Ghaly *et al.*, 2014; Arslan *et al.*, 2016). Many national, supranational, and/or local administrations establish maximum release standards for discharges into the environment, into wastewater collectors, and into public sewers that may apply directly to the textile industry or more generally to industrial residues (ZDHC, 2015). Table 1.2 compares typical representative ranges for some of the most relevant physicochemical properties of textile wastewaters with three sets of standard limits established (i) for discharges into surface waters and sewers by the Legislative Decree No. 152 of the Italian Code on the Environment (2006), and (ii) for discharges into collecting systems in Madrid (Spain) by the Industrial Liquid Dumping Law to Integrated System of Sanitation of the Statute of Autonomy of the Community of Madrid (2015) (ZDHC, 2015). As depicted, the release of textile wastewaters entails the application of treatment processes that can ensure (depending on the intended discharge route) pollutant removal rates described by parameters such as COD, BOD₅, or TSS as high as 99%. The development of wastewater treatment facilities within the textile mill is therefore fundamental to certify the legal bounds imposed by standard discharge codes and avoid severe environmental damage (Arslan *et al.*, 2016).

1.2 Azo dyes: environmental impact and treatment solutions

1.2.1 Textile dyes and dyeing: basic principles and environmental strain

Dyes used by the textile industry are largely synthetic and typically derived from coal tar and petroleum-based intermediates (OECD, 2004; Volmajer Valh *et al.*, 2011; Sarayu & Sandhya, 2012). They are usually small molecules capable of absorbing visible light at certain wavelengths and producing vivid colours in aqueous solution even when present in small amounts. The major structural element responsible for light absorption is called the chromophore group and consists of a delocalized electron system with conjugated double or simple bonds (Pereira & Alves, 2012). In addition to these structures,

Table 1.2 | Typical physicochemical properties of textile wastewaters and selected limits for discharges into surface waters, public sewers, and discharge collectors (after Ghaly *et al.*, 2014; ZDHC, 2015)

Physicochemical parameters	Typical ranges in untreated textile effluents (Ghaly <i>et al.</i> , 2014)	Standard discharge limits (ZDHC, 2015)		
		into surface waters Legislative Decree No. 152 (2006)  ITA	into public sewers Legislative Decree No. 152 (2006)  ITA	into discharge collectors Industrial Liquid Dumping Law to Integrated System of Sanitation (2015, Madrid)  ESP
pH (–)	6–10	5.5–9	–	6–10
Temperature (°C)	35–45	30	30	40
BOD ₅ (mg O ₂ L ⁻¹)	80–6,000	40	250	1000
COD (mg O ₂ L ⁻¹)	150–12,000	160	500	1750
TSS (mg L ⁻¹)	15–8,000	80	200	1000
TDS (mg L ⁻¹)	2,900–3,100	–	–	–
Oil & grease (mg L ⁻¹)	10–30	20	40	100
Colour	50–2,500 Pt-Co ^a	not perceived after 1:20 dilution	not perceived after 1:40 dilution	–

^a The Platinum-Cobalt (Pt-Co) Scale is a colour scale developed to evaluate pollution levels in wastewater; it relies on a visual comparison between a test sample and serial dilutions of a standard solution prepared with potassium hexachloroplatinate (IV), cobalt (II) chloride hexahydrate and hydrochloric acid (Spartan Environmental Technologies, 2017)

dye molecules contain one or several ionizable substituents – generally referred to as auxochromes – that either directly contribute to or intensify the colour and provide the dye with a higher affinity to the fibre during the dyeing process (Carmen & Daniela, 2012; Pereira & Alves, 2012; Sarayu & Sandhya, 2012). Common chromophores include azo (–N=N–), carbonyl (–C=O), methine (–CH=), nitro (–NO₂), and quinoid groups, whereas the most frequent auxochromes are amines (–NH₂), carboxyl (–COOH), sulfonate (–SO₃H), and hydroxyl (–OH) (Pereira & Alves, 2012; Sarayu & Sandhya, 2012; Holkar *et al.*, 2016). Electron delocalization in between these groups is usually carried through a core aromatic structure (normally benzene, naphthalene, or anthracene rings) called the chromogen to form a large auxochrome-chromogen-chromophore system (Pereira & Alves, 2012).

Synthetic dyes exhibit considerable structural diversity and thus possess very different chemical and physical properties. The chemical classes more frequently employed on an industrial scale are azo, anthraquinone, indigoid, xanthene, arylmethane, and phthalocyanine derivatives (Pereira & Alves, 2012). Systematic names for dyes used in industrial applications are regulated by a general classification system developed by the Society of Dyers and Colourists in 1924 and named Colour Index (CI) (O'Neill *et al.*, 1999; Pereira & Alves, 2012). The system lists dyes firstly by a generic name based on its application and colour (using three-word constructs such as Acid Blue 16 or Reactive Red 4), and then by assigning a 5-digit CI number based on its chemical structure (if known) (O'Neill *et al.*, 1999; Carmen & Daniela, 2012; Pereira & Alves, 2012). Table 1.3 succinctly describes the main dye application methods employed within the context of textile finishing and used as a base for the nomenclature of the CI (also referred to as dye classes). Common chemical families of dyes applied using each method are also provided. As of August 2017, the CI system provided commercial names for over 44,800 dyes (Society of Dyers and Colourists & AATCC, 2017). Estimates for the worldwide production of synthetic dyes place the annual output at 7×10^5 tonnes (Chequer *et al.*, 2013), of which as much as two thirds are consumed by the textile industry alone (Pereira & Alves, 2012).

Table 1.3 | Application classes of dyes, their chemical types and degrees of fixation (after O'Neill *et al.*, 1999)

Class	Method of application	Chemical types	Degree of fixation (%)
Acid	Usually applied from neutral to acidic dyebaths	Azo, triphenylmethane, azine, xanthene, nitro, and nitroso	89–95 on polyamide fibres
Basic	Applied from acidic dyebaths	Diazocarbocyanine, cyanine, hemicyanine, diazohemicyanine, diphenylmethane, triarylmethane, azo, azine, xanthene, acridine, oxazine, and anthraquinone	95–100 on acrylic fibres
Direct	Applied from neutral or slightly alkaline baths containing additional electrolyte	Azo, phthalocyanine, stilbene, and oxazine	70–95 on cellulosic fibres
Disperse	Fine aqueous dispersions often applied by high temperature/pressure or lower temperature carrier methods; dye may be padded on fabric and baked on or thermofixed	Azo, anthraquinone, styryl, nitro, and benzodifuranone	90–100 on polyester fibres
Reactive	Reactive site on dye reacts with functional group on fibre to bind dye covalently under influence of heat and pH (alkaline)	Azo, anthraquinone, phthalocyanine, formazan, oxazine, and basic	50–90 on cellulosic fibres
Sulphur	Aromatic dyes mixed with sodium sulphide and re-oxidized to insoluble sulphur-containing products on fibre	Indeterminate or poorly understood structures	60–90 on cellulosic fibres
Vat	Water-insoluble dyes solubilised by reducing with sodium hydrosulphite, then exhausted on fibre and re-oxidized	Anthraquinone and indigoids	80–95 on cellulosic fibres

During dyeing, fibres can take up colourants as a result of van der Waals forces, hydrogen bonds, hydrophobic interactions, or covalent bonds (EIPPCB, 2003; dos Santos *et al.*, 2007). The adsorptive strength is controlled by several factors – including the contact time between the fibres and the dye, process temperatures and pH levels, and the presence of several auxiliary chemicals – and directly affects the outcome of the operation (Correia *et al.*, 1994; Carmen & Daniela, 2012). As displayed in Table 1.3, fixation efficiencies vary quite significantly with the class of dye used, ranging from levels as low as 50% in the case of reactive dyes to 100% with basic dyes. As a result, dyebaths are discharged from process units with residual concentrations of dyes as high as 800 mg L^{-1} , generating strongly coloured wastewaters (O'Neill *et al.*, 1999). It has been estimated that approximately 9% of the total mass of dyestuffs produced worldwide is released in textile wastewaters (O'Neill *et al.*, 1999; Pereira & Alves, 2012). Depending on the class of dye and several specific process conditions, dye concentrations in dyehouse effluents can range from $10\text{--}50 \text{ mg L}^{-1}$ up to the previously stated maximum limit, which can nonetheless be exceeded in selected cases (O'Neill *et al.*, 1999). As even small amounts of dyes ($<1 \text{ ppm}$ in some cases) are highly visible in aqueous solution, dyeing effluents can significantly degrade the aesthetic merits of receiving water bodies if unsuitably treated before release. In addition, synthetic dyes contribute to a reduction in the activity of aquatic photoautotrophic organisms – with over-arching effects on dissolved oxygen concentrations – by absorbing and reflecting the sunlight entering the water, and can significantly disturb the normal biological functions of the entire ecosystem (Pereira & Alves, 2012; Ghaly *et al.*, 2014). Due to their synthetic nature and mainly aromatic structure, most dyes can cause allergies, dermatitis, skin and upper respiratory tract irritations, and can, in specific cases, display carcinogenic activity (Carmen & Daniela, 2012; Khan & Malik, 2014). The removal of colour from dye-

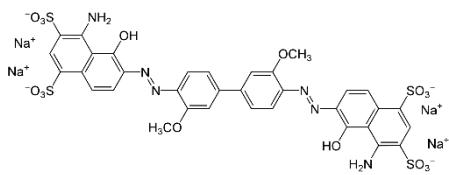
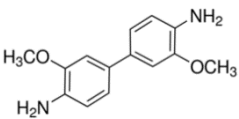
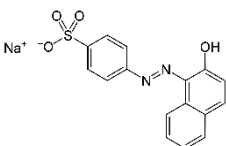
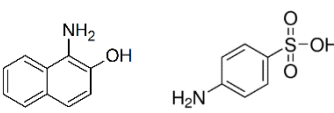
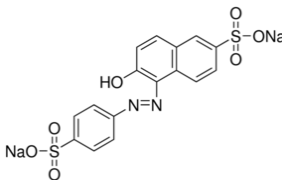
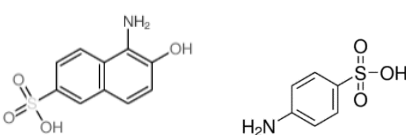
containing wastewaters is therefore, as stated above, an eminent concern for treatment facilities operating with effluents from textile processing mills (Pereira & Alves, 2012).

Along with the dyes themselves, a large range of chemicals can be found in dyeing effluents at any one time (Correia *et al.*, 1994). The full chemical composition of dyeing baths is dependent on the method of dye application and may include mineral acids, bases, and buffers for pH control; reducing and oxidising agents to solubilize and insolubilize dyes (common with sulphur and vat dyes); salts to reduce the electrostatic forces on the surface of the fibre and promote the penetration of the dye; and dispersing and surface-active agents to ensure fabric softness (Correia *et al.*, 1994; EIPPCB, 2003). As a whole, these auxiliaries account for the bulk of dissolved solids (mostly salts, acids, and alkalis), COD, and BOD values in dyeing wastewaters (Correia *et al.*, 1994; Bisschops & Spanjers, 2003). Furthermore, heavy metals such as cadmium, chromium, copper, lead, and zinc can arise in exhausts in association with the dyes themselves, either as impurities attendant to their synthesis or as integral structural elements (in metallized dyes) (Correia *et al.*, 1994; EIPPCB, 2003).

1.2.2 Azo dyes: demand, environmental releases and specific ecotoxic properties

Azo colourants represent the overwhelming majority of dyestuffs currently employed in industrial applications. They are characterized by one or more chromophoric azo functions ($-N=N-$) combined with a variety of auxochromic substituents – including, *e.g.*, methyl ($-CH_3$), nitro ($-NO_2$), amino ($-NH_2$), hydroxyl ($-OH$) and sulfonic acid ($-SO_3H$) groups – and stand out among known colourant families owing to their simple production processes, durability, stability and variety (Saratale *et al.*, 2011). According to statistics compiled by Pinheiro *et al.* (2004), they account for 60-70 per cent of the total volume of textile dyes currently in use and show up in the composition of over 3,000 dyestuffs with declared applications (including both dyes and pigments) (O'Neill *et al.*, 1999; Pinheiro *et al.*, 2004; Pereira & Alves, 2012). Textile manufacturing emerges as the largest consumer market for azo dyes, accounting for roughly two-thirds of the overall sales volume. Out of these, ~12% is estimated to be released directly into the environment as a result of incomplete dyeing yields and poor recovery strategies (Pinheiro *et al.*, 2004). These figures render azo dyes one of the principal pollutants specifically associated with the textile industry and have raised concerns for decades among manufacturers and researchers regarding their impacts on natural ecosystems. Some synthetic azo dyes are known to be toxic, carcinogenic and/or mutagenic, and can produce prolonged polluting effects on account of their fastness, stability and potential to accumulate in the environment (Saratale *et al.*, 2011; Khan & Malik, 2014). Moreover, even in those ecosystems where natural azo dye biodegradation functions are known to exist, the combination of governing biological and physicochemical factors involved in the degradation of these compounds may not always yield non-toxic or less toxic metabolites. In fact, in certain conditions, these environmental processes can lead to the conversion of non-toxic dyes into toxic breakdown products, effectively creating a secondary pollution problem (Rawat *et al.*, 2016). Understanding the determinants of both direct and indirect azo dye toxicity is therefore an important pre-requisite if their impact over natural communities is to be mitigated.

Table 1.4 | Chemical structures of selected azo dyes and their toxic moieties (after Rawat *et al.*, 2016)

Dye structure	Toxic moieties in structure
<p>Direct Blue 1</p> 	<p>3,3'-dimethoxybenzidine</p> 
<p>Acid Orange 7</p> 	<p>1-amino-2-naphtol; 4-aminobenzenesulfonic acid</p> 
<p>Sunset Yellow FCF</p> 	<p>5-amino-6-hydroxynaphthalenesulfonic acid; 4-aminobenzenesulfonic acid</p> 

Inherently toxic azo dyes are generally characterized by low molecular weights and high lipophilicity, and can easily diffuse through the cell membrane. They include a number of *N*-substituted aryl compounds and free arylamines – often with additional electron-donating substituents in *ortho*- or *para*-positions – which undergo biochemical activation to generate mutagenic and carcinogenic nitrenium intermediates that can bind to DNA and RNA molecules (Khan & Malik, 2014; Rawat *et al.*, 2016). Based on these structural cues, intrinsic dye toxicity has often been sidestepped through the development of bulky chemical structures with several polar moieties (e.g., sulfonic acid and carboxyl groups) – to restrict diffusion through the cell membrane – and by altering, when required, the relative position of amino groups to increase steric hinderance and inhibit the metabolic activation of amines (Pinheiro *et al.*, 2004; Rawat *et al.*, 2016). However, this strategy can carry some negative consequences to the remediation of coloured wastewaters and has often proven inefficient in fully eliminating azo dye toxicity (Pinheiro *et al.*, 2004; Rawat *et al.*, 2016). On the one hand, the introduction of multiple polar groups in the structure of azo dyes results in increased aqueous solubility and may ultimately hinder dye removal during biological wastewater treatment by affecting biosorption mechanisms (Pinheiro *et al.*, 2004). On the other hand, noxious action has, as stated, been known to emerge indirectly from the dye's breakdown products even when exposure to the undegraded colourant does not produce any effect (Rawat *et al.*, 2016).

When in natural environments, azo dyes are susceptible to both oxidative and reductive biodegradation by action of several microbial species (Pereira & Alves, 2012; Solís *et al.*, 2012; Rawat *et al.*, 2016). Under anaerobic conditions, microbes decolourise dyes via azo bond cleavage, releasing colourless aromatic amines that are resistant to further degradation and which can accumulate if low oxygen

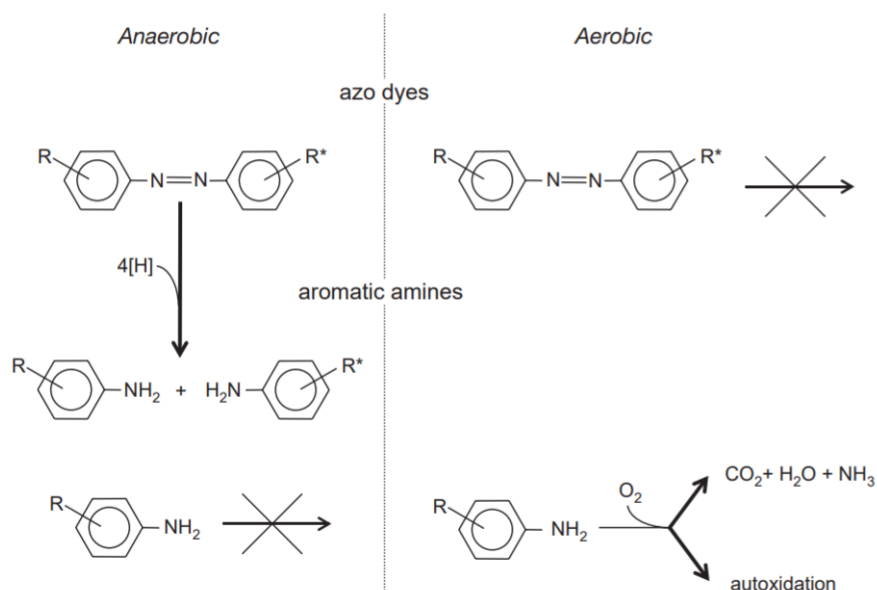
concentrations persist (Rawat *et al.*, 2016). As discussed above, arylamines, such as substituted and unsubstituted anilines or benzidines, are known genotoxic and carcinogenic compounds and can therefore inflict significant damage where their parent azo dyes could not (Pinheiro *et al.*, 2004; Rawat *et al.*, 2016). Table 1.4 displays several examples of toxic aromatic amine moieties in selected chemical structures of intrinsically non-toxic azo dyes. Metabolites derived from the degradation of azo dyes in aerobic environments (through asymmetric – *i.e.*, non-chromophoric – cleavage) can similarly display high mutagenicity and even damage cell viability by promoting the development of oxidative stress conditions (Rawat *et al.*, 2016). Azo dye-containing wastewater treatment strategies should therefore be devised to promote both decolourization and the complete breakdown of any intermediate metabolites (van der Zee & Villaverde, 2005). The use of combined sequential anaerobic-aerobic bioreactors has been suggested as an effective solution for the complete mineralization of azo dyes and will be discussed in detail in the next section after a brief recap of other treatment methods currently established in the literature.

1.2.3 Treatment strategies for azo dye-laden wastewaters: the case of anaerobic-aerobic biodegradation

Seeing as traditional wastewater treatment processes are generally unsuccessful in the degradation of synthetic textile dyes (Forgacs *et al.*, 2004), several alternatives have been studied over the course of the last few decades in order to achieve suitable dye conversion and colour removal rates. The amassed knowledge has yielded a wide range of technologies for the treatment of dye-laden wastewaters, including (i) physical methods – such as membrane filtration and sorption techniques –, (ii) chemical methods – such as coagulation-flocculation, standard and advanced oxidation processes (*e.g.*, with ozone, hydrogen peroxide and/or UV radiation), and electrochemical treatments –, and (iii) biological methods – designed to promote anaerobic and/or aerobic dye degradation by pure microbial populations, mixed microbial communities, or isolated enzymes (Pereira & Alves, 2012).

Most physicochemical dye removal methods have inherent drawbacks because they are expensive, have limited versatility, are greatly interfered by other wastewater constituents, and/or generate large volumes of waste products that must be handled (van der Zee & Villaverde, 2005). In contrast, biological wastewater treatment processes provide an economical alternative with low running costs, reduced water requirements and waste sludge generation, and the potential to metabolize (and, in some cases, fully mineralize) coloured pollutants into non-hazardous substances (Saratale *et al.*, 2011; Pereira & Alves, 2012; Holkar *et al.*, 2016). Several organisms have been tested for their potential to degrade synthetic dyes in aqueous solution, including algae, filamentous fungi, yeasts, pure and mixed bacterial cultures, and plants (Saratale *et al.*, 2011; Pereira & Alves, 2012; Solís *et al.*, 2012; Holkar *et al.*, 2016). Among these groups, the use of bacteria has produced the largest volume of research on the decolourisation of azo dyes (Holkar *et al.*, 2016).

Figure 1.1 | General overview of the fate of azo dyes and aromatic amines during anaerobic–aerobic treatment processes (from van der Zee & Villaverde, 2005) ►



Generally, bacterial azo dye biodegradation proceeds in two stages. The first stage involves the reductive cleavage of the dyes' azo linkages, resulting in the formation of (typically) colourless but potentially toxic aromatic amines; the second stage involves the degradation of the aromatic amines. Azo dye reduction usually requires anaerobic conditions, whereas bacterial biodegradation of aromatic amines is an almost exclusively aerobic process. A wastewater treatment strategy in which anaerobic and aerobic conditions are combined is therefore the most logical concept for removing azo dyes from wastewater (van der Zee & Villaverde, 2005). In order to establish some basic information about the mechanisms and operational factors affecting the degradation of azo dyes and the fate of the breakdown products during such treatments, the next few pages will go into some detail on the workings of each phase using data from multiple studies and different classes of anaerobic-aerobic bioreactors. Key discussion topics are schematically summarized in Figure 1.1.

The process of anaerobic azo dye reduction involves a transfer of four electrons (reducing equivalents) that proceeds in two stages at the azo linkage; in each stage, two electrons are transferred to the dye, which acts as a final electron acceptor (dos Santos *et al.*, 2007). The exact mechanism behind this reductive transformation is somewhat uncertain but is generally believed to involve a co-metabolic reaction in which reducing equivalents or reduced cofactors produced via oxidation of a primary substrate – such as NADH, NAD(P)H, FMNH₂, and FADH₂ – channel electrons to support the enzymatic cleavage of the azo bond (dos Santos *et al.*, 2007). Enzyme functions involved in azo bond reduction (designated as azoreductases) are thought to be located either in the outer membrane of bacterial cells (in the case of Gram-negative bacteria) or in the extracellular medium, where they can make direct contact with the azo dye substrate (Pearce *et al.*, 2003). Redox mediators, such as anthraquinone sulphonates or lawsone, have been shown to facilitate the reduction of azo dyes in the extracellular environment and are believed to act as electron shuttles between the azoreductases and the final acceptor (Pearce *et al.*, 2003; dos Santos *et al.*, 2007). In aerobic conditions, this reduction mechanism is inhibited by oxygen – due to the preferential oxidation of the reduced redox mediator by O₂ – and the decolourisation efficiency by means of reductive degradation significantly drops (Pearce *et al.*, 2003).

Other theories circulated in the literature concerning the mechanisms of azo bond cleavage include intracellular reduction by cytoplasmic, flavin-dependent reductases and purely chemical reactions in the extracellular medium with reduced inorganic compounds such as ferrous iron or sulphide – formed as end-products of strictly anaerobic bacterial metabolic reactions (Stolz, 2001). Their relevance for the overall decolourization performance is, however, thought to be low in the case of most azo dyes and the processes are mostly written off as secondary transformations (Russ *et al.*, 2000; van der Zee & Villaverde, 2005; dos Santos *et al.*, 2007; Popli & Patel, 2015).

Aromatic amines produced as a result of azo bond cleavage are typically recalcitrant to further anaerobic conversion and will persist in the mixed liquor for as long as the environmental conditions remain unchanged (dos Santos *et al.*, 2007); oxygenic transformations have, however, been reported by many authors. These transformations fall along two main lines – bacterial degradation (Libra *et al.*, 2004; van der Zee & Villaverde, 2005; Franca *et al.*, 2015; Pereira *et al.*, 2015) or auto-oxidation (van der Zee *et al.*, 2001; Kudlich *et al.*, 1999; Coughlin *et al.*, 2002). Effective biodegradation has been associated with the presence of specialized bacterial strains that use aromatic amines as a carbon source and oxygen as a co-substrate for the hydroxylation of the amino group and for the oxygenolytic cleavage of the aromatic ring (Pereira *et al.*, 2015). Complete amine mineralization is also possible in specific cases, and typically involves a range of specialized dioxygenase activities and ubiquitous metabolites such as catechol, protocatechuate, and gentisate responsible for establishing the bridge with central metabolic pathways to secure the full oxidation of the aromatic substrate (Çinar & Demiröz, 2010). These specialized microbial activities can typically be found in bacterial inocula collected from areas with a history of exposure to aromatic amines, suggesting degrading functions can be developed naturally if sufficient and persistent selective pressures are exerted on resident microbial communities (Tan *et al.*, 2005; Barsing *et al.*, 2011). In a clear demonstration of this idea, Franca *et al.* (2015) described the development of an aromatic amine-degrading activity in an aerobic granular sludge SBR after 71 days of back-to-back anaerobic-aerobic cycles designed to treat a simulated textile effluent loaded with the azo dye Acid Red 14. After that point, bioconversion of the amine moieties released from dye reduction occurred in all cycles up until the end of the operation, even when the inlet dye concentration was trebled. The authors correlated their results with the high biomass retention capacity of aerobic granular sludge systems (further discussed ahead) and suggested that this property has the potential to improve the treatment efficiency of arylamine-laden wastewaters by allowing the development of a diverse microbial population. Clara *et al.* (2005) advanced similar conclusions after testing the effects of sludge retention time (SRT) over the degradation of multiple synthetic organic compounds (including pharmaceuticals such as ibuprofen and diclofenac, and natural oestrogens), suggesting that a minimum SRT was indeed required to achieve meaningful levels of biodegradation and correlating them with the proliferation of specific slow-growing microorganisms that provided the sludge community with relevant enzyme activities.

Besides the cases of successful aerobic biodegradation, one other staple of the aerobic treatment stages of azo dye-laden wastewaters has been found to be arylamine auto-oxidation. Auto-oxidation is a common phenomenon that takes place with unstable amines in the presence of oxygen (Pereira *et al.*, 2015). Substituted anilines and naphthylamines are among the most common aromatic amines to undergo auto-oxidation (Kudlich *et al.*, 1999; Pereira *et al.*, 2015) and have been thoroughly investigated

to determine the main chemical transformations that can take place under aerobiosis. In one of those investigations, Kudlich *et al.* (1999) examined the chemical mechanisms behind the auto-oxidation of three different sulfonated arylamines and documented the production of quinone derivatives or dimers depending on the number and relative position of substituents. Polymerisation reactions have similarly been reported for multiple hydroxylated aromatic amines, including 1-amino-2-naphthol and 4-hydroxyaniline (Coughlin *et al.*, 2002; Pereira *et al.*, 2015), and found to result in the production of insoluble humic-like molecules that can settle out from the liquid phase to form a *de novo* solid phase (Pereira *et al.*, 2015). Many of these products boast extensive delocalized π electron systems and strong natural colours, and have been noted to impart a distinctive hue to the wastewater throughout the aerobic stage (van der Zee *et al.*, 2001; Kudlich *et al.*, 1999; Pereira *et al.*, 2015). Because they are often recalcitrant to further aerobic biodegradation, these compounds can therefore substantiate a major setback for the overall colour removal goal of sequential anaerobic-aerobic treatment settings (Libra *et al.*, 2004; Pereira *et al.*, 2015). Nevertheless, some isolated cases of successful secondary colour removal during normal bioremediation cycles can be found in the available literature. The clearest example is perhaps that advanced by Kudlich *et al.* (1999), who reported the aerobic degradation of the blue naphthoquinone imine derivative obtained following the decolourisation of Reactive Black 5 after a 27-day lag phase in the presence of activated sludge. These results suggest, once again, that specialized microbial populations might be capable of curbing the negative effects of secondary colour development and advocate further research efforts in order to find a suitable solution for each case.

1.2.4 Bioreactor systems for the application of sequential anaerobic-aerobic treatments: the case of the sequencing batch reactor (SBR)

Well beyond their appeal in the context of textile wastewater treatment, anaerobic-aerobic processes represent one of the most promising technological tools currently available for the remediation of industrial effluents as a whole, standing out from other processes on account of their characteristically high treatment efficiencies – a natural effect emerging from the imposition of two distinct and complementary bioremediation stages – and their inherent potential to address a number of common concerns in industrial settings – such as energy savings and resource recovery (e.g., through biogas collection in anaerobic units) (Butirón *et al.*, 2006). Lab-, pilot- and process-scale studies describing the implementation of such processes are extraordinarily numerous and run the gamut on all topics from effluent sourcing to process conditions and bioreactor design. Reviewing efforts have identified treatment results for industrial sectors as distinct as pulp and paper, dairy, meat packing, textiles, general chemicals and pharmaceuticals and have found a seemingly disorderly wealth of design logics for process units that pop up somewhat randomly across the literature. Examples include multiple combinations of anaerobic and aerobic high-rate reactors – the likes of the upflow anaerobic sludge blanket, fluidized bed reactors and membrane reactors –, conventional systems made up of separate, serially connected aerated and non-aerated ponds, and a number of integrated anaerobic-aerobic bioreactors where the two conditions are provided either temporally or spatially separated (Chen *et al.*, 2009). Looking specifically to the case of azo dye remediation in textile wastewaters, however, preferences seem to settle more or less firmly on one key system drawn from this vast pot: the sequencing batch reactor (SBR).

The SBR is a modification of the widely applied activated sludge process (ASP) where time-sequenced processes of flow equalization, aeration, clarification, and biomass wasting are conducted cyclically in a single tank (Dutta & Sarkar, 2015; Mullai *et al.*, 2016). The technology provides for the conversion of continuous ASP-based systems into a batch process by condensing treatment stages that are usually conducted in different units (e.g., bioreactors for aeration and pollutant removal, secondary clarifiers for settling, external pumping and flow-dividing circuits for sludge recirculation and discharge) into a temporal series. This arrangement delivers relevant advantages in terms of equipment design and process control that render the SBR an easily automatable system and can ensure reductions in running costs as high as 60% when compared to a conventional ASP (Dutta & Sarkar, 2015). Because of their periodic operation, SBRs execute temporally defined selective pressures that can be easily modulated to enrich desired microbial populations and enhance BOD, nutrient, and micropollutant removal. In order to ensure optimum environmental conditions for each conversion process, alternating aerobic and anaerobic phases can be implemented through the control of aeration and arranged in adequate succession during a single SBR cycle (Chan *et al.*, 2009; Dutta & Sarkar, 2015; Mullai *et al.*, 2016). Because of these properties, the technology has been pointed as a suitable solution for bioremediation strategies aiming to limit discharges of xenobiotic compounds into the environment, and has found particular resonance in the field of wastewater decolourisation (Chan *et al.*, 2009; Mullai *et al.*, 2016). The main characteristics of each process stage in an SBR engaged in textile wastewater treatment are described below (Singh & Srivastava, 2011; Metcalf & Eddy *et al.*, 2004; Mullai *et al.*, 2016).

- (i) *Fill*. The influent wastewater is added to the biomass that was left in the tank from the previous cycle under either static or aerated conditions (depending on effluent characteristics and bioremediation goals). The length of the fill period is determined by the volume of the bioreactor and by the flow rate of the wastewater.
- (ii) *React*. Wastewater flow to the tank is stopped, while aeration and/or mixing are initiated or continued from the previous stage. As stated, air flow can be modulated or stopped to produce anaerobic or aerobic conditions in adequate succession; if required, fully anaerobic environments can be provided by injecting nitrogen gas into the vessel. Treatment efficiency, as described by colour, nutrient, and COD removal yields, is a function of the chosen arrangement and of the time allotted for mixing and aeration.
- (iii) *Settle*. Aeration and mixing are ceased to ensure static conditions and facilitate liquid-solid separation in the form of supernatant and sludge.
- (iv) *Draw*. After settling, the clarified supernatant is discharged from the reactor as the process effluent. Pumps and weirs are typically arranged to ensure sludge withdrawal is minimized during effluent removal.
- (v) *Idle*. A quiescent buffer period between draw and fill is applied to complete the cycle time. Idle periods are frequent in full-scale multi-tank systems to ensure that filling is carried out separately in separate units and/or to equalize the duration of all cycles.

Much like the ASP, the simplest conception of the SBR system employs a flocculent suspension of microorganisms for pollutant removal. Most studies investigating the use of anaerobic-aerobic SBRs for textile wastewater treatment have subscribed to this design logic and have reported satisfactory results in terms of simultaneous colour, COD, and nutrient removal (Lourenço *et al.*, 2001; Cabral Gonçalves

et al., 2005; van der Zee & Villaverde, 2005). Various other choices of sludge technology are, however, available for application in SBRs and have often proven superior in the context of wastewater decolourisation (Singh & Srivastava, 2011; Dutta & Sarkar, 2015). Among them, aerobic granular sludge (AGS) has shown the greatest deal of promise and has been the subject of much attention in recent years (Muda *et al.*, 2010; Franca *et al.*, 2015, 2017a; Lourenço *et al.*, 2015). The following chapter will delve into the principles behind this technology. Throughout the exposition, the reader is advised to bear the basic operating specs of the sequencing batch reactor in mind in order to understand the many connections and intersections that meld the two subjects together.

1.3 Aerobic granular sludge (AGS) technology

1.3.1 General characterization and application to textile wastewater treatment

Aerobic granular sludge systems have emerged as one of the most promising bioprocesses for wastewater bioremediation over the last few years and currently enjoy a fully proven track record in the full-scale treatment of municipal sewage (Giesen *et al.*, 2013; Inocêncio *et al.*, 2013; Pronk *et al.*, 2015a). They can be developed from conventional activated sludge inocula in response to an adequate balance of selective pressures, cell-to-cell interactions, and hydrodynamic shear forces and are normally established by manipulating a number of operational conditions in SBR settings. The process of aerobic granulation results in the establishment of large, strong-structured biomass aggregates with regular outlines called aerobic granules (AGs), which are composed by densely packed, self-immobilized microbial consortia enmeshed in a net of extracellular polymeric substances (EPS) (de Bruin *et al.*, 2004; Singh & Srivastava, 2011). Owing to their unique structural properties, AGS systems are characterized by (i) an excellent settling behaviour, resulting in good solid–liquid separation over a short settling period; (ii) a good biomass retention capacity, allowing high accumulation in the SBR and a consequent reduction in reaction time and/or reactor volume; and (iii) an increased ability to withstand toxicity and high organic loading rates (highly desirable for the treatment of industrial wastewaters) (de Bruin *et al.*, 2004; Lourenço *et al.*, 2015). Aerobic granules are additionally characterized by aerobic and anoxic/anaerobic internal zones – developed as a result of oxygen mass transfer gradients along the EPS matrix – that render them an attractive solution for the simultaneous removal of organic matter and nutrients (nitrogen and phosphorus) by segregated microbial populations (Singh & Srivastava, 2011; Lourenço *et al.*, 2015). Combined with the high biomass retention capacity of AGS SBRs, the establishment of these localized biological niches provides unique conditions for the proliferation of multiple bacterial species with a capacity to degrade a wide range xenobiotic compounds (Dutta & Sarkar, 2015) and therefore substantiates a strong incentive for the use of aerobic granules in the bioremediation of aggressive industrial wastewaters.

In a clear demonstration of the technology's potential for industrial applications, several recent studies have reported largely positive results in terms of bioremediation performance and long-term process stability during the treatment of textile wastewaters in anaerobic-aerobic AGS SBRs. In a preliminary proof-of-principle investigation, Muda *et al.* (2010) explored the use of an aerobic granular sludge SBR operated with intermittent aerated and non-aerated periods for the treatment of a simulated effluent

loaded with three different textile dyes. AGS was developed from a mixed flocculent inoculum containing samples from textile mill sludge and successfully adapted to the feeding conditions to provide maximum COD and ammonia removal yields of 94 and 95% (respectively) and a maximum decolourisation yield of 62%. Colour removal during the aerobic reaction periods contributed as much as one third of the final decolourisation efficiency, demonstrating the ability of anaerobic microorganisms growing in the inner regions of the granules to degrade the dye even when bulk dissolved oxygen concentrations reached high levels (Muda *et al.*, 2010).

More recently, Lourenço *et al.* (2015) documented superior anaerobic and overall COD removal yields in an AGS SBR when compared to a similar reactor operated with flocculent biomass. Even though both systems attained comparable decolourisation yields during the treatment of Acid Red 14, the AGS bioreactor performed better in terms of detoxification of the dye reduction products as evaluated by yeast-based cyto- and genotoxicity assays. The findings were attributed to an aerobic arylamine-degrading activity developed in the AGS SBR and demonstrated by means of HPLC analysis (Lourenço *et al.*, 2015). In a different study, the same azo dye substrate was found to provide a long-term stabilizing effect to the structure of aerobic granules when compared to a control bioreactor fed with a dye-free synthetic wastewater. Fluorescence *in situ* hybridization (FISH) analysis was used to demonstrate the compact structure of dye-fed granules and confirmed the presence of a strong microbial activity down to the granule core. In contrast, aerobic granules in the dye-free control displayed significantly diminished FISH signals in their innermost regions, which were correlated with an increased tendency for creasing and breakup and with a rampant deterioration in sludge settleability. These results were attributed to the role of the azo dye substrate as an electron acceptor for the metabolism of obligate or facultative anaerobic microorganisms in the interior of aerobic granules and provided further validation for the use of AGS in the decolourisation of azo dyes. Despite the relevance of these findings, however, the observed developments in granule stability were found to have little effect on the carbon load removal activity of the dye-free control, which maintained performance levels similar to those of the dye-fed reactor (around 80% removal) (Franca *et al.*, 2015). This demarcation between granule structure and treatment performance underlines the need for parallel monitoring devices during bioreactor operation and is a cornerstone of AGS technology. Thorough descriptions of aerobic granular sludge properties, the principles of aerobic granulation, and the factors affecting granule stability will be provided further ahead as a conceptual basis for the experimental work described herein.

1.3.2 Physical and biological properties of aerobic granules (AGs)

Aerobic granules (AGs) are self-established microbial aggregates characterized by a robust and clearly-defined three-dimensional structure and high settling velocities. They boast a number of distinctive physicochemical features that set them apart from conventional activated sludge (CAS) flocs – ranging from size to density and shape – and play a major role in establishing the unique characteristics of AGS systems (de Kreuk *et al.*, 2005a). Among these features, the key defining elements laid out in the closing communiqué from the International Water Association's first session on AGS (de Kreuk *et al.*, 2005a) and in early review works by Adav *et al.* (2008a) and Gao *et al.* (2011a) can be summarized as follows:

- AGs are entirely microbial in origin, meaning they are established exclusively through auto-aggregation without the need for external carrier materials; the process of AG development is called aerobic granulation.
- AGs display significantly higher settling velocities (ranging from 10 to 100 m h⁻¹) than CAS flocs (no higher than 5 m h⁻¹); likewise, they boast fairly smaller sludge volume indexes (SVI; below 80 mL/g on the majority of cases and reaching as low as 20 mL/g), a descriptive parameter used to characterize sludge settleability and compressibility. These properties relate directly to the prime biomass retention and solid-liquid separation capacities of AGS bioreactors.
- Unlike CAS flocs, AGs have clear outlines, describing nearly spherical or elliptical shapes.
- Unlike CAS flocs, where resident populations can occupy both central and peripheral coordinates indiscriminately and interchangeably at any moment in time, microorganisms in AGs are tightly embedded in the EPS matrix and have relatively fixed positions within the three-dimensional structure.
- AGs have enough physical strength to maintain their granular form and structure during operation and do not coagulate under the nominal weight of surface abrasion and hydrodynamic shear stress.

In between studies, aerobic granules have been known to display significant variability, depending on inoculum structure, wastewater composition, existing selection pressures, and a number of specific operating conditions (Gao *et al.*, 2011a). Granule colour has been found to be deeply dependent on chemical composition and microbial population, with reports of yellow, black (Zheng *et al.*, 2006; Zhu *et al.*, 2008), white and red granules (Ni *et al.*, 2010; Winkler *et al.*, 2011a) making the rounds across the literature. Likewise, average AG diameters documented in dedicated studies have ranged from a few hundred micrometers – typically over 200 μ m (de Kreuk *et al.*, 2005a) – to as much as 5 mm (Bassin *et al.*, 2018), shifting up and down in tune with the parameters of bioreactor operation – high organic loading rates, for example, seem to stimulate the formation of larger AGs (Li *et al.*, 2008), whereas smaller-sized granules appear to emerge more commonly under high shear conditions or in association with long starvation periods (Gao *et al.*, 2011b).

Granule density typically falls close to the average values of CAS flocs but can shift upwards to as much as 1.3 kg dry weight m⁻³ owing to precipitate formation inside the EPS matrix (Winkler *et al.*, 2017). Significant differences in density can emerge even within a single aerobic granular sludge system, causing an uneven distribution of biomass particles across the sludge bed and effectively creating different environmental niches inside the bioreactor for each of them (Winkler *et al.*, 2011a,b). These differences are typically caused by disparities in the microbial structure of the aerobic granules and pertain directly to the physical properties and metabolic abilities of the resident microorganisms (Winkler *et al.*, 2013).

In line with their remaining properties, microbial communities in AGs differ significantly from those found in CAS flocs. Multiple authors have reported wide-ranging shifts in the number and prevalence of specific bacterial families during the transition from flocculent to granular sludge and even along the growth and maturation stages of the AG life cycle (Li *et al.*, 2008; Zhang *et al.*, 2011; Lv *et al.*, 2014). However, the predominant organisms in both types of sludge share common phylogenies and physiological functions for nitrogen, carbon, and phosphate removal, implying that granule formation may be population-

independent (Winkler *et al.*, 2017). This assertion is further backed by the multitude of different CAS inocula used thus far to develop AGs, which ranges in scope from defined mixed and simple bacterial or fungal populations (Hailei *et al.*, 2006; Adav *et al.*, 2008b) to uncharacterized sludge samples from pre-existing wastewater treatment units (Morgenroth *et al.*, 1997; Dangcong *et al.*, 1999; de Kreuk *et al.*, 2005b).

In those cases where complex communities are used as seeds, developed AGs can host a wide variety of microorganisms from all domains of life, including archaea, bacteria, yeasts, fungi, protozoa and simple metazoans such as nematodes. As a rule, *Proteobacteria* represent the most common phylum, followed by *Firmicutes*, *Actinobacteria* and *Bacteroidetes*. Out of these phyla, several populations of fast-growing heterotrophs known to produce EPS are commonly identified, including isolates from the genera *Zoogloea*, *Thauera*, *Pseudomonas*, *Flavobacterium*, *Chryseobacterium*, *Stenotrophomonas* and *Acinetobacter* (Winkler *et al.*, 2017). The specific make-up of the microbial community is dependent on a range of external and internal factors, including, as stated, inoculum structure, as well as granule size and wastewater composition (Gao *et al.*, 2011; Winkler *et al.*, 2017).

To date, granulation has been achieved using both synthetic feed solutions with defined concentrations of simple organic substrates (such as glucose, acetate, ethanol or phenol) (de Kreuk *et al.*, 2005b; Adav *et al.*, 2008b) and real wastewaters from municipal and industrial sources (Arrojo *et al.*, 2004; Su & Yu, 2005; Weber *et al.*, 2007; Ni *et al.*, 2009; Derlon *et al.*, 2016). In each case, inoculated microbial communities were shown to evolve and adapt to the presence of specific wastewater constituents, aggregating to form AGs with different grades of species richness and diversity and, often, different morphologies. In a comparative example, glucose-fed aerobic granules were observed to contain significant numbers of filamentous bacteria at their surface while acetate-fed AGs hosted mostly rod-shaped bacteria and no filaments (Tay *et al.*, 2001a). Filamentous bacteria were similarly shown to be the predominant species in an AGS system developed with brewery wastewater, with significant populations identified as part of *Thiothrix* spp. and *Sphaerotilus natans* (Weber *et al.*, 2007).

In AGs developed for phenol degradation, yeast genera such as *Rodotorula*, *Trichosporon* and *Candida* have been identified in association with relevant activities involved in the breakdown of phenolic compounds (Gao *et al.*, 2011a; Adav *et al.*, 2007a), whereas populations of aerobic ammonium oxidizers, nitrite oxidizers, denitrifiers and, in some cases, ANAMMOX bacteria have been shown as a recurring staple in systems performing nitrogen removal (Tsuneda *et al.*, 2003; Adav & Lee, 2009; Ni *et al.*, 2010; Winkler *et al.*, 2011a; Winkler *et al.*, 2012). Finally, AGS reactors engaged in enhanced biological phosphorus removal are characterized by significant numbers of polyphosphate-accumulating organisms (PAOs) – the likes of *Candidatus Accumulibacter phosphatis* and *Tetrasphaera* – and competing specimens of glycogen-accumulating organisms (GAOs) – such as *Candidatus Competibacter phosphatis* (Gonzalez-Gil & Holliger, 2011; Zhang *et al.*, 2011).

Conceptually, these populations can all coexist simultaneously within a single AG, occupying specific niches across the granular volume to form a clearly stratified architecture. In all, three main microbial strata can be distinguished – a layer of heterotrophic, aerobic bacteria occupying the outermost sections, a layer of denitrifying bacteria, PAOs and GAOs developed across the middle range, and a layer of

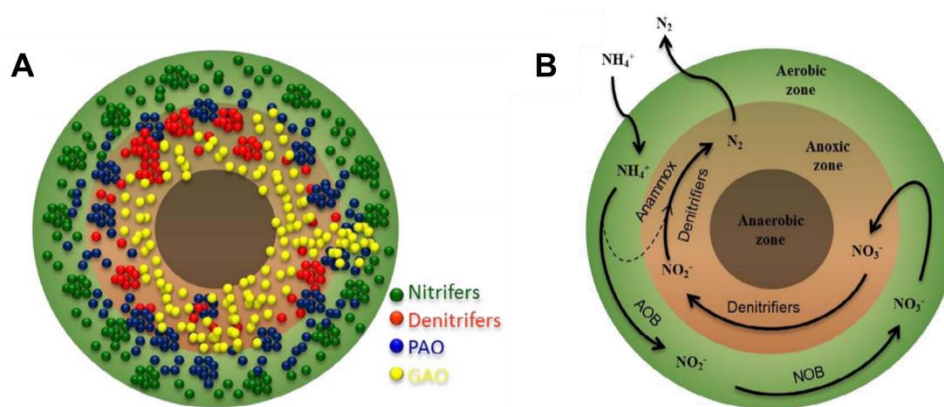


Figure 1.2 | Microbial community structure and metabolic functions inside an aerobic granule. Graphical representation of segregated (A) population and (B) nitrogen removal pathway distributions within the structure of a conceptual aerobic granule (after Nancharaiah & Reddy, 2018)

facultative and obligate anaerobes established closer to the core (Gao *et al.*, 2011a). Distribution patterns across these layers follow oxygen diffusion gradients through the AG matrix and demarcate discrete aerobic, anoxic and anaerobic microenvironments. The specific depth of each layer is determined by granule porosity and pore clogging and is intimately connected to AG size (Adav *et al.*, 2008a). Examples available in the literature report a prevalence of *Ca. Accumulibacter* spp. at a depth of 200 μm – followed by *Ca. Competibacter* spp. in slightly deeper regions (Lemaire *et al.*, 2008a) –, the presence of aerobic ammonium oxidizers from the genus *Nitrosomonas* at a depth of 70–100 μm and a pocket of anaerobic bacteria stretching from 800 μm to 1 mm (Tay *et al.*, 2002), and a layer of dead cells and proteinaceous matter stretching far into the granular core (Toh *et al.*, 2003). Metabolic interactions between microorganisms at different depths create the conditions for multiple simultaneous conversion processes within the granular volume and offer countless possibilities for the removal of organic carbon, nitrogen, phosphorus and micropollutants (such as pharmaceuticals and personal care products, recalcitrant or toxic xenobiotic compounds and metal ions) (Nancharaiah & Reddy, 2018). An example of one such chain of interactions – specifically associated with N removal – is provided in Figure 1.2 along with a schematic representation of population distributions inside a conceptual AG.

1.3.3 AG formation and maintenance: insights from biochemistry, SBR engineering and microbiology

Aerobic granulation is commonly thought to evolve according to a comprehensive four-step mechanism combining elements of physicochemical interaction with microbial physiology and biochemistry. These steps include (i) an initial cell-to-cell attachment stage to start the process, (ii) the development of microaggregates by self-attached cells, (iii) a period of extensive EPS biosynthesis by the aggregated microorganisms, and (iv) a final granule maturation stage elicited in response to external hydrodynamic parameters – as determined by bioreactor configuration and operating conditions – and involving both sustained sessile cell growth and continued EPS production within the three-dimensional structure (Sarma *et al.*, 2017). A schematic overview of this mechanism is shown in Figure 1.3.

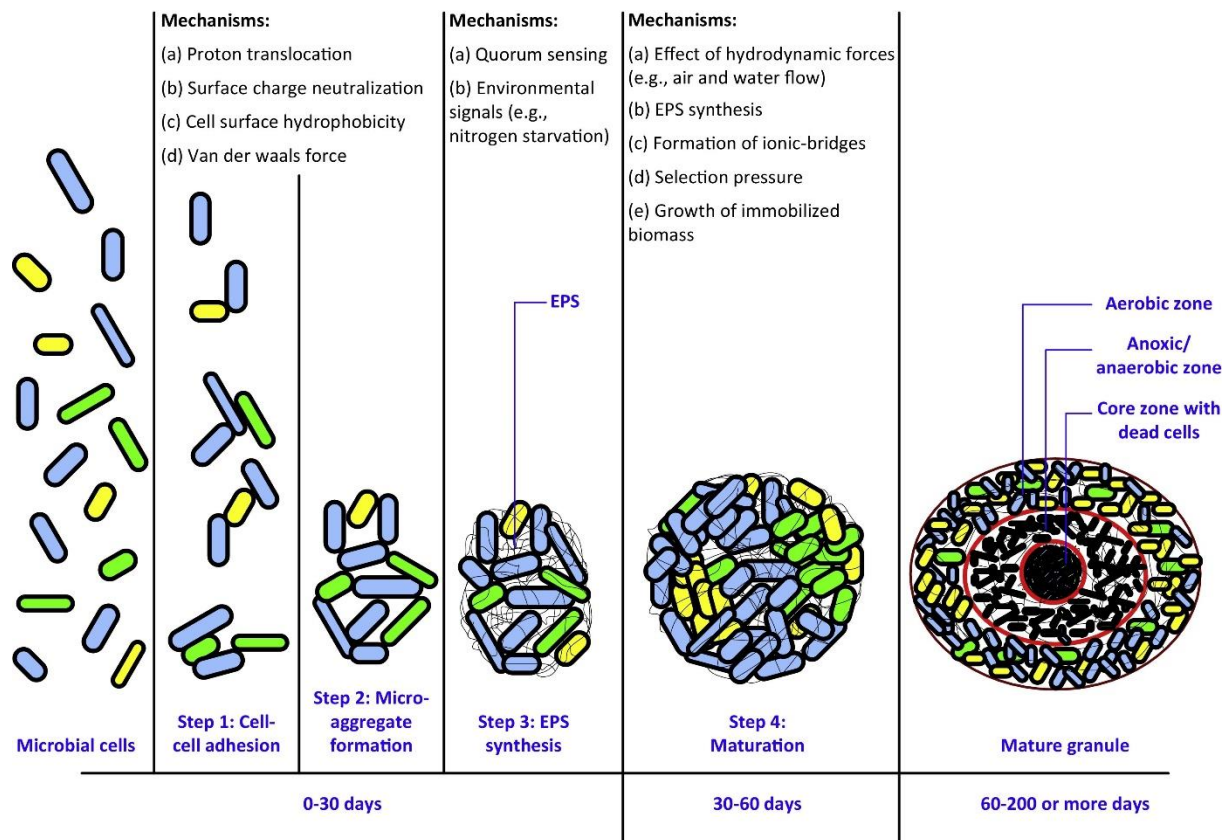


Figure 1.3 | The aerobic granulation process. Schematic representation of the aerobic granulation process and the mechanisms involved in each step (after Sarma *et al.*, 2017)

Cell-to-cell contacts during the initial stages of granule formation are mostly thought to be the product of physical and thermodynamic forces – including hydrodynamic and diffusion forces and Brownian movements – as well as cell mobility (Liu & Tay, 2002; Sarma *et al.*, 2017). Upon contact, attractive physicochemical and biological interactions between communicating cells promote the development of tight bilateral connections and provide for the establishment of self-attached precursor microcolonies. Among the adhesive forces listed in the literature as possible drivers for microbial aggregation, van der Waals interactions between cell surface components, surface tension, cell membrane fusion, and bridging effects resulting from the presence of filamentous bacteria constitute some of the most common examples (Liu & Tay, 2002). In addition to these factors, the introduction of divalent cations (e.g., Ca^{2+} , Mg^{2+} , Fe^{2+}) to the sludge system has been highlighted repeatedly for its positive, multilateral action in the process, most notably for its roles in the neutralization of negative cell surface charges – acting to minimize cell repulsion – and in the development of scattered, solid, inorganic nuclei for microbial aggregation through the formation of insoluble precipitates (including calcium carbonate and multiple phosphates) (Jiang *et al.*, 2003; Li *et al.*, 2009; Nancharaiiah & Reddy, 2018)

Amid the flood of putative aggregative stimuli, the most consensual view seems, however, to hold the development of hydrophobic interactions between microbial cell surfaces as the most crucial factor affecting the formation of seed bacterial aggregates (Liu & Tay, 2002; Sarma *et al.*, 2017). Reports of rising relative biomass hydrophobicity over the various stages of granule development have accumulated over the years (Tay *et al.*, 2001b; Wang *et al.*, 2005; Zheng *et al.*, 2005), hinting at

consistent changes on either a biomolecular or physiological level that lead to the dehydration of external cell surfaces and promote cell-to-cell attachment as a way of lowering the system's free energy (Liu & Tay, 2002). Sharp rises in proton translocation towards the extracellular medium (leading to surface charge neutralization and decreased solvation) have been listed as possible causes, but the actual molecular developments operating behind this phenomenon during the early phases of granulation remain unknown (Sarma *et al.*, 2017).

Following the formation of precursor microcolonies, the aggregated microorganisms initiate a stage of significant EPS production that continues side by side with attached cell growth throughout the remaining steps of the granulation process. During these final steps, microscopic microbial clusters develop first into unstructured and immature granules with small sizes, and later into large, compact structures displaying discrete environmental niches (Sarma *et al.*, 2017) and measuring anywhere between a few hundred micrometers and 5 mm (Bassin *et al.*, 2018). Transition from one state to the other relies on a tight balance between structural growth, resulting from microbial propagation, EPS biosynthesis, and/or two-way bioaggregate coalescence, and structural strain, a consequence of surface attrition and/or granule sloughing that manifests in response to the external hydrodynamic shear forces exerted by aeration and dispersive particle-particle collisions (Liu & Tay, 2002; Verawaty *et al.*, 2012; Zhou *et al.*, 2014).

The EPS matrix developed during this period comprises a complex mix of proteins, polysaccharides, humic substances, nucleic acids and lipids that acts both as a scaffold for bacterial adhesion and as the basic structural foundation of the aerobic granule (Adav *et al.*, 2008a; Nanchaiah & Reddy, 2018; Sarma *et al.*, 2017). Research papers investigating the roles of the various chemical classes of EPS during aerobic granulation have amassed over the years, generating a number of different theories striving to rationalize the link between the properties of EPS molecules, granule structuration and cellular aggregation. The accumulation of hydrophobic components – such as amino acids and proteins –, for instance, has been suggested to contribute for a direct increase in cell surface hydrophobicity and to promote microbial attachments through hydrophobic interactions (Zhang *et al.*, 2007). Bound EPS in general, and proteins specifically, have similarly been proposed to foster microbial adhesion by reducing the negative surface charges of bacterial cells, contributing to maintain a tightly packed assembly through the minimization of repulsive cell-to-cell interactions (Gao *et al.*, 2011a; Zhang *et al.*, 2007).

On the subject of structure, early interpretations of EPS composition and distribution in AGS systems led authors to suggest the development of a protein core within the aerobic granule as the most crucial pre-requisite for mechanical stability (McSwain *et al.*, 2005; Zhang *et al.*, 2007). More recently, however, Adav *et al.* (2008) demonstrated that the structural stability of aerobic granules is less dependent on the composition of the core and more on the presence of an external EPS layer with an elastic, $\beta(1\rightarrow3)$ -linked polysaccharide backbone onto which other polymeric compounds with non-architectural functions can adhere. Unlike the removal of proteins, lipids, and α -polysaccharides, selective enzymatic hydrolysis of this carbohydrate skeleton in mature granules was shown to result in immediate fragmentation, hinting at an important role in structural maintenance. In a different study, Seviour *et al.* (2009) struck a similar chord by conflating granule architecture with a single, high-molecular weight exopolysaccharide fraction isolated from lyophilized aerobic granules via gel permeation

chromatography. The extracted polysaccharide was shown to exist as a gel under neutral to slightly acidic pH conditions (similar to those found in wastewater treatment units), forming pearl-necklace-like, intramolecularly condensed assemblies that were suggested to hold the basic structural matrix of the granule in place. Apart from these exopolymer-specific considerations, many authors have defended a general role for divalent metal cations in the preservation of granule integrity, emphasizing their ability to endorse polymer cross-linking across the EPS matrix and promote tighter connections between individual molecular units (Sarma *et al.*, 2017; Wilén *et al.*, 2018).

Even through the fog of all this information on the underlying molecular mechanisms, continuous efforts have been made to optimize the granulation process. Engineering parameters such as the organic loading rate (OLR) (Tay *et al.*, 2004), shear stress (Liu & Tay, 2002; Tay *et al.*, 2001b), hydraulic retention time (HRT) (Pan *et al.*, 2004), sludge retention time (SRT) (Li *et al.*, 2007), selection pressures (Qin *et al.*, 2004a) and periodic starvation stages (Li *et al.*, 2006), and microbiological parameters such as quorum sensing (QS) signalling (Tan *et al.*, 2014) have all been investigated to establish their roles in granule formation and maintenance (Sarma *et al.*, 2017). Views on the operational dimension behind these processes suggest complex trade-offs are at work at all times in any AGS system and that multiple parameters can be differentially and individually regulated to steer and mold AG development and properties in whatever way seems suitable (Adav *et al.*, 2008a; Gao *et al.*, 2011a; Franca *et al.*, 2017b).

The three criteria most often cited as granulation drivers are (i) the application of high hydrodynamic shear forces, (ii) feast-famine alternation, and (iii) the removal of non-granulated biomass (Wilén *et al.*, 2018). High sludge wash-out rates are thought to act as an accelerant by creating a hydraulic selection pressure that encourages the removal of slow-settling flocs while promoting the physical selection of bigger particles and can be achieved by imposing short settling periods at the end of SBR cycles (Adav *et al.*, 2008a). Shorter settling times have also been found to result in increased cell surface hydrophobicity and EPS production, suggesting biomass particles might respond to the selection pressure with increased aggregation in a bid to raise the chances for retention in the bioreactor (Qin *et al.*, 2004a; Qin *et al.*, 2004b). Similar developments have been reported as a response to the imposition of periodical aerobic starvation (famine) periods and high shear forces, further backing their relevance in the process (Tay *et al.*, 2001b; Liu & Tay, 2002; Li *et al.*, 2006). Regulating the magnitude of shear stresses and the duration of famine phases – as well as a number of other conditions such as OLRs and SRT – can, however, have a significant impact on AG structure and has been reported to have a momentous influence over their stability (Franca *et al.*, 2017b). In one example, Liu and Tay (2008) showed that a short starvation time could speed up the formation of granules but had a negative long-term impact, leading to fluffy morphologies with filamentous outgrowths that limited substrate penetration, caused settleability decays and ultimately forced the bioreactor into shutdown. Likewise, a study into the effects of aeration intensity and the associated shear stresses conducted by Adav *et al.* (2007b) with phenol-degrading AGs showed that insufficient aeration could similarly lead to the development of unstable and excessively large fluffy granules that significantly damaged long-term bioreactor operation. An in-depth review on the makings and undoing of AGS stability has recently been published by Franca *et al.* (2017b) detailing all the ways in which process condition have been shown to influence granular sludge SBRs over lengthy operation periods and available strategies to avoid instability. One such strategy – the use of anaerobic feeding phases for the selection of slow-growing

microorganisms – is at the core of most of the work described in this document and will be analysed in greater detail over the following section. The review is recommended as follow-up reading to the interested reader looking for information on other alternatives.

More recent strides in AGS research have yielded important information regarding AG integrity and stability at the levels of energy metabolism and cell-to-cell communication (Franca *et al.*, 2017b). The role of cellular interactions specifically has been mainly explored by detecting autoinducer molecule-producing bacteria (*Aeromonas* sp., *Pseudomonas* sp., and *Acinetobacter* sp.), quorum sensing (QS) molecules – mainly *N*-acyl-homoserine lactones (AHLs) and autoinducer-2 (AI-2) – and quorum quenching (QQ) enzymes with an ability to degrade QS signals in AGs (Nancharaiah & Reddy, 2017), or by observing the effects of exogenous QS molecule additions and augmentation with QS and QQ bacteria. In one example, the concentration of AHLs, a common autoinducer produced by Gram-negative bacteria, was shown to increase with granulation (Jiang & Liu, 2012) and AGS was demonstrated to have a higher content of AHLs than floccular sludge (Li *et al.*, 2014; Lv *et al.*, 2014). When an SBR was inoculated with floccular sludge and operated to promote AG development, strong positive correlations between EPS production and AHL concentrations were seen to arise over the course of granulation; likewise, parallel AHL add-back studies were shown to result in increased EPS synthesis, hinting at a causality link between the two processes. In the same study, over 50% of the 50 most common microbial isolates were shown to bear strong simultaneous positive correlations with at least one AHL and with granulation, pointing at a community level coordination of QS-regulated AG development (Tan *et al.*, 2014). Quorum quenching has also been found to have an important impact on granule development, acting as an effective modulator of QS activity in the transition from flocculent to granular morphology. Coherent shifts in microbial community structure were observed during granulation, with a higher proportion of QQ active bacteria in the floccular sludge and a higher proportion of bacteria with QS activity in the granules (Tan *et al.*, 2015).

Despite the wealth of information on granule formation, however, data on the relation between AG maintenance and decay and QS mechanisms is much sparser. In one of the most relevant examples out of the few, Tan *et al.* (2014) found AHL levels tended to drop during later stages of granule maturation and disintegration and once again observed a community shift during structural breakdown, favoring microorganisms that correlated negatively with granulation. Likewise, very few studies have been published establishing the link between macroscopic operational conditions known to impact granule formation/stability and communicational responses at the microscopic level. In a rare examples, AI-2 levels in AGs were shown to increase throughout the aerobic starvation stages of SBR cycles and to promote the production of EPS with high molecular weights, leading to cell adhesiveness enhancement and granule formation. In the long run, signal concentrations were shown to be higher in bioreactors operated with a 5-h famine phase as compared to 3-h and 7-h periods, suggesting bacterial communication was maximized along the middle ground (Liu *et al.*, 2016). To patch some of these information holes, we describe the analysis of sludge QS signal (specifically, AHL) levels over the course of a long-term operation in two SBRs operated according to different feeding strategies (known to impact on AG stability) and different hydrodynamic shear stresses (known to impact AG development). The experimental design will include the identification of specific AHL production patterns associated with each of these conditions both in an initial granulation phase and in the long run and will be combined

with other analytical methods to fully characterize sludge properties. To better understand the setting and goals of the work at hand, a full context will be provided over the next two sections.

1.4 AGS stability and feeding configuration

1.4.1 The link between anaerobic feeding in AGS SBRs and AG stability

Among the challenges currently facing the dissemination of AGS systems as the default treatment solution for industrial wastewaters, the development of structurally stable aerobic granules able to withstand long operation periods without losing their integrity or faltering in terms of treatment performance remains one of the toughest hurdles to clear (Lee *et al.*, 2010; Zhang *et al.*, 2016; Franca *et al.*, 2017b). Granule disintegration and washout episodes in lengthy operations have been reported by multiple authors since the inception of AGS research and have been consistently associated with severe decays in sludge settleability, effluent quality (owing to the presence of high suspended solids concentrations) and treatment performance (Schwarzenbeck *et al.* 2005; Zheng *et al.*, 2006; Liu & Tay, 2008), a combination of undesirable scenarios that has inspired a measure of caution even as AGS technology is transitionally implemented in existing large-scale treatment facilities (Lee *et al.*, 2010; Pronk *et al.*, 2015a). Efforts to prevent or curtail the impacts of granule disintegration in lab-scale research have thus far relied on the modulation of specific bioreactor operating parameters – including organic loading rates, food-to-microorganism ratios, sludge retention times, starvation periods and feeding regimes – with a view to fine tune specific granule properties bindingly associated with AGS stability, such as granule diameter (Zhu *et al.*, 2013), precipitate build-up within the granule (Isanta *et al.*, 2012), the presence (or absence thereof) of filamentous bacteria (Chen *et al.*, 2007), or the average growth rate of the microbial community (Liu *et al.*, 2004; de Kreuk & van Loosdrecht, 2004). Among these strategies, the imposition of an anaerobic feeding period prior to the onset of aeration constitutes one of the best reported case studies and currently represents an inescapable staple of AGS research (de Kreuk & van Loosdrecht, 2004; Rocktäschel *et al.* 2013; Franca *et al.*, 2015; Pronk *et al.*, 2015a; Franca *et al.*, 2017a).

Effectively in continuous use since its first description 14 years ago, anaerobic feeding in AGS SBRs has been repeatedly shown to promote the development of stable aerobic granules by enriching slow-growing bacterial populations within the sludge community (de Kreuk & van Loosdrecht, 2004; Pronk *et al.*, 2015b) – a trait long since demonstrated, as discussed above, to bear a positive influence over the density and structural cohesion of granules and biofilms (Picioreanu *et al.*, 1998). Among the enriched populations, the examples of polyphosphate- and glycogen-accumulating organisms (PAOs and GAOs), a heterogenous group of bacterial genera sharing an ability to assimilate and convert dissolved, readily biodegradable COD into intracellular storage polymers, are those most commonly listed in the dedicated literature (Winkler *et al.*, 2017). Selection of PAOs and GAOs works across the entire feeding and reaction stages and relies on the definition of clearly segregated anaerobic feast and aerobic famine periods (Franca *et al.*, 2017b). During the feast phase, these bacteria strip the mixed liquor of simple carbon sources – in most cases volatile fatty acids (VFAs; *i.e.*, acetate and propionate) – and amass

significant endogenous energy reserves in the form of polyhydroxyalkanoate (PHA) granules. After the available COD in the influent wastewater is exhausted and the aerated reaction is initiated, the stored PHA acts as the sole carbon and energy source for cell maintenance and growth and secures the survival and proliferation of PAOs and GAOs over the length of the famine phase (Oehmen *et al.*, 2007). In the absence of similar endogenous resources, fast-growing aerobic heterotrophs, such as filamentous bacteria (a typical root cause of granule instability), are effectively starved out of the system, leading to a relative enrichment of slow growers and ultimately providing for the development of stable granular structures (de Kreuk & van Loosdrecht, 2004; Pronk *et al.*, 2015b).

1.4.2 Bioreactor geometry and anaerobic feeding configurations as determinants of AG stability

The first report on the use of an anaerobic feeding stage during the operation of an AGS SBR was advanced by de Kreuk & van Loosdrecht (2004) and described a tubular system ($H/D = 14$) operated with a prolonged, non-aerated and non-mixed (*i.e.*, static) plug-flow filling phase expressly designed to promote a meaningful contact between the settled biomass and the influent substrate. Steep concentration gradients between the bulk influent and the granular matrix allowed the substrate to penetrate the entire granule depth and to be converted by relevant bacterial populations into storage polymers. Rapid COD consumption throughout the anaerobic feeding (feast) phase resulted in the establishment of a long aeration period with limited available substrate (famine phase), effectively providing for the domination of GAOs and PAOs. Throughout the monitored operation window, slow growth of PAOs and GAOs on the internally stored substrate occurred across the entire granular structure and ensured adequate conditions for long-term granule maintenance and a stable bioreactor operation (de Kreuk & van Loosdrecht, 2004). The use of an anaerobic plug-flow filling period in tubular SBRs has since become a dependable process tool to secure the establishment of stable aerobic granules and has featured in multiple studies relating directly to or otherwise entirely unconcerned with the issue of stability (Liu *et al.*, 2010; Winkler *et al.*, 2011b; Pronk *et al.*, 2015b; Bassin *et al.*, 2012). Moreover, the configuration is currently disseminated as a key feature of the full-scale municipal wastewater treatment system Nereda®, an AGS-based technology in extant use or pending implementation in 12 countries across 4 continents – including the Netherlands, Portugal, South Africa, Brazil, Australia, and the US (Royal HaskoningDHV, 2018).

Despite its popularity, however, the success of this strategy in the treatment of strong industrial wastewaters seems to depend on reactor geometry to a non-negligible degree. Unlike the case of tubular bioreactors, plug-flow feeding in SBRs with low H/D ratios has been associated with uneven flow patterns and channelling effects across the granular sludge bed that can limit the effective contact time between the biomass and the influent substrate and impact on anaerobic carbon uptake (Franca *et al.*, 2017a; Rocktäschel *et al.* 2013). As a result, significant amounts of unconsumed COD might leak from the anaerobic feeding stage into the aeration period, acting as substrate for fast-growing aerobic heterotrophs distributed along the outer regions of the aerobic granules and contributing for granule instability by limiting substrate accessibility in the inner regions (Franca *et al.*, 2017a; Rocktäschel *et al.*

2013). These outcomes take on an even more concerning dimension when the ultimate goal of full-scale implementation is considered, seeing as non-tubular bioreactors represent the default choice in virtually all existing and projected wastewater treatment plants (Henriet *et al.*, 2016).

In an effort to sidestep this scenario, Rocktäschel *et al.* (2013) proposed the implementation of an alternative anaerobic feeding arrangement consisting of a fast filling step followed by a period of anaerobic mixing. Using an AGS SBR ($H/D = 2$; non-tubular reactor) fed with PAO-rich and stable aerobic granules, the authors applied a plug-flow feeding strategy over 70 days and subsequently switched the feeding method to their proposed alternative as a way of evaluating the system's behaviour in both conditions. COD depletion during plug-flow feeding proved insufficient, paving the way for fast consumption during the first 60 minutes of aeration. As a result, heterotrophic filamentous bacteria proliferated in large numbers, leading to the development of fluffy and unstable granules. Upon the introduction of an anaerobic mixing period, COD consumption profiles described the canonical structure of an anaerobic feast phase followed by an aerobic famine period, allowing for the re-establishment of granules with even outlines and no filamentous outgrowth. Even though the introduction of mechanical stirring proved detrimental in terms of biomass concentration and the contribution of the fast filling stage for carbon removal was deemed negligible, the authors concluded that high anaerobic COD uptake and stable granule maintenance can be efficiently achieved regardless of bioreactor geometry by applying a mixed period that ensures an even substrate distribution throughout the entire reactor working volume and facilitates a homogenous substrate consumption (Rocktäschel *et al.*, 2013).

In a recent investigation conducted by our research group (Franca *et al.*, 2017a), this strategy was combined with the static plug-flow arrangement advanced by de Kreuk & van Loosdrecht (2004) in a bid to ascertain whether a combined configuration could provide any advantage for granule stability. Using a non-tubular SBR engaged in the treatment of a synthetic textile wastewater, the fast equalization stage proposed by Rocktäschel *et al.* (2013) was replaced with a long (1-hour) anaerobic plug-flow filling phase so as to establish an initial period of residual COD consumption. To build on the contribution from filling and secure a meaningful anaerobic carbon conversion yield, a shortened (1-hour), non-aerated mixing period was provided before the onset of aeration. The bioreactor was run for 315 days and continually subjected to shifts in feed concentration and substrate composition in order to assess long-term granule stability and the system's response to external perturbations. A geometrically identical control SBR run with a fast filling stage (30 minutes) and a longer stirring phase (1 hour and 30 minutes) – more closely aligned with the model proposed by Rocktäschel *et al.* (2013) – was operated in parallel and monitored concurrently for granule development, sludge settleability and treatment performance (Franca *et al.*, 2017a). Interestingly, the hybrid feeding strategy was shown to allow for faster AGS recovery in response to the imposed disturbances in feed composition, with significantly less dramatic rebounds in terms of biomass concentration, sludge settling properties, and sludge retention time than recorded in the control SBR. Fluorescence micrographs of biomass samples collected from both bioreactors revealed sizeable PHA reserves that remained intact in the hybrid feeding system and seemed to subside over the course of the famine phase in the control, suggesting that microorganisms in the latter system might have been in carbon starvation towards the end of the reaction cycle (Franca

et al., 2017a). The combination of these results hints at a better case for the maintenance of long-term operational stability in association with the alternative feeding scheme suggested by the authors and substantiates a new and largely unexplored avenue for granule stabilization through anaerobic feeding.

In an effort to advance the knowledge on this novel arrangement, the present study was framed as a test to the reproducibility of the results described by Franca *et al.* (2017a) and as a deeper investigation of the drivers behind granule stabilization in plug-flow-fed, anaerobically-mixed SBR systems. The bioreactors employed in the initial report were once again operated using a synthetic textile wastewater – prepared with a hydrolysed, starch-based sizing agent, an azo dye and a high dose of Ag NPs – and fed with a nominally constant composition for 192 days to assess long-term process stability and eliminate the variability produced by changes in the feed solution. Stability was evaluated in terms of granule number and structure, macroscopic biomass properties (settleability and inventory) and treatment performance (as judged by COD and colour removal yields) and interpreted simultaneously as a product of feeding configuration and Ag NP loading. Context for the action of Ag NPs over granule stability will be provided in the following section.

1.5 Silver nanoparticles (Ag NPs) and AGS: environmental impact and fate during wastewater treatment

1.5.1 Antimicrobial finishing of textiles and Ag NPs: basic principles, antimicrobial action and environmental impact

In recent years, the antimicrobial finishing of textiles has become extremely important in the production of protective, decorative, and technical textiles (Simoncic & Tomsic, 2010). The growth of microorganisms on textiles inflicts a range of unwanted effects, including the generation of unpleasant odour, stains, decolourisation of the fabric, a reduction in fabric mechanical strength, and an increased likelihood of contamination (Gao & Cranston, 2008). Antimicrobial finishes are therefore desirable or otherwise indispensable in articles as diverse as industrial fabrics (especially those exposed to weather), home furnishings (e.g., carpets, mattresses, shower curtains), utensils for outdoor activities (e.g., tents, screens, ropes), technical textiles for healthcare applications, sportswear, and intimate apparel (e.g., brassieres, underwear, socks) (Schindler & Hauser, 2004).

On account of their eclecticism and importance, the number of antimicrobial agents suitable for textile applications on the market has increased dramatically in the recent past (Simoncic & Tomsic, 2010). Conventional choices tend to fall on chemicals with proven antimicrobial action in other industrial applications (e.g., as food preservatives, disinfectants, swimming pool sanitizers, or components of wound dressings) (Gao & Cranston, 2008) and include quaternary ammonium compounds, triclosan, chitosan, *N*-halamine, peroxyacids, polyhexamethylene biguanide, metal salts, and nanostructured metallic materials (Schindler & Hauser, 2004; Gao & Cranston, 2008; Simoncic & Tomsic, 2010). Among these examples, nano-sized metals and metal oxides (*i.e.*, metallic materials with at least one dimension inferior to 100 nm) have benefitted from the greatest deal of attention over the course of the last decade on account of their unique physicochemical properties, biological activity and their potential to enhance

textile functionalities (Simoncic & Tomsic, 2010; Rivero *et al.*, 2015). On par with titanium dioxide (TiO₂) and copper (II) oxide (CuO) (Simoncic & Tomsic, 2010), silver nanoparticles (Ag NPs) have yielded some of the most promising results in terms of antimicrobial action, regarding both efficiency and durability (Radetic, 2013). Zhang *et al.* (2009) reported 99.01 and 99.26% reductions in *Staphylococcus aureus* and *Escherichia coli* populations, respectively, after treating a cotton fabric with 88 mg kg⁻¹ of a nano-silver colloid developed from aqueous silver nitrate. The antimicrobial activity was maintained at over 98.77% bacterial reduction levels even after 20 consecutive home laundering cycles (Zhang *et al.*, 2009). Similar results were described by Gerber *et al.* (2011) after testing the effect of silver-tricalcium phosphate nanoparticles applied onto polyamide 6 fibres to build a reactive system against bacteria such as *E. coli* and *Streptococcus sanguinis*, with a reported killing efficiency of 99.99 or 100% within 24 h of contact time, respectively (Gerber *et al.*, 2011). In addition to their enhanced antimicrobial action, Ag NPs have proven advantageous in producing little or no changes to fabric colour, breathability, and handle, and hence superior to simpler finishes with ionic silver (which can significantly alter fibre properties) (Radetic, 2013).

The mechanisms underpinning the antimicrobial action of silver nanoparticles are yet to be fully elucidated, but are generally suggested to result from the combined effects of three interconnected toxicity pathways involving (i) the release and uptake of silver ions (Ag⁺), (ii) the generation of reactive oxygen species (ROS) on the surface of the nanoparticles or by action of Ag⁺, and (iii) cell membrane damage inflicted directly by Ag NPs (Marambio-Jones & Hoek, 2010). The release of Ag⁺ from silver nanoparticles is regarded as the main toxicity effector (Le Ouay & Stellacci, 2015) and has been reported to occur in aqueous solution under oxic conditions according to a dissolution reaction where dissolved O₂ acts as an oxidant to produce a soluble silver oxide (Marambio-Jones & Hoek, 2010; Radetic, 2013; Le Ouay & Stellacci, 2015). Ionic silver is known for its high affinity towards organic amines, phosphates, and sulphur-containing compounds, and can inactivate a range of vital enzymes by binding several key functional groups in their structure (especially thiolates in cysteine residues and selenates in selenocysteine residues) (Prabhu & Poulouse, 2012). Unlike conventional antibiotic systems used to target specific components of the cell cycle, the highly reactive nature of Ag⁺ elicits a non-specific antimicrobial response that impacts multiple metabolic pathways and cellular functions simultaneously. This indiscriminate action is often regarded as one of the main reasons for the antimicrobial activity of silver against a broad spectrum of microorganisms and constitutes one of the primary appeals of Ag NPs in the context of textile finishing (Le Ouay & Stellacci, 2015).

In addition to the direct inactivation of key biological molecules, several authors have suggested the generation and concentration of ROS in the intracellular medium as an important part of the biocidal action of Ag NPs (Park *et al.*, 2009; Le Ouay & Stellacci, 2015). Exposure to excess concentrations of ROS is associated with a range of damaging effects in multiple cellular structures, including proteins, lipids, and DNA, and can ultimately result in the shutdown of important physiological functions leading to cell death (Apel & Hirt, 2004). Besides these effects, silver nanoparticles are currently recognised to interact directly with cell membranes, inflicting serious structural damage and penetrating microbial cells to unleash a range of reactive biomolecular transformations (Marambio-Jones & Hoek, 2010; Prabhu &

Poulose, 2012; Radetic, 2013). Much to the similarity of ionic silver, native Ag in the nanoparticle surface is thought to interact with sulphur-rich proteins and phosphate groups in DNA molecules, causing a severe disruption in key cellular functions (including the selective permeability of the cell membrane and respiration), and either inhibiting DNA replication or provoking the outright destruction of genetic material (Morones *et al.*, 2005; Prabhu & Poulose, 2012; Radetic, 2013). These effects are exclusive to nanoparticle systems and are the direct result of their reduced dimensions and of the surface properties imparted on Ag NPs during synthesis (Le Ouay & Stellacci, 2015).

Because of their physicochemical and biological features, silver nanoparticles have attracted attentions far and wide, way beyond the horizons of textile manufacturing. As of October 2017, the Project on Emerging Nanotechnologies' Consumer Products Inventory listed 442 products containing Ag NPs, including items as diverse as throat and nasal sprays, air and water purifiers, air conditioners, vacuum cleaners, blow dryers, curling irons, fabric softeners, antibacterial socks and insoles, toothpastes, toothbrushes, and beauty creams (The Project on Emerging Nanotechnologies, 2017). The number of entries has seen a 41% increase from 2013 to 2017 and is expected to keep rising consistently as commercial nanotechnological commodities establish a comfortable position in the global economy (Tran & Le, 2013). Given the vast number of products leveraging the benefits of silver nanomaterials, fundamental concerns regarding the potential human and ecosystem hazards associated with their increased utilization have been raised in the recent past (Marambio-Jones & Hoek, 2010).

Silver nanoparticles may be released to the environment from discharges at the point of production, from erosion of engineered materials in household products (e.g., antibacterial coatings and silver-impregnated water filters), and from washing or disposal of silver-containing products (Benn & Westerhoff, 2008; Marambio-Jones & Hoek, 2010; Hou *et al.*, 2012; Kaegi *et al.*, 2013; Demirel, 2016). Results from simulated material flows suggest that the majority of Ag NPs in consumer products will be released into sewer systems, reaching wastewater treatment plants (WWTP) in significant concentrations to be retained in the process biomass (Blaser *et al.*, 2008; Gottschalk *et al.*, 2009; Kaegi *et al.*, 2011). Using estimated release loads from consumer goods sold in European markets, Blaser *et al.* (2008) predicted that Ag loads in sewage treatment plant inflows (combining industrial and common household discharges) should fall between 2–18 $\mu\text{g mL}^{-1}$ in the year 2010. These estimates are in reasonable agreement with experimental data collected by Deycard *et al.* (2017) between 2010 and 2011 at the Louis Fargue WWTP in Bordeaux (France), indicating average daily influent and effluent silver concentrations of 0.90–1.7 $\mu\text{g mL}^{-1}$ and 100–270 ng mL^{-1} , respectively. The retention of silver nanoparticles in conventional activated sludge WWTPs has stoked concerns over eventual negative impacts on treatment efficiency arising from their antimicrobial properties and has been the subject of prolific research efforts focusing both on repercussions at the process scale and on the chemical and biochemical interactions between Ag NPs and wastewater sludge (Zhang *et al.*, 2016). An in-depth analysis of studies investigating the fate, transformations, and bearings of Ag NPs on wastewater bioremediation will be provided further ahead after a brief review of technologies for the treatment of dye-laden textile effluents.

1.5.2 Fate and impacts of Ag NPs during biological wastewater treatment: the effects of environmental silver transformations and microbial growth mode

As previously stated, the bactericidal activity of Ag NPs is in great part attributable to the release of Ag^+ ions under oxygenated conditions through oxidative dissolution (Le Ouay & Stellacci, 2015). The rate of Ag^+ release can be regulated by various parameters such as the physicochemical properties of the NP (including size, shape and capping material) and several environmental conditions (pH, ionic strength, light), and can have a remarkable impact on the antibacterial activity of Ag NPs (Pareek *et al.*, 2018). Additionally, metallic Ag is well-known for its thermodynamic instability and will oxidize or react with (in)organic ligands to form a range of derivatives. For example, silver is known to react strongly with sulfide, chloride and organic matter. Silver corrosion agents are ubiquitous in nature and induce multiple environmental transformations of Ag NPs that can strongly affect their surface properties and consequently their transport, reactivity and toxicity (Levard *et al.*, 2012). In an example of one such transformation, Levard *et al.* (2011) reported the effects of surface sulfidation on the dissolution rate of Ag NPs and concluded that the release of silver ions decreases as the sulfide-to-silver concentration ratio increases. This behavior relates to the lower solubility of silver sulfide (as compared to metallic silver) and can contribute to limit the environmental impact of Ag NPs by reducing the amounts of available Ag^+ (Levard *et al.*, 2012). Similar results have been obtained in association with silver chloride and silver phosphate (Levard *et al.*, 2013), and even simple, common molecules relevant in aqueous environmental media – such as glucose or soluble microbial products – have been found to have a decelerating effect on Ag NP dissolution (Loza *et al.*, 2014). Effective silver nanoparticle toxicity in wastewater bioremediation units is therefore largely dependent on the abating action produced by whatever surface transformations take place upstream from the treatment works – during transport through sewage networks – and inside the bioreactor and can be significantly reduced when compared to pristine NPs (Zhang *et al.*, 2016).

In addition to these elements, bioreactor configuration can be used to control the biological effects of silver nanoparticles by modulating the growth processes of the microbial population. Microbes in an attached-growth system appear, for instance, to be less susceptible to antimicrobial agents such as Ag NPs than suspended flocculent cultures because they enjoy more protection (Zhang *et al.*, 2016). This protection emerges in association with two key factors: physical structure and community structure. The physical structure of microbial aggregates – brought about by strong cohesion and a polymeric matrix – provides a dense physical barrier against cell exposure to NPs. Abundant EPS in the matrix of the aggregate entrap NPs near the outside of aggregates, thus protecting microorganisms residing in the interior. On the other hand, adaptation mechanisms such as the proliferation of resistant individual strains, community resilience (understood as the ability to counteract antimicrobial action with increased microbial growth) and functional redundancy (*i.e.*, the presence and prevalence of equivalent microbial functions to those provided by susceptible microorganisms) are accentuated by microbial diversity and social interactions within microbial aggregates (Tang *et al.*, 2018).

The example of AGS technology, characterized by self-established, dense microbial aggregates, is therefore regarded as one of the most suitable solutions available for the treatment of Ag NP-loaded wastewaters. To date, however, only two published studies have been submitted with direct mentions to the subject. In a demonstrative investigation, Gu *et al.* (2014) compared the removal of Ag NPs by flocculent and granular sludge as well as their short- (12 hours) and long-term (22 days) inhibitory impacts. Flocculent sludge proved better in terms of absolute Ag NP removal owing to the larger surface area of sludge flocs, but was shown to be more susceptible to silver exposure, sustaining reductions of up to 25% in ammonia oxidizing rate when exposed to 1–100 mg Ag NPs L⁻¹ for up to half a day and ~20% in specific oxygen uptake rates in the long run. Even though it proved less efficient in removing Ag NPs, AGS showed increased resistance in both time-frames, with no significant drops in either activity. More recently, Quan *et al.* (2015) exposed two equivalent AGS systems to 5 and 50 mg Ag NPs L⁻¹ for 69 days and evaluated the impacts of exposure over microbial activities, pollutant removal and sludge properties by comparison with a silver-free control. Both systems were able to operate with no significant reduction in activity until day 35, but experienced drops in the respiration, ammonia oxidizing and denitrification rates thereafter. Despite these setbacks, overall COD and ammonia removal efficiencies remained above 90% throughout the entire operation and no significant impacts seemed to bear over sludge settleability, granule architecture or community structure.

While promising as preliminary dashes into the feasibility of AGS treatments for Ag NP removal, these studies are limited in temporal scope and focus mainly on microbial activities to characterize toxicity. Longer operation times are required to clarify just how far silver dosing can go before reaching a retention limit or forcing the system into shutdown and a deeper focus on the micro- and microscopic parameters associated with granule stability is necessary to understand whether negative impacts are to be expected solely in association with microbial activities. Moreover, clarifying the ways in which bioreactor operation can impact on silver toxicity is required if negative effects are to be averted. In order to answer some of these questions, this study used two SBRs with different operating parameters known to impact on sludge properties (namely shear stress and feeding strategy) and investigated the bearings of persistent silver dosing at 10 mg Ag NPs L⁻¹ on bioreactor operation for 192 days.

2 Materials and methods

2.1 Synthetic textile wastewater

2.1.1 Carbon source and azo dye stock solutions

Emsize E1 (Emsland-Stärke GmbH, Germany), a starch derivative (hydroxypropyl starch) used as a sizing agent in the cotton textile industry, was used as carbon source for the preparation of the synthetic textile wastewater. Under the alkaline conditions applied in the desizing step of cotton manufacturing, Emsize E1 is hydrolysed and released in the effluent. The preparation of the stock solution (100 g L^{-1}) was based on one set of desizing conditions provided by the manufacturer and previously described by Lourenço *et al.* (2000) (Lourenço *et al.*, 2000). Briefly, 100 g of Emsize E1 and 40 g of sodium hydroxide were dissolved in distilled water and stirred for 15 hours at room temperature. The hydrolysed solution was then neutralized to $\text{pH } 7.0 \pm 0.05$ with 37%(m/m) HCl and diluted to 1 L with distilled water.

The azo dye stock solution (5.0 g L^{-1}) was prepared by dissolving Acid Red 14 (AR14; Chromotrope FB, 50% dye content, Sigma-Aldrich Química, S.L., Portugal) in distilled water.

2.1.2 Synthetic wastewater composition

The synthetic textile effluent used as a feed solution was prepared by diluting the carbon source to a COD content of $1,000 \text{ mg O}_2 \text{ L}^{-1}$ (1.15 g L^{-1} Emsize E1) and the azo dye to a final concentration of 40 mg L^{-1} . Each component was added from equal volumes of two separate concentrated solutions containing the carbon (Feed C) and nitrogen sources (in the form of ammonium chloride; Feed N), and supplemented with macro- (magnesium, calcium, and iron salts) and micronutrients (manganese and zinc sulphates, boric acid, and ammonium molybdate) respectively. pH buffering phosphates were added to the final wastewater along with the remaining components of Feed N to produce an influent COD:N:P mass ratio of 100:3.7:37. The final composition of the simulated wastewater was as follows: $2,310 \text{ mg L}^{-1} \text{ Na}_2\text{HPO}_4 \cdot 12\text{H}_2\text{O}$, $762 \text{ mg L}^{-1} \text{ KH}_2\text{PO}_4$, $143 \text{ mg L}^{-1} \text{ NH}_4\text{Cl}$, $27.5 \text{ mg L}^{-1} \text{ CaCl}_2$, $22.5 \text{ mg L}^{-1} \text{ MgSO}_4 \cdot 7\text{H}_2\text{O}$, $250 \text{ } \mu\text{g L}^{-1} \text{ FeCl}_3 \cdot 6\text{H}_2\text{O}$, $40 \text{ } \mu\text{g L}^{-1} \text{ MnSO}_4 \cdot 4\text{H}_2\text{O}$, $57 \text{ } \mu\text{g L}^{-1} \text{ H}_3\text{BO}_3$, $43 \text{ } \mu\text{g L}^{-1} \text{ ZnSO}_4 \cdot 7\text{H}_2\text{O}$, and $35 \text{ } \mu\text{g L}^{-1} (\text{NH}_4)_6\text{Mo}_7\text{O}_{24} \cdot 4\text{H}_2\text{O}$. Reported concentrations represent net inlet loads after dilution with an Ag NP suspension fed separately to the SBRs according to a 4:1 (other components:Ag NP) volume ratio. All salts were analytical grade.

2.1.3 Silver nanoparticle suspension

Ag NPs with a maximum particle size of 100 nm (with added polyvinylpyrrolidone as dispersant) were purchased as a powder from Sigma-Aldrich Química, S.L. (Portugal). Silver nanoparticle stock suspensions (100 mg L^{-1}) were prepared by dispersing 200 mg Ag NPs in 2 L of MilliQ water and stabilized by ultrasonication on ice (150 W, 20 kHz) for 30 minutes using a Sonoplus HD 3200 ultrasonic homogenizer (Bandelin, Germany). The suspensions were stored in tinted glass bottles next to the bioreactor system and fed to the SBRs from a top inlet port over a 15-minute period simultaneous with

the introduction of fresh simulated textile wastewater. To ensure a homogeneous amount of Ag NPs was loaded into the bioreactors at the beginning of each cycle, continuous stirring was provided in the feed bottle throughout the filling stage using a magnetic bar.

2.2 Sequencing batch reactor (SBR) setup and operation

Two non-tubular bubble column SBRs with a working volume of 1.5 L and a height-to-diameter (H/D) ratio of 2.5, SBR1 and SBR2, were seeded with conventional activated sludge harvested from a full-scale municipal wastewater treatment plant in Chelas, Lisbon (Portugal), and operated in parallel for 192 days. The reactors were run in 6-hour cycles comprising five individual stages – fill, reaction (which included a mixed anaerobic stage and an aerobic stage), settling, drain, and idle (Figure 2.1) – with a volumetric exchange ratio (VER) of 50% and a hydraulic retention time (HRT) of 12 h. At the beginning of each cycle, synthetic textile wastewater was fed in static and anaerobic conditions from the bottom of the reactors according to a volumetric organic loading rate (OLR) of $2.0 \text{ kg COD m}^{-3} \text{ day}^{-1}$ using one of two different strategies: an uprising plug flow developed from the centre bottom and spread out through the sludge bed (in SBR2), or a rapid discharge at a peripheral site followed by a fast and channelling rise across the settled biomass (in SBR1) (Figure 2.1). Towards the end of the filling stage, 150 mL of a concentrated Ag NP suspension (100 mg L^{-1}) were added from the top of the reactors to produce an added silver concentration of 10 mg L^{-1} at the onset of the reaction phase. The distribution of the synthetic textile wastewater and the Ag NP suspension from the feed containers to the reactors was performed using peristaltic pumps (Mini-S 660, Ismatec, Switzerland).

Sequencing batch cycles were timed to include 30 and 60 minutes of anaerobic feeding in SBR1 and SBR2 respectively, followed by a stirred anaerobic phase stretching to the 2-hour mark (*i.e.*, 1.5 h in SBR1 and 1 h in SBR2) and a 3.5-hour aeration period (Figure 2.1). Mechanical mixing was provided by a magnetic anchor impeller ($\phi = 6 \text{ cm}$) at 70 rpm in SBR1 and by a pitched-blade turbine ($\phi = 5 \text{ cm}$) at 280 rpm in SBR2. During the aerobic stage, fine bubble diffusers installed at the bottom of the reactors and connected to air compressors (SPP-20GJ-L, Hiblow, Japan) provided aeration at a flow rate of 2 vvm. After settling, supernatant withdrawal was performed over 1 minute using gear pumps (Reglo-Z, Ismatec, Switzerland) and the reactors were left in a quiescent state until the start of the next cycle. Figure 2.1 offers a schematic representation of SBR1 and SBR2 during a full batch cycle complete with a summary of the main operational specifics and the duration of each stage.

The operation was conducted at room temperature with no pH control and sustained pH variations in the 6.1–6.9 range along each cycle. All pumping, aeration and agitation functions were automatically controlled via an interface by a dedicated software installed in a personal computer. Figure 2.2 displays a simplified equipment diagram of the experimental system including both SBRs and the associated auxiliary gear.

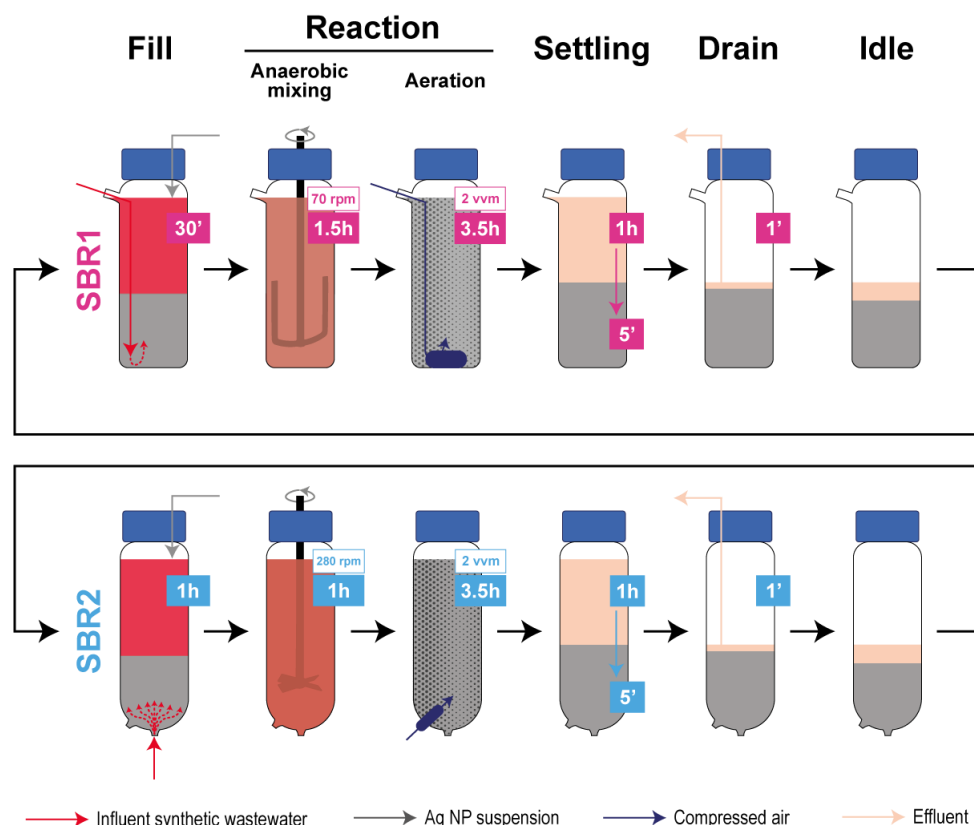


Figure 2.1 | Schematic representation of a full 6-h sequencing batch cycle in SBR1 and SBR2. The duration of each operating stage is shown in pink (SBR1) or blue (SBR2) boxes and complemented with relevant process conditions in white boxes. A settling time of 5 minutes was applied from day 28 onwards after a progressive reduction (down from 1 hour) over the first 4 weeks of operation.

2.3 SBR inoculation and aerobic granulation

SBR1 and SBR2 were seeded with 1.30 and 1.50 g TSS L⁻¹ of activated sludge, respectively, and operated during the first 3 days with a settling time of 60 minutes so as to minimize biomass wastage and provide a suitable adaptive period to the new feeding conditions. Aerobic granulation was induced by applying progressively smaller settling times, high hydrodynamic shear stress, and a feast-famine regime for biomass culture. The sedimentation time was shortened in a stepwise manner during the first 4 weeks of operation in order to select fast-settling sludge particles, starting at 40 minutes (days 3–7) and going down to 30 minutes (days 7–10), 20 minutes (days 10–14), 15 minutes (days 14–17), 10 minutes (days 17–24), 7 minutes (days 24–28) and 5 minutes (from day 28 onwards). The final step reduction defined a minimum settling velocity of 1.5 m h⁻¹ for biomass retention throughout the remaining operation time. Settling periods larger than 15 minutes were accommodated by reducing the aeration time accordingly in order to maintain a total cycle time of 6 hours. Feast-famine conditions were developed by allotting a relatively short feeding period and promoting a rapid consumption of the carbon source during the mixed anaerobic stage, thereby limiting the externally available COD for the remainder of the cycle time. The required shear stress was achieved by mechanical mixing during the anaerobic phase (described by a maximum tip speed of 26 and 88 m min⁻¹ in SBR1 and SBR2, respectively) and by aeration during the aerobic phase (described by an upflow air velocity of 0.4 m min⁻¹ in both reactors).

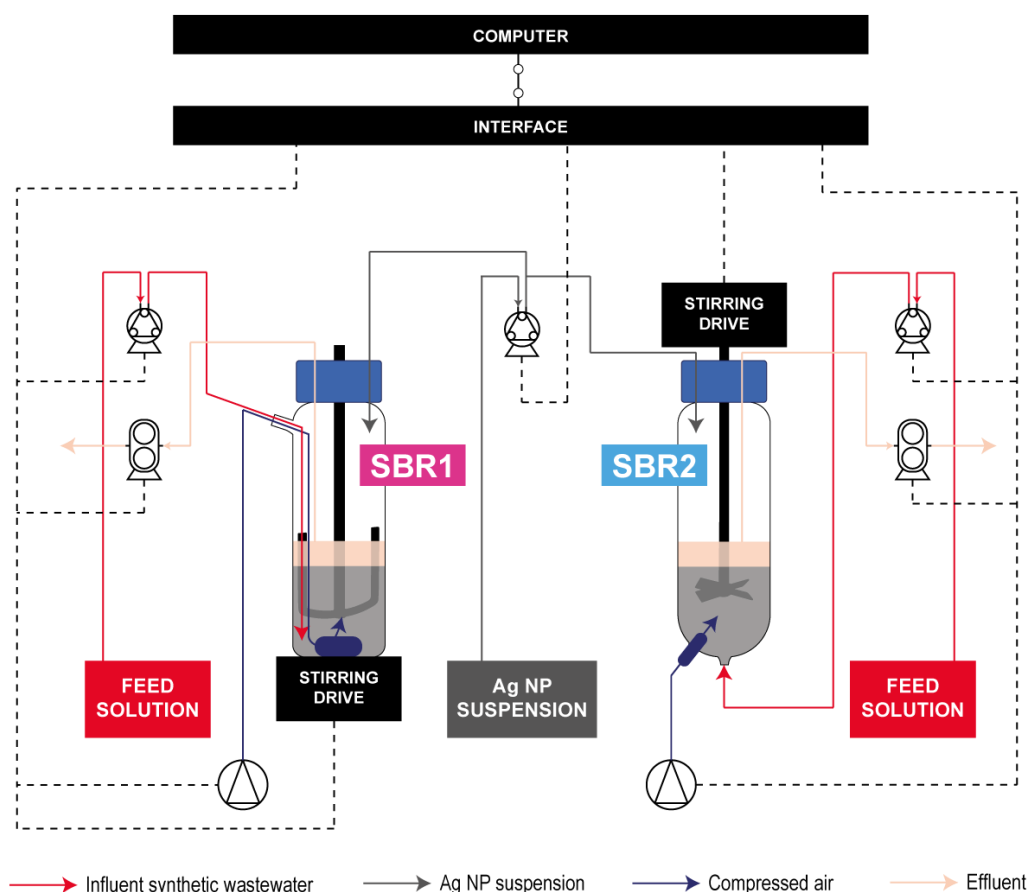


Figure 2.2 | Simplified equipment diagram of the experimental sequencing batch reactor system. All pumping, aeration and mixing functions were controlled automatically by a dedicated software via an interface. Dashed lines represent electrical connections between the interface and the equipment; the software link between the controlling unit and the interface is denoted by a full line spaced by open circles.

2.4 SBR performance monitoring

Throughout the course of the operation, the reactors were monitored with respect to (i) biomass inventory, size distribution, settling properties and morphology; (ii) chemical oxygen demand and azo dye conversion; (iii) pH variations relating to biological activity; and (iv) shifts in *N*-acyl-L-homoserine lactone-based quorum sensing in response to process conditions. Representative cycles were sampled at 3- to 4-day intervals during the first 6 weeks of operation so as to clearly describe the granulation process, and on a weekly basis thereafter.

2.4.1 Sludge properties

Total and volatile suspended solids. Total (TSS) and volatile suspended solids (VSS) were measured in the effluent discharged from the reactors and in mixed liquor samples collected at the beginning of the aerated phase using standard methods (APHA, 1995). 10 mL of mixed liquor and 20 mL of effluent were filtered using previously weighed glass fibre filters in a vacuum filtration system consisting of a vacuum pressure pump (EMD Millipore, USA) and a stainless-steel filtration support. For TSS analysis, the filters were dried to constant mass in a drying balance (HB-43-S, Mettler Toledo, Switzerland) at

~105 °C and then weighed in an analytical balance (AE160, Mettler Toledo, Switzerland). Taking A as the mass of the filter with the solid residue and B as the mass of the empty filter (both in grams), TSS concentrations were calculated using the following expression:

$$\text{TSS, mg mL}^{-1} = \frac{(A - B) \cdot 1000}{\text{sample volume, mL}} \quad (0.1)$$

Mixed liquor (MLTSS) and effluent total suspended solids (ETSS) were measured in duplicate and mean values are presented (mean relative standard deviations (RSD) of 1.6% and 8.3% for MLTSS and ETSS respectively).

In order to determine VSS contents, the residue produced after TSS analysis was ignited at 550°C for 90 minutes in a muffle furnace (L3/S27, Nabertherm, Germany) and the sample was reweighed. Taking C as the mass of the filter with the leftover ash produced during baking (in grams), VSS concentrations were computed according to equation (2.2). As with TSS values, means of duplicate mixed liquor (MLVSS) and effluent volatile suspended solids (EVSS) measurements are reported (mean RSD of 1.7% and 6.8% for MLVSS and EVSS respectively).

$$\text{VSS, mg mL}^{-1} = \frac{(A - C) \cdot 1000}{\text{sample volume, mL}} \quad (0.2)$$

Sludge retention time. The batch-wise average sludge retention time (SRT) was estimated for each monitored cycle using the TSS measurements collected from mixed liquor and effluent samples. Considering the working volume of each reactor, V_R , and the total volume of mixed liquor extracted for sampling purposes (both in litres), V_s , SRT values were computed as:

$$\text{SRT, days} = \frac{\text{MLTSS} \cdot V_R}{\text{ETSS} \cdot Q_E + \frac{\text{MLTSS} \cdot V_s}{\text{sampling period, days}}}, \quad (0.3)$$

where Q_E represents the volumetric rate of effluent removal (in L day⁻¹) and the sampling period encompasses every day in between two consecutive representative cycles. The values thus calculated neglect possible changes in MLTSS contents between the two cycles and assume that ETSS concentrations are approximately constant over the entire sampling window. The procedure constitutes a simplistic take on sludge age monitoring with little quantitative power and was mainly performed to detect broad trends regarding biomass accumulation in the SBRs.

Sludge volume index. The sludge volume index (SVI) was determined by measuring the volume occupied by the sludge settled from 1 L of mixed liquor after 5 (SVI₅) and 30 (SVI₃₀) minutes of settling, and dividing it by the MLTSS content as suggested by equation (2.4). SVI measurements were carried out offline in an Imhoff cone, and the mixed liquor samples were promptly returned to the reactors.

$$\text{SVI, mL g}^{-1} \text{ TSS} = \frac{\frac{\text{settled sludge volume, mL}}{\text{mixed liquor sample volume, mL}}}{\text{MLTSS, mg TSS mL}^{-1}} \cdot 1000 \quad (0.4)$$

Granule size distribution. The proportion of large granules (sizes above 0.65 mm), small granules (sizes within the 0.2–0.65 mm range) and flocs (sizes under 0.2 mm) in the SBRs was estimated by sifting 20-mL mixed liquor samples through 0.65-mm and 0.2-mm net sieves and determining the biomass content in each collected fraction using the TSS analysis protocol.

Aerobic granular sludge morphology. Biomass samples collected weekly from both reactors during the aerated phase were observed at magnifications of 40x and 100x under a light transmission microscope (BA200, Motic, China) fitted with a digital camera and respective software (Moticam 1000, Motic, China) in order to trace changes in sludge morphology.

2.4.2 Treatment performance: pollutant conversion and pH profiles

In order to evaluate the treatment performance of the bioreactors during the monitored cycles, 10-mL mixed liquor samples were collected at different time coordinates along the cycle and centrifuged at 4,000 rpm and 21 °C for 10 minutes (centrifuge model 5810 R, Eppendorf, Germany) to remove the biomass. The collected supernatants were analysed in terms of AR14 concentration, soluble COD content, and pH level so as to establish the respective time profiles and quantify pollutant conversion.

Colour removal, aromatic amine accumulation and conversion. Sample colour was determined spectrophotometrically by reading the absorbance at 515 nm (the wavelength of maximum absorbance in the visible range by AR14) using a Specord 200 spectrophotometer (Analytik Jena, Germany). Colour contents were expressed as equivalent Acid Red 14 concentrations using a previously established calibration curve. Each sample was measured in duplicate and mean values are presented (mean RSD of 0.61%). UV-visible absorption spectra were plotted for all collected samples in order to validate the mechanism of colour removal and track the accumulation and conversion of aromatic amines. Reporter wavelengths were selected from the absorption spectrum of a 7.3 mg L⁻¹ standard solution of the aromatic amine 4-amino-naphtahlene-1-sulphonic acid (4A1NS, Fluka, USA), one of the constitutive moieties of AR14 admitted to result from the reductive cleavage of the azo bond. Amine conversion was evaluated under aerobic conditions in terms of percent reductions in the absorbance of the mixed liquor at the chosen wavelengths during the aerated reaction stage. All absorbance measurements were performed against a distilled water blank.

COD removal. Soluble COD in the collected samples was determined following a closed reflux titrimetric standard method. The procedure relies on the oxidation of organic matter to CO₂ and H₂O in a boiling mixture of chromic and sulfuric acids prepared with a known excess of potassium dichromate (K₂Cr₂O₇). Under these conditions, the dichromate ion (Cr₂O₇²⁻) acts as an oxidant and reacts with the sample to yield the reduced form Cr³⁺. After digestion, the remaining unreduced potassium dichromate is titrated with ferrous ammonium sulphate (Fe(NH₄)₂(SO₄)₂, FAS) to determine the amount of K₂Cr₂O₇ consumed and the oxidizable matter is calculated in terms of O₂ equivalents (APHA, 1995).

To determine the COD contents in each of the collected samples, 1.5 mL of the isolated supernatants were mixed with 1 mL of 0.01667 M K₂Cr₂O₇ and 2 mL of a sulfuric acid reagent (containing 5.5 g AgSO₄ kg⁻¹ H₂SO₄) in glass tubes and digested at 170 ± 2 °C for 15 minutes in a HT200S high temperature thermostat (Hach, USA). Reaction blanks were prepared by replacing the sample with 1.5 mL of reagent

water and refluxed along with the remaining test tubes. After cooling, the samples were transferred to 50-mL Erlenmeyer flasks and the leftover volume in the glass vials was washed into the mix using distilled water. Excess dichromate was determined by titration with FAS (~0.0125 M) using a ferroin solution as the endpoint indicator. After every analysis, FAS standardization was performed by titrating 1 mL of a potassium dichromate standard solution (12.2073 g L⁻¹) mixed with 2 mL of concentrated H₂SO₄. Knowing the molarity, M, of FAS, and the volumes (in mL) of titrant used with each sample, B, and with the blank, A, the amount of oxidizable matter was calculated as chemical oxygen demand using the expression:

$$\text{COD, mg O}_2 \text{ L}^{-1} = \frac{(A - B) \cdot M \cdot \text{O}_2^{\text{eq}} \cdot 1000}{\text{sample volume, mL}}, \quad (0.5)$$

where the factor $\text{O}_2^{\text{eq}} = 8 \text{ mg O}_2 \text{ mol}^{-1}$ FAS symbolises the equivalent mass of oxygen involved in the oxidation of one mole of ferrous iron (Fe^{2+} , from FAS). COD measurements were performed in duplicate for each sample and mean values are reported (mean RSD of 3.2%).

pH profiles. pH levels were measured on each centrifuged sample according to a standard procedure (APHA, 1995) using a Metrohm 6.0202.100 glass electrode connected to a Metrohm 691 potentiometer (Switzerland).

2.5 *N*-acyl-L-homoserine lactone-based quorum sensing analysis

2.5.1 Biosensor strain and growth conditions

Biosensor *Agrobacterium tumefaciens* NTL4(pZLR4) was kindly provided by Ramón Peñalver from Instituto Valenciano de Investigaciones Agrarias (IVIA, Valencia, Spain). The strain is a Ti plasmid-cured derivative of the model *A. tumefaciens* C58 (Luo *et al.*, 2001) and is incapable of producing detectable levels of endogenous *N*-acyl-L-homoserine lactones (AHLs). The pZLR4 plasmid confers resistance to gentamicin and carbenicillin and provides a response system for the detection of exogenous AHLs comprising two separate genetic motifs: a sequence encoding the AHL-responsive transcription activator TraR and a TraR-regulated *traG::lacZ* fusion. AHL-mediated induction of the *traG::lacZ* reporter gene via TraR leads to the production of β -galactosidase (LacZ) and can be quantified by a suitable enzyme assay (Yin *et al.*, 2012).

A. tumefaciens NTL4(pZLR4) was initially stored in 20%(v/v) glycerol at -80 °C. The cells were thawed on ice for 1 hour and activated in overnight cultures (28 °C, 150 rpm) developed with lysogeny broth (LB) containing 50 $\mu\text{g mL}^{-1}$ of gentamicin. These cultures were plated on LB agar supplemented with gentamicin to the same concentration, grown overnight at 28 °C and then stored at 4 °C. Before each AHL bioassay, the biosensor strain was grown at 28 °C with orbital shaking (150 rpm) for 16–18 hours in AT minimal medium (10.5 g L⁻¹ K₂HPO₄, 4.5 g L⁻¹ KH₂PO₄, 2 g L⁻¹ (NH₄)₂SO₄, 200 mg L⁻¹ MgSO₄ · 7H₂O, 15 mg L⁻¹ CaCl₂ · 2H₂O, 10 mg L⁻¹ FeSO₄ · 7H₂O, 3 mg L⁻¹ MnSO₄ · H₂O) containing 0.2%(w/v) glucose and 50 $\mu\text{g mL}^{-1}$ of gentamicin.

2.5.2 Model AHL and auxiliary chemicals

N-(3-oxododecanoyl)-L-homoserine lactone (3OC12-HSL) was purchased from Sigma-Aldrich Química, S.L. (Portugal) and dissolved in distilled water to produce a 1 μ M stock solution. The stock was serially diluted to test the response of biosensor *A. tumefaciens* NTL4(pZLR4) in the presence of 0–10 nM 3OC12-HSL and obtain a reference calibration curve (see 2.5.5).

AHL bioassays were conducted using 5-bromo-4-chloro-3-indolyl- β -D-galactopyranoside (X-gal, nzytech, Portugal) as a chromogenic substrate of β -galactosidase (see 2.5.4). The substrate was dissolved in dimethyl sulfoxide (DMSO) to a concentration of 50 mg mL⁻¹ and stored at -20°C before the bioassay.

2.5.3 AHL extraction

Mixed liquor samples containing 10 mg TSS were harvested from both SBRs towards the end of the aerated reaction phase and centrifuged at 6,000 rpm and 4 °C for 10 minutes. The supernatants (S1) were separated and stored at -20 °C along with the sludge pellets until further use.

AHL concentrations were assayed in intracellular extracts prepared from aerobic granules of sludge pellets through sonication. Cell lysis and sample handling were performed according to the method described by Ren *et al.* (2010) (Ren *et al.*, 2010) with some modifications. Sludge pellets were thawed at room temperature for 30 minutes, resuspended in 3 mL of MilliQ water and divided into two 1.5 mL aliquots. The aliquots were sonicated on ice at an acoustic intensity of 30 W for 10 minutes (Sonoplus HD 3200, Bandelin, Germany) and then centrifuged for an additional 10 minutes at 4 °C and 10,000 rpm. The resulting supernatants (S2) were isolated as cell-free sludge extracts without further purification and stored at -20 °C before the AHL bioassay.

2.5.4 Development of the AHL bioassay

Outline of the AHL bioassay. Induction of the *lacZ* reporter fusion in *A. tumefaciens* NTL4(pZLR4) was measured using a colorimetric assay with X-gal as the chromogenic substrate. The assay was performed with whole biosensor cells in liquid culture medium and was designed to promote the AHL-induced synthesis of β -galactosidase (β -gal) in tandem with microbial growth. In the presence of β -gal, X-gal is hydrolysed to yield an insoluble blue product, 5,5'-dibromo-4,4'-dichloro-indigo (henceforth referred to simply as indigo), that can be quantified turbidimetrically and used to estimate enzyme activity. In a whole-cell assay layout, however, optical density (OD) read-outs reflect a combined effect of absorption and light scattering by bacterial cells and by the blue pigment that render the measurement of enzyme activities a challenging task. Moreover, minor differences in inoculum density can develop into strong demarcations in cell and β -gal concentrations during microbial growth and produce unreliable spectrophotometric results if single wavelength values are considered. Knowing the individual contributions of each species to light scattering is therefore desirable if β -gal activities normalized by cell density are to be obtained (Tang *et al.*, 2013). The AHL bioassay described herein used a dual wavelength approach developed mathematically by extending the principles of the Beer-Lambert law to

turbidity analysis to isolate light scattering from indigo and biosensor cells. Experimental methods and data handling strategies were applied as described by Tang *et al.* (2013) with minor modifications.

A. tumefaciens NTL4(pZLR4) inocula were grown overnight in AT minimal medium containing 0.2%(w/v) glucose and 50 $\mu\text{g mL}^{-1}$ of gentamicin as described in 2.5.1. Seed cultures were diluted to an optical density at 600 nm (OD600) of 0.02 using fresh minimal medium (without antibiotics) and supplemented with X-gal (250 $\mu\text{g mL}^{-1}$, added from stock) to produce the AHL bioassay solution. 15 μL of cell-free sludge extracts were mixed with 235 μL of this solution in 96-well plates and incubated in the dark with gentle shaking for 13 hours using a Stat Fax-2200 shaker-incubator (Bio-Rad, USA) at 28 °C. After incubation, colour development was monitored with a SPECTROstar® Nano microplate reader (BMG LABTECH, Germany) at 504 nm (OD504) and 629 nm (OD629) (against distilled water) and the measured optical densities were described as additive contributions from indigo and biosensor cells using equations (2.6) and (2.7). Working wavelengths were selected from the light scattering spectrum of a pure indigo suspension to describe the activity of the tested samples around the regions of maximum (504 nm) and minimum (629 nm) transmittance.

$$\text{OD629} = \text{OD629}_{\text{indigo}} + \text{OD629}_{\text{cells}} \quad (0.6)$$

$$\text{OD504} = \text{OD504}_{\text{indigo}} + \text{OD504}_{\text{cells}} \quad (0.7)$$

Simultaneous resolution of equations (2.6) and (2.7) to isolate each of the previous terms was achieved by relating light scattering at 504 nm and 629 nm in pure indigo and biosensor cell suspensions using the principles of light absorption. According to the Beer-Lambert law, extinction coefficients are intensive (*i.e.*, independent of quantity) and chemically specific properties that vary as a function of incident radiation wavelength. Therefore, for a given concentration of absorber, the ratio of absorbances at two different wavelengths is a constant and equals the ratio of extinction coefficients under the same conditions. Applying the same principle to the spectral properties of indigo and *A. tumefaciens* NTL4(pZLR4) cells, two additional parameters, α and γ , can be defined in the form:

$$\alpha = \frac{\text{OD629}_{\text{cells}}}{\text{OD504}_{\text{cells}}} \quad (0.8)$$

$$\gamma = \frac{\text{OD504}_{\text{indigo}}}{\text{OD629}_{\text{indigo}}} \quad (0.9)$$

Rearranging and solving the previous four equations for $\text{OD629}_{\text{indigo}}$ and $\text{OD504}_{\text{cells}}$, normalized β -gal activities, defined as the ratio between the contributions of indigo and biosensor cells, were computed from the collected OD measurements using equation (2.10).

$$\text{Normalized } \beta\text{-gal activity} = \frac{\text{OD629}_{\text{indigo}}}{\text{OD629}_{\text{cells}}} = \frac{\text{OD629}_{\text{indigo}}}{\alpha \cdot \text{OD504}_{\text{cells}}} = \frac{\alpha \cdot \text{OD504} - \text{OD629}}{\alpha \cdot (\gamma \cdot \text{OD629} - \text{OD504})} \quad (0.10)$$

Several independent normalized β -gal activity values were obtained per AGS sample using different combinations of biological and technical replicates. AHL extracts obtained from independently processed AGS aliquots were regarded as biological replicates, whereas measurements of AHL concentrations performed on the same extract with independently developed biosensor cultures were classified as technical replicates. Whenever only one extract was deemed usable for application in the bioassay, five technical replicates were performed. In any other case, reported values are the result of three technical replicates performed with two independent AHL extracts (six replicates).

Obtaining factors α and γ for the normalization of β -galactosidase activity. In order to obtain the value of factor α , an overnight culture of biosensor developed as described in 2.5.1 was inoculated in AT minimal glucose medium without antibiotics to produce an initial OD600 of 0.02. After incubation at 28 °C and 150 rpm for 24 hours, the culture was serially diluted and the optical densities at 629 nm and 504 nm were measured. Linear regression analysis was performed to establish OD629_{cells} as a function of OD504_{cells} and the slope was defined as factor α .

In order to obtain factor γ , a fresh biosensor culture was prepared from an overnight inoculum as described above and supplemented with 3OC12-HSL to a final concentration of 2.5 nM. After incubation for 24 hours (28 °C, 150 rpm), the culture was sonicated on ice in a Sonoplus HD3200 ultrasonic homogenizer (Bandelin, Germany) using five on-and-off cycles of 30 seconds with an amplitude output of 30%. The supernatant of the culture was collected after centrifugation at 13,000 *g* and 4 °C for 10 minutes and filtered through a sterilizing filter with a porosity of 0.2 μ m. The filtrate (considered as a cell-free β -galactosidase solution) was mixed with X-gal to a final concentration of 250 μ g mL⁻¹ (added from stock) and incubated in the dark at 28 °C and 150 rpm for 16 hours. After incubation, the blue pigment was serially diluted and the optical densities at 629 nm and 504 nm were measured. Linear regression analysis was performed to establish OD504_{indigo} as a function of OD629_{indigo} and the slope was defined as factor γ .

2.5.5 Reference calibration curve

In order to compare the normalized β -gal activities produced by AHL extracts with those generated by a model AHL, the bioassay was applied to standard solutions with increasing concentrations of 3OC12-HSL (in the 0–10 nM range) and a calibration curve was plotted using second-degree polynomial regression analysis. β -gal activities obtained for each standard concentration are presented as the mean \pm standard error (SEM) of three technical replicate measurements. All results derived from AHL extracts were confronted with the reference calibration curve and converted to equivalent 3OC12-HSL concentrations (presented as mean \pm SEM).

2.6 Statistical analysis

Statistical analyses were performed using Excel® (Microsoft, USA) and GraphPad Prism 6 (GraphPad Software, USA). One-way analysis of variance (ANOVA) with Holm-Šidák post-test was conducted to examine differences in equivalent 3OC12-HSL concentrations along the operation of each reactor and adjusted *p*-values are reported. Multiple unpaired *t*-tests were used to compare weekly results of AHL-based quorum sensing in between the two SBRs and family-wise error rate corrections were provided using the Holm-Šidák method (adjusted *p*-values are reported). Finally, Pearson correlation coefficients, *r*, were determined to investigate the relations between biomass inventory, settling properties, and AHL levels. In all cases, statistical significance was evaluated at *p* < 0.05.

3 Results and Discussion

3.1 Biomass properties, inventory and morphology

Over the course of the experimental run, sludge properties in SBR1 and SBR2 were monitored using five different analytical methods with a view to evaluate the formation, development and maintenance of aerobic granules (AGs) and to clarify the relation between each system's microscopic and macroscopic traits. To track the establishment of AGs and study the remaining morphological and microbiological features of the sludge, transmission light micrographs were collected weekly and complemented with periodic sieving analyses of mixed liquor samples describing the overall size distribution of sludge particles. To monitor the inventory and maturation state of the granular sludge, biomass concentrations were measured in terms of total and volatile suspended solids in both mixed liquor and effluent samples collected during each representative cycle and subsequently used to calculate the batch-wise sludge retention time. Finally, sludge volume index measurements were performed after each sampled cycle on the mixed liquor of both bioreactors and used to complement the remaining elements as analytical descriptors of sludge settleability. Over the length of the following pages, the main evolutionary trends identified throughout the operation using each of these methods will be described individually and correlated whenever relevant to paint a clear picture of the recorded progresses. In an effort to reconcile all the extracted information sustainably, discussion topics will be provided both in combination with relevant results and as separate elements at the end of the exposition. The analysis will orbit around data depicted in Figures 3.1 through 3.5 and will strive to evaluate the recorded evolutions in light of their relation to specific operating parameters. In all, three key themes will be debated: (i) the effects of prolonged exposure to Ag NPs; (ii) the differentiating action exerted by anaerobic feeding configuration; and (iii) the differentiating action exerted by stirring speed and hydrodynamic shear. To foster mutual intelligibility between the chosen discussion structure and the information provided in each figure, the operational run will be informally divided into three phases: (i) the period of aerobic granulation proper (days 0–31), (ii) a subsequent stage of biomass accumulation (days 31–70), and (iii) a long-running period of sludge instability recorded towards the end of the experimental run (days 70–192). As will become apparent along the following sections, the chosen division applies loosely to both bioreactors with occasional comparative divergences; in order to ensure these divergences do not assume a heightened importance and deviate the course of analysis to the exploration of minor events, the partition will be used exclusively as a source of revisionary terms for specific phases of the operational run subdivided *a priori* into relevant temporal intervals.

3.1.1 Aerobic granular sludge morphology

The main morphological features of the aerobic granular sludge in SBR1 and SBR2 are summarized in Figures 3.1 and 3.2 by representative transmission light micrographs collected along the experimental run. As depicted, the activated sludge inoculum was comprised of large numbers of low-density pinpoint flocs that developed into compact, dense, and loose structures during the first days of operation and persisted as the dominant feature of sludge morphology throughout the entire run. Aerobic granules with

ovoid shapes and irregular outlines were identified in SBR1 as soon as day 10 (data not shown) and were disseminated in both bioreactors by day 16. During this period, clearly individualized structures with large diameters developed in SBR1, whereas complex nets of small granules and densely packed flocs proliferated in SBR2. Granule breakup between days 16 and 30 significantly reduced the size of biomass aggregates, with particularly manifest effects in SBR1. However, several small light-coloured aggregates with even outlines, likely containing high concentrations of bound extracellular polymeric substances (EPS), were seen in combination with the biomass in both bioreactors between days 22 and 52 (Figure 3.2A), suggesting the presence of bacterial strains with high EPS-producing capacities despite the tendency for granule disintegration.

Sludge morphology traits developed during these first few weeks would persist mostly unchanged throughout the entire operation (Figure 3.1), leaving both bioreactors to operate a mixture of aerobic granules and dense sludge flocs that varied only with respect to AG number and size. Small granules established from dense nuclei within meshes of flocs were dominant in SBR2 all through the experimental run and generally underwent minimal growth before reaching an equilibrium size. Several large structures could be identified between days 107 and 150 (Figure 3.1A,B), but progressively gave way to granules with more evenly distributed sizes that thrived until the end of the operation. In SBR1, biomass aggregates were able to develop into larger granules (generally with diameters over 250 μm) but fluctuated more sharply in size along the operational period – with particularly visible effects between days 79 and 122 (Figure 3.1B). From day 143 on, AGS samples collected from SBR1 consisted of a heterogeneous mixture of small granules with irregular shapes and large round or oval granules that were maintained up until the moment the operation was stopped.

Full granulation – *i.e.*, a state of 100% granular morphology – was, however, never achieved, signalling some inherent impediment working behind the specifics of each bioreactor to keep small flocs from growing excessively. This could be related to the minimum settling velocity threshold imposed on the bioreactors after the final reduction in sedimentation time on day 28 (1.5 m h^{-1}), which is similar to that found in CAS systems (up to 5 m h^{-1}) and therefore likely to have provided little in the way of selective pressures for the elimination of CAS flocs. Early studies on the subject of hydraulic selection pressure have suggested a minimum retention threshold of 10 m h^{-1} as a way of reaching full granulation (Beun *et al.*, 2002) and reported mixed granular and flocculent morphology – in accordance with current results – whenever lower settling velocities were imposed as a minimum (Liu *et al.*, 2005). However, recent work by Kong *et al.* (2009) suggested that stringent minimum settling velocities *per se* are not the most important parameter defining granule development and growth, reporting the establishment of a fully granulated, stable AGS system with a retention threshold as low as 2 m h^{-1} . In explaining the apparent dissonance between these findings and the results obtained in SBR1 and SBR2, several operational differences – such as the use of mechanical mixing (exclusive to this work), bioreactor geometry (H/D ratios over 1.5 times higher in the work by Kong *et al.*) or Ag NP dosing – might be advanced as possible reasons. Determining which of these factors had a dominant impact over granulation grade is, however, a matter for future studies.

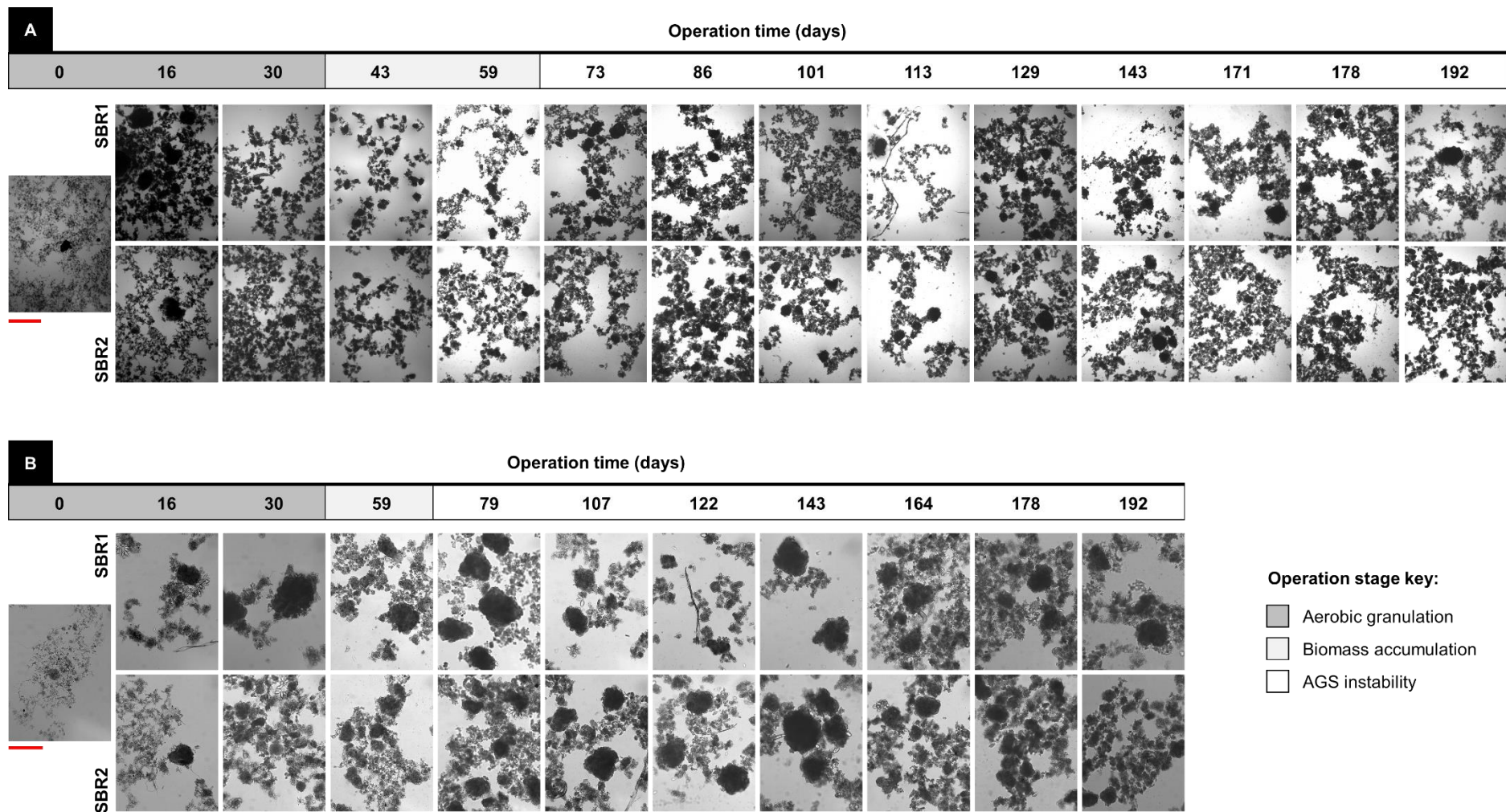


Figure 3.1 | Morphological development of granular sludge along the experimental run. Transmission light micrographs – magnification: (A) 40x, (B) 100x – of biomass samples harvested from the conventional activated sludge inoculum (centre left-hand side), from SBR1 (top row), and from SBR2 (bottom row). Scale bars (in red, left-hand side): (A) 600 μm , (B) 250 μm

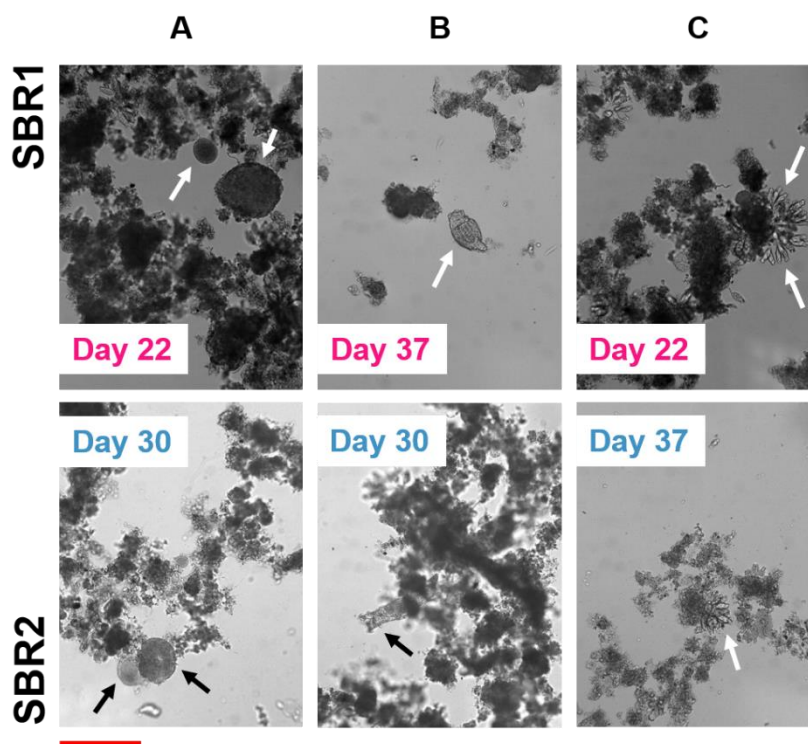


Figure 3.2 | Representative morphological and microbiological features of AGS samples collected during the initial granulation and biomass accumulation stage. Transmission light micrographs – 100x magnification – of biomass samples collected from SBR1 (top row) and SBR2 (bottom row) highlighting the presence of (A) light-coloured EPS-rich aggregates, (B) rotifers, and (C) stalked ciliates. Scale bar (in red, bottom): 250 μm

Free-swimming ciliates, stalked ciliates (most likely *Epistylis* spp., *Vorticella* spp., and *Opercularia* spp.), and rotifers were found in large numbers in samples collected from both bioreactors during the first 52 days (Figure 3.2B,C), but became gradually less common over the following weeks until only small clusters of sessile protozoa could be identified on the surface of aerobic granules. The diversity of microscopic protozoa and metazoans in complex sludge communities is a good indicator of process maturation and varies significantly in response to changes in environmental and operating conditions (e.g., severe biomass washout, toxic shock loads). The presence of rotifers in sludge systems is associated with mature microbial communities (Wanner, 1998) and is coherent with the observed increase in sludge retention time during the initial biomass accumulation stage. Similarly, the relative abundance of free-swimming and stalked ciliates reflects the developmental stage of sludge communities and usually varies from an initial phase dominated by motile species that feed on dispersed bacteria in the bulk liquid to a mature phase, where species with sessile growth proliferate on the surface of flocs and granules (Wanner, 1998; Madoni, 2011). The observed results therefore suggest a reduction in the number of planktonic bacteria during the granulation and sludge build-up stage, allowing for the dominance of stalked ciliates throughout the remaining operation time. In addition to these conclusions, and seeing as the rotifer population is often regarded as a toxicity model (Rico-Martínez *et al.*, 2016), the recorded reduction in the number of rotifers after the first 7 weeks of operation might be regarded as evidence of a cumulative toxic effect brought about by the accumulation of silver nanoparticles and/or dye degradation metabolites in the bioreactors.

3.1.2 Biomass particle size distribution

Figure 3.3 displays the mass fractions of sludge flocs ($d < 0.2$ mm), small granules ($0.2 \text{ mm} < d < 0.65$ mm), and large granules ($d > 0.65$ mm) in SBR1 and SBR2 as assayed on mixed liquor samples collected along the experimental period. As depicted, the conventional activated sludge inoculum – which, in accordance with results from morphology analysis, consisted mostly of small flocs (94%) – successfully aggregated to form granular structures in both bioreactors during the first 16 days of operation. Along this period, the proportion of small granules significantly increased in both SBRs, while the large granular fractions saw a small increase in SBR1 (from 1.1 to 1.9%) and a slight reduction in SBR2 (from 1.1 to 0.7%). The collapse of biomass aggregates with large diameters in SBR2 might be associated with the use of a higher stirring speed during the mixed anaerobic stage (280 rpm, as compared to 70 rpm in SBR1) and interpreted as a consequence of (i) higher hydrodynamic shear forces near the impeller, promoting sloughing or disruption of large granules; and (ii) higher fluid and sludge circulation velocities, resulting in stronger attrition upon collision of biomass particles. Despite the successful development of aerobic granules in both systems, biomass aggregation seemed to occur at a faster rate in SBR1 along the first two weeks of operation, resulting in granular fractions of 11% on day 16 as compared to 7.8% in SBR2. Once again, the governing mixing conditions in SBR2 might be invoked as one of the main reasons for this evolution and associated with an operational counterbalance between the drive for microbial agglomeration and the application of strong dispersive shear forces. The two processes will be discussed further ahead.

As previously concluded, after the initial aggregation stage both SBRs experienced granule breakup episodes that resulted in the disruption of either all or most large aggregates and in reduced overall granular fractions ($d > 0.2$ mm) – 4.5 and 2.0% in SBR1 and SBR2, respectively, on day 59. The most significant drop in the proportion of granules was recorded between days 16 and 30, suggesting an early loss in granule stability during a stage of the operation where settling times were continually reduced to achieve the opposite goal, *i.e.*, favour the selection of fast-settling biomass aggregates and foster the development of mature aerobic granules. In analysing the causes behind this event, the presence of individualized, light-coloured and EPS-rich structures along the same period (discussed in the previous section; Figure 3.2A), indicative of an excessive production of bacterial exopolymers, might be looked on for some context. Intensive EPS production has been suggested by a number of authors to result in the clogging of granule pores, causing severe restrictions in the transport of substrates and metabolites into and out of the EPS matrix and often leading to cell death in the inner layers – through starvation or prolonged exposure to toxic by-products – and drops in the overall biological activity of the AG (Zheng & Yu, 2007; Lemaire *et al.*, 2008b; Corsino *et al.*, 2016). Over time, this phenomenon can destabilize the granule core, causing the structure to become brittle and eventually leading to the disruption of the granular architecture under the weight of external shear (Toh *et al.*, 2003; Zheng *et al.*, 2006; Corsino *et al.*, 2016). The heightened EPS producing capacity developed in SBR1 and SBR2 during granulation could therefore have impacted negatively (and counterintuitively) on AG stability, causing disruption and motivating a sharp drop in granulation grade. In an interesting final note on the issue, it should be noted that concerns with EPS overproduction in aerobic granules were first reported by Lemaire *et al.* (2008b)

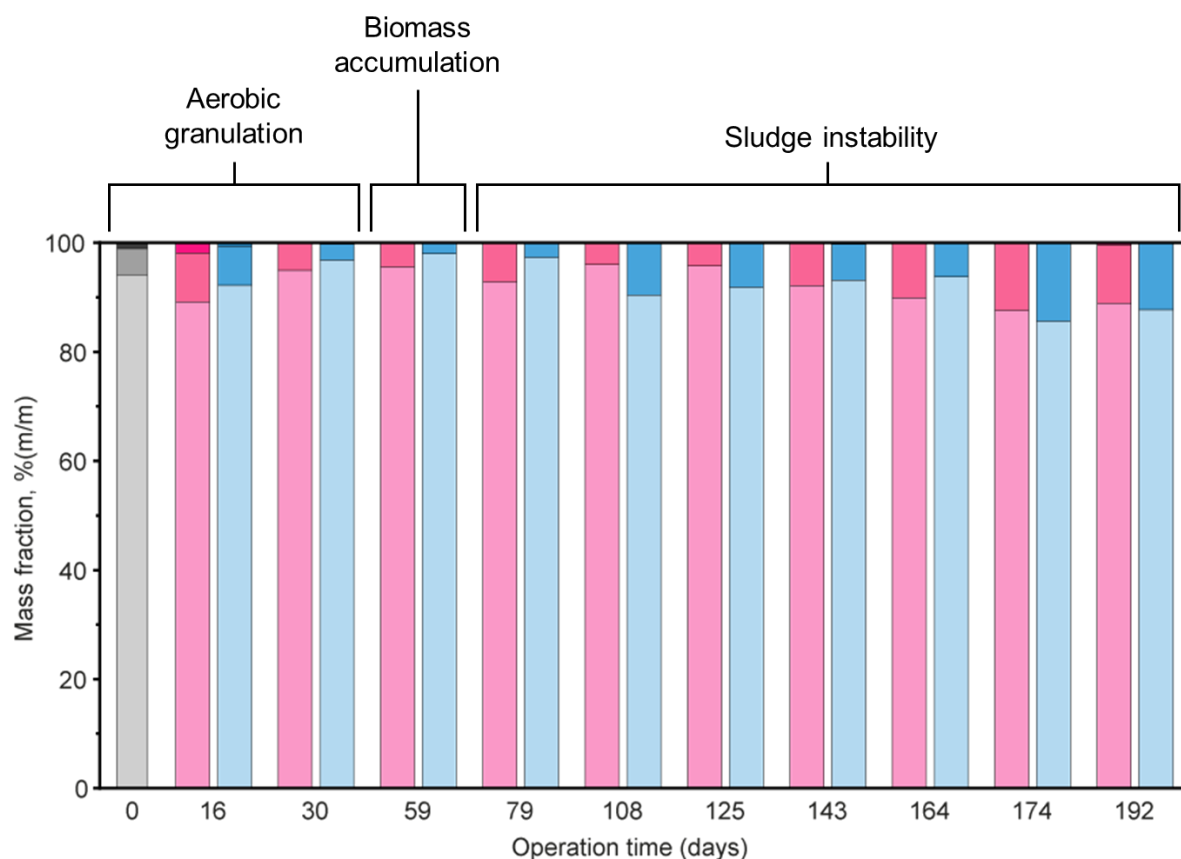


Figure 3.3 | Biomass particle size distribution (in terms of mass fraction) along the experimental run. Comparison between the mass fraction of sludge flocs (■, ■, ■; $d < 0.2$ mm), small granules (■, ■, ■; $0.2 \text{ mm} < d < 0.65$ mm), and large granules (■, ■, ■; $d > 0.65$ mm) in the conventional activated sludge inoculum (grayscale), in SBR1 (pink gradient), and in SBR2 (blue gradient).

in a study investigating the treatment of a real abattoir wastewater and were suggested to result from the presence of particulate and colloidal matter in combination with high concentrations of fats, grease and oils. While absent within the context of this study, these components are, as stated before, a constitutive part of most real textile wastewaters produced in wet processing mills (Table 1.1) and should therefore be looked on attentively if AGS-based bioremediation strategies are under consideration.

From day 59 on, granular structures in SBR1 and SBR2 were partially and slowly recovered up until the end of the operation (on day 192), following distinct patterns in each bioreactor. In SBR1, the proportion of aerobic granules initially surged (from day 59 to day 79), but subsequently declined back to stable levels at approximately 4%. From day 125 onwards, biomass aggregation promoted the development of a large number of small granules, which accounted for 10.7% of the total sludge mass by day 192. In SBR2, granular fractions increased from 2.7 to 9.6% between days 79 and 108 only to decrease slowly over the course of the following eight weeks; during the final month of operation (from day 164 onwards), the bioreactor quickly accumulated small granules up to a final mass fraction of 12%. Amid these successive restructuring and breakup episodes, granular fractions in SBR2 overtook those of SBR1 on day 108 and then again on day 174, thereby proving the influence of factors other than hydrodynamic shear in dictating the comparative edge between the granulation grade of the two systems. At any rate, the proportions of large granules in both SBRs were consistently maintained below 0.50%, signalling an inability to redevelop aggregates with large diameters in the long run.

3.1.3 Sludge settleability, biomass inventory and sludge retention time

The sludge volume index profiles obtained in each bioreactor are provided in Figure 3.4 and complemented with the respective biomass concentration and sludge retention time curves in Figure 3.5. Biomass concentrations in the SBRs were assessed by measuring TSS and VSS values in the mixed liquor and in the discharged effluent along the operational run. In order to evaluate microorganism concentrations in the process sludge, biomass contents were analysed in terms of VSS (Figure 3.5A), whereas SRT calculations (Figure 3.5B) were referred to the corresponding TSS concentrations.

As depicted in the SVI profiles, adaptation to the operating conditions in each bioreactor progressed differently and resulted in broadly contrasting sludge settling properties for most of the first month-and-a-half. In SBR1, SVI_{30} values decreased sharply from inoculum levels to $192 \text{ mL g}^{-1} \text{ MLTSS}$ during the first day of operation and initiated a declining trend that stabilized quickly around $60 \text{ mL g}^{-1} \text{ MLTSS}$ after day 7. During the same period, the corresponding SVI_5 profiles evolved in a similar manner, reaching levels below the $100 \text{ mL g}^{-1} \text{ MLTSS}$ mark within one week (Figure 3.4). The prime settling properties developed throughout this period proved sufficient to overcome the rising hydraulic selection pressure of the following weeks, ensuring a period of relative stability between days 7 and 24, characterized by SVI_5 and SVI_{30} plateaus around 93 and $59 \text{ mL g}^{-1} \text{ MLTSS}$ (mean values, respectively), despite the progressive reductions in settling time. These plateaus suggest the development of biomass structures with significantly higher settling velocities than those required for retention in the bioreactor and is consistent with the formation of dense aerobic granules in response to the operational conditions applied during the first week of the experimental run (as suggested by the results of sieving analysis). As a direct consequence of the devolved retention capacity, SBR1 enjoyed a long period of sludge build-up with minimum biomass removal along the first three weeks that resulted in a steep rise in MLVSS concentrations from a minimum of 1.1 g L^{-1} on day 3 to a local maximum of 6.2 g L^{-1} on day 24 (Figure 3.5A). After the imposition of settling times below 7 minutes (on day 24), however, significant biomass washout episodes recorded between days 24 and 28 brought MLVSS levels to a standstill that stretched until day 31 (Figure 3.5A), indicating that the sludge retention threshold was finally crossed. In the wake of these washout events, SVI_5 and SVI_{30} values dropped from their long-standing constant levels to 78 and $47 \text{ mL g}^{-1} \text{ MLTSS}$ (respectively) on day 31, reflecting the removal of slow-settling biomass particles from the system following the last two step reductions in sedimentation time ($10 \rightarrow 7$ minutes on day 24 and $7 \rightarrow 5$ minutes on day 28).

In the case of SBR2, developments in sludge settling properties and biomass accumulation progressed slowly and more measuredly than described for SBR1. During the first day of operation, SVI_5 values soared from inoculum levels to $548 \text{ mL g}^{-1} \text{ MLTSS}$, while the 30-minute index underwent a modest reduction (Figure 3.4). The recorded evolution hints at the disruption of fast-settling biomass flocs and/or larger aggregates present in the seed sludge and might be regarded as one of the initial effects of the high shear forces applied in the bioreactor during anaerobic mixing. Despite the brief climb, SVI_5 values

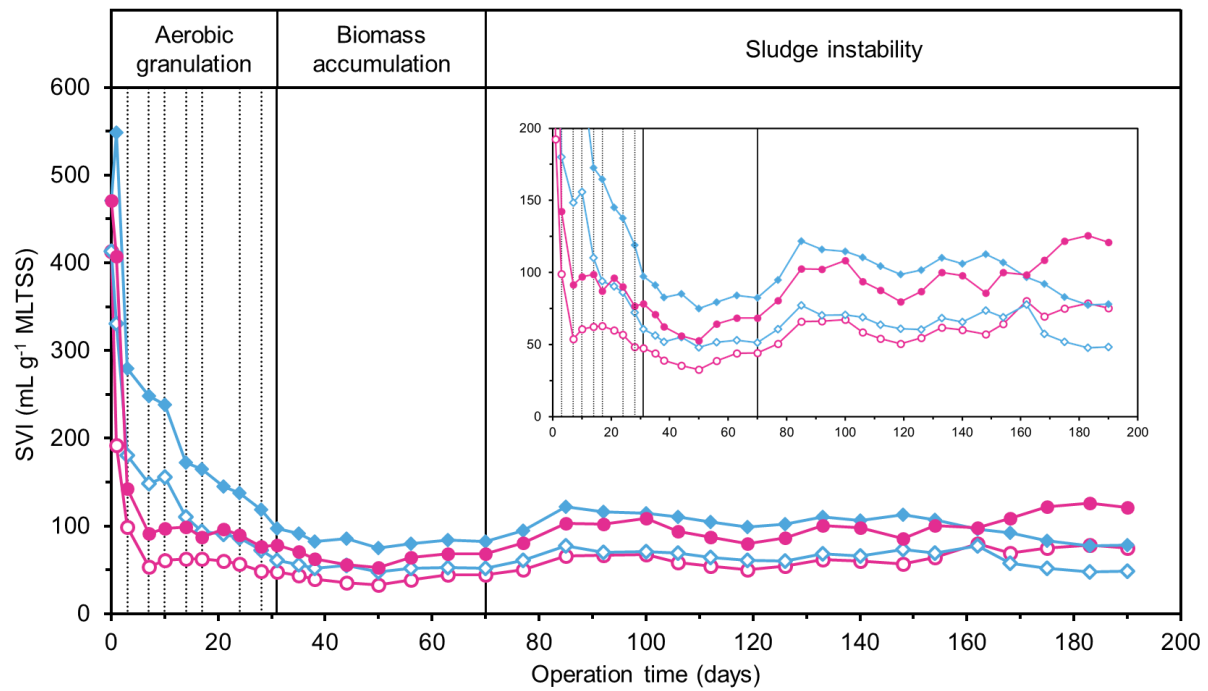


Figure 3.4 | Sludge volume index (SVI) profile along the experimental run. SVI values measured after a 5-minute settling period (SVI_5) in SBR1 (●) and SBR2 (◆), and after a 30-minute settling period (SVI_{30}) in SBR1 (○) and SBR2 (◇). The inset plot displays a focused profile for $SVI \leq 200 \text{ mL g}^{-1} \text{ MLTSS}$. Vertical dotted lines on the left-hand side denote the days where step reductions in settling time were applied.

decreased significantly after day 1, reaching $279 \text{ mL g}^{-1} \text{ MLTSS}$ (on day 3) before any changes were made to the initial 60-minute sedimentation period. Progress thereafter occurred modestly and according to a quasi-linear trend that culminated in SVI_5 and SVI_{30} values of 97 and $61 \text{ mL g}^{-1} \text{ MLTSS}$ shortly after the final step reduction in settling time (on day 31; Figure 3.4). Along the way, MLVSS concentration profiles described a very steep initial curve that raised the minimum levels of day 1 to a peak at 4.6 g L^{-1} on day 21 (Figure 3.5A). Much like the case of SBR1, this hike followed a period of very low EVSS contents – below 70 mg L^{-1} – that stretched at least until day 14 (Figure 3.5A). The described growth curve can be interpreted as a reflection of the good biomass retention capacity in the bioreactor and correlated with the development of fast-settling aerobic granules throughout the first two weeks of operation (once again consistent with sieving analysis). Despite the initial evolution, the sludge system proved sensitive to the increasing hydraulic selection pressure, recording severe washout events on days 17, 24, and 28 after the definition of settling periods below 15 minutes. As a result, biomass accumulation slumped towards the end of the granulation stage, reaching a maximum of 4.7 g L^{-1} on day 31 (Figure 3.4). While similar to SBR1 in describing an initial period of biomass accumulation driven by prime sludge settling properties and a subsequent stage of heavy washout, the picture of aerobic granulation described above for SBR2 hints at a much more gradual formation of aerobic granules in the latter bioreactor and offers some context to the comparative superiority – in terms of granular fractions – of SBR1 along the initial leg of the operation (Figure 3.3).

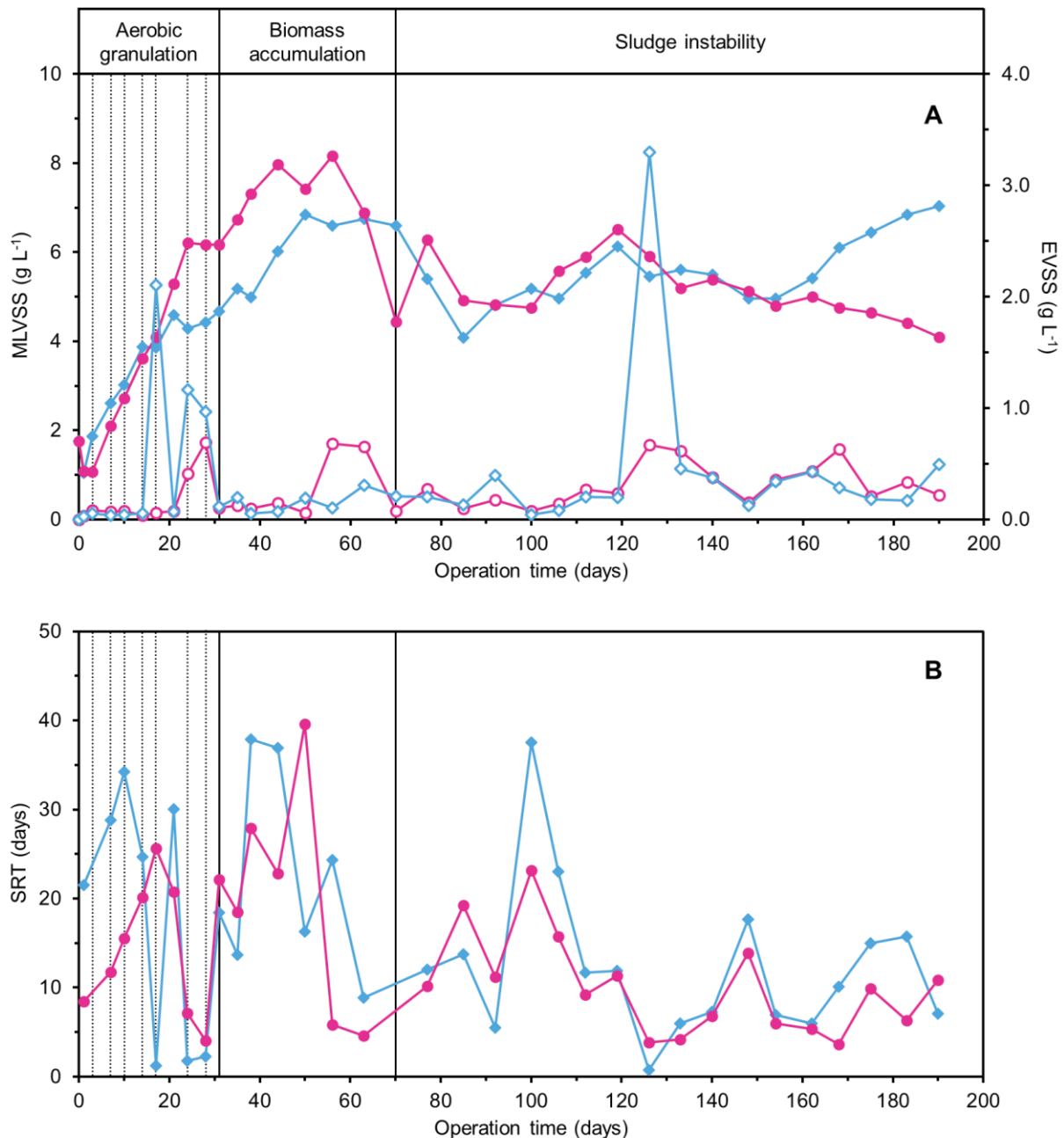


Figure 3.5 | Biomass concentration and sludge retention time (SRT) along the experimental run. (A) Volatile suspended solids contents in the mixed liquor (full symbols) and in the effluent (open symbols) from SBR1 (●,○) and SBR2 (◆,◇). (B) SRT profiles in SBR1 (●) and SBR2 (◆). Vertical dotted lines on the left-hand side denote the days where step reductions in settling time were applied.

Beyond the final settling time reduction, sludge volume indexes continued to decrease in both bioreactors despite the evidence for granule disruption between days 16 and 59 (Figure 3.3), reaching minimum levels on day 50 – SVI₅ and SVI₃₀ values of 53 and 33 mL g⁻¹ MLTSS in SBR1, and 75 and 48 mL g⁻¹ MLTSS in SBR2, respectively. These results suggest the presence of dense sludge fragments, produced upon the structural disintegration of aerobic granules formed along the first two weeks, that developed to adopt higher settling velocities after the definition of a constant hydraulic selection pressure (on day 28). In response to the improvement in sludge settleability, biomass accumulated once again until day 50, reaching maximum concentrations of 8.2 g VSS L⁻¹ in SBR1 (on

day 56) and 6.8 g VSS L^{-1} in SBR2 (on day 50). The comparatively higher levels achieved in SBR1 during this stage and throughout most of the experimental run are the product of inferior SVI values that allowed the bioreactor to retain a more compact sludge system with superior microbial concentrations. Much to the similarity of what had been observed during previous sludge build-up episodes, EVSS concentrations measured after the imposition of a 5-minute sedimentation period on day 28 significantly declined when compared to the levels of previous days and were maintained at around $100 \text{ mg VSS L}^{-1}$ until day 56. As a combined reflection of the trends described by the MLVSS and EVSS curves, the sludge retention time increased during the first month-and-a-half (Figure 3.5B) to maximum values of 40 days in SBR1 (day 50) and 38 days in SBR2 (day 38), sustaining marked oscillations concomitant with the washout episodes recorded towards the end of the aerobic granulation period. As described in chapter 2, the chosen method for SRT calculations is based on a simplistic approach that assumes constant MLTSS concentrations and effluent solids contents and is therefore largely susceptible to the quality of the data collected during the representative cycles. Using this strategy, high ETSS concentrations will result in low SRT values that do not necessarily reflect the average sludge age throughout the relevant sampling period and should thus be interpreted with caution. Along this initial period, however, this strategy provides a reliable measure of the retention capacity developed in the SBR systems that clearly integrates all previous considerations.

Following the accumulation stage, biomass concentrations reached the maximum retention capacity of the bioreactors and stagnated around the previously mentioned maxima for several weeks – between days 44 and 56 in SBR1 and between days 50 and 70 in SBR2 (Figure 3.5A). Throughout this period, sludge settling properties underwent a gradual deterioration that progressed until day 85 to reach local maximum levels in SBR1 (SVI₅ and SVI₃₀ values of 103 and 66 $\text{mL g}^{-1} \text{ MLTSS}$) and SBR2 (SVI₅ and SVI₃₀ values of 122 and 77 $\text{mL g}^{-1} \text{ MLTSS}$) (Figure 3.4). As a result, two intense periods of biomass washout recorded between days 63 and 85 caused MLVSS contents to drop steeply from their plateaus to local minima of 4.4 mg L^{-1} in SBR1 (day 70) and 4.1 mg L^{-1} in SBR2 (day 85) (Figure 3.5A). This episode marked the beginning of a long period of dynamic changes in sludge properties that progressed, with only minor distinctions between the two bioreactors, according to mirror images in the SVI and MLVSS profiles. The recorded evolution is best subdivided in the following three stages (Figures 3.4 and 3.5A):

- (i) a paced sludge accumulation between days 85 and 119 driven by gradually decreasing SVI₅ and SVI₃₀ values (effective in SBR1 only from day 100 on); peak MLVSS contents were recorded on day 119 at 6.5 and 6.1 g L^{-1} in SBR1 and SBR2, respectively;
- (ii) a reversal of the previous progress, characterised by heavy biomass washout after day 126 and stretching until day 148 (when comparable MLVSS levels of $\sim 5.0 \text{ g L}^{-1}$ were reached in both systems);
- (iii) a period of divergence from day 148 on to the end of the operation, characterised by an improvement in sludge settleability in SBR2 and by increasing SVI values in SBR1; as a result, biomass concentrations increased in the former case (up to 7.0 g L^{-1}) and decreased in the latter (down to 4.1 g L^{-1}); this final period marks the only instance of the whole experimental run where SVI and MLVSS levels in SBR2 surpassed those of SBR1.

These episodes follow multiple variations in the mass proportion of granules in the sludge bed (as revealed by sieving analysis) that relate differently to sludge settleability in each reactor. In the case of SBR2, the succession of granule formation and breakdown events previously inferred in section 3.1.2 concurs with the SVI profiles in describing a stage of granule restructuring concomitant with the progressive improvement in sludge settleability recorded between days 85 and 119 (SVI₅ and SVI₃₀ values of 99 and 61 mL g⁻¹ MLTSS down from 122 and 77 mL g⁻¹ MLTSS). Following this period, the final fast granulation phase led to a similar decrease in SVI values (from day 148 until the end of the operation) that further validates a correlation between the two variables. In contrast, the SVI profiles obtained for SBR1 suggest variations in sludge settleability that are largely unrelated to the changes in the proportion of granules. Despite the apparent recovery of biomass aggregates between days 59 and 79 and the progressive granule reformation observed from day 125 onwards (Figure 3.3), sludge settleability markedly waned along the same periods rather than improving. These results suggest that, beyond the first few weeks of operation, where sludge aggregation resulted in dense structures that significantly reduced SVI values, biomass flocs in SBR1 aggregated to form aerobic granules with poor settling properties.

During this final period of sludge instability, EVSS measurements revealed consistently higher levels than those registered along the first 85 days, with a minimum at just under 600 mg L⁻¹ and a maximum at 3.3 g L⁻¹. All throughout, assayed concentrations peaked and fell indiscriminately according to patterns that could not always be trivially correlated with the recorded changes in sludge settleability and with bioreactor capacity. In the face of this inconsistent progression, SRT values oscillated sharply towards the end of the experimental run between vastly diverging extremes that hold little meaning as descriptors of sludge age and maturation. Combined with the data from sieving analysis, these results describe two SBR systems with an erratic behaviour inconsistent with the realisation of a steady-state operation and with the development of a mature aerobic granular sludge bed.

3.1.4 Hydrodynamic shear as a determinant of granulation grade and sludge settleability

As described in 2.3, hydrodynamic shear in SBR1 and SBR2 was provided by mechanical mixing during the anaerobic reaction period and by aeration during the aerobic phase. In order to provide a serviceable measure of the governing shear forces in each stage, fluid deformation was indirectly and informally evaluated using the tip speed attained by the impellers (26 and 88 m min⁻¹ in SBR1 and SBR2, respectively) and the average upflow air velocity achieved during aeration (0.4 m min⁻¹ in both systems). In the case of mechanical shear, the chosen representative values characterise the rate of deformation in the boundary layer around the impeller tip and document only the maximum fluid displacement in the bioreactors. Albeit restrictive, these values provide a general notion of the average shear forces that can be anticipated in each system and establish a useful comparative tool for analytical purposes. Assuming the mixed liquors of the two SBRs retain similar rheological characteristics, the pitched blade turbine installed in SBR2 can therefore be expected to generate higher shear stresses during anaerobic

mixing than the magnetic anchor impeller fitted in SBR1. This demarcation constitutes a defining factor for the course of the operation and is likely to have impacted several key properties of the granulated sludge systems.

As previously discussed, the high shear forces applied in SBR2 can be regarded as the main factor behind the differences in the granulation rates and granular fractions achieved in each bioreactor during the first few months of the experimental run (roughly spanning the aerobic granulation and biomass accumulation periods; Figures 3.1 and 3.3). The process of aerobic granulation is promoted by an equilibrium between microbial adhesion forces (including, e.g., van der Waals interactions, hydrophobic interactions, Brownian movements, ion pairs, and/or cell membrane fusion) (Liu & Tay, 2002; Adav *et al.*, 2008a) and dispersive shear forces with both direct effects (produced by, e.g., biomass-stirrer collisions or collapsing air bubbles in the mixed liquor) and indirect effects (collisions between biomass particles promoted by fluid circulation). The balance between these forces manifests as a competition between surface grinding and internal cohesion that simultaneously determines the kinetics of granule growth and the equilibrium dimensions achieved by mature aerobic granules (Verawaty *et al.*, 2013). Considering the different stirring speeds applied in each reactor (70 rpm in SBR1 vs. 280 rpm in SBR2), it is thus possible to infer a sharper shift in the direction of granule disaggregation in the case of SBR2 that might justify the inferior granular fractions registered throughout the first weeks of the operation (Figure 3.3). The same reasoning might also be invoked to explain the overall smaller dimensions of aerobic granules developed in SBR2 and the rapid disintegration of large bacterial aggregates observed during the first 16 days (Figures 3.1 and 3.3). Outside the aerobic granulation period, however, the role of shear in defining the microscopic characteristics of the aerobic granular sludge systems in SBR1 and SBR2 was superseded by other factors, forcing granule dimensions and mass fractions to oscillate profusely and with no clear trend.

On a macroscopic level, the meaningful differences identified throughout the entire operation between the settling properties in SBR1 and SBR2 can similarly be attributed to the different stirring speeds and shear forces imposed in each system. Hydrodynamic shear has been shown to play an important role in defining the settling velocity of aerobic granules by promoting the development of dense three-dimensional structures (Beun *et al.*, 1999; Liu & Tay, 2002). While studying the association between the two variables, Tay *et al.* (2001) found a negative correlation between the dispersive forces provided by increasing superficial upflow air velocities (SUAV) and the SVI of aerobic granules developed in an SBR. The results were explained by codirectional increases in cell surface hydrophobicity and EPS production that resulted in the formation of high-density aerobic granules with high structural cohesiveness and integrity (Tay *et al.*, 2001b). In a similar note, Chen *et al.* (2007) reported average SVI values of 41 and 27 mL g⁻¹ MLTSS for mature granules cultivated in two column sequencing batch reactors operated under a SUAV of 2.4 and 3.2 cm s⁻¹, respectively (Chen *et al.*, 2007). Even though no equivalent conclusions regarding the effects of mechanical shear over sludge settleability have been advanced to this day, simple conceptual parallels between the work at hand and these results would suggest the development of aerobic granules with superior settling velocities in SBR2 – on account of the higher governing shear forces – and not in SBR1, as observed throughout the better part of the experimental

run (until day 162; Figure 3.4). Alternative conclusions advanced in SBR studies with activated sludge seem, however, to suggest that the correlations described above can only be observed over a limited range of average shear rates (associated with increasing air flow rates) whose upper limit corresponds to a maximum average sludge settling velocity and a minimum SVI value. Beyond that limit, the covariation trend is inverted, resulting in rising sludge volume indexes that will deviate more sharply from the minimum as the difference between the threshold and effective shear forces increases (Feng *et al.*, 2015). In light of these results, it is therefore possible to speculate that the governing mixing conditions in SBR2 exceeded an unspecified shear threshold and promoted the development of a sludge system with poorer settling properties than those achieved in SBR1, where lower stirring speeds allowed the formation of denser biomass structures. This demarcation reflected in inferior biomass compressibility and resulted in a reduced sludge retention capacity that was clearly manifested in the MLVSS profiles plotted for SBR2 over the first 148 days of operation (Figure 3.5A). The factor most likely to have influenced settleability from this point on will be discussed independently ahead.

3.1.5 Contradictory short- and long-term impacts of Ag NP dosing

While no independent method was employed throughout this work to evaluate Ag NP accumulation in the sludge and silver releases in the effluent extracted from SBR1 and SBR2, several key evolutionary trends detected in the SVI and MLVSS profiles can be associated with results from previous studies investigating the impacts of silver nanoparticle on wastewater sludge systems to reach important conclusions. These trends are best subdivided along the temporal plane and relate to both bioreactors' responses in the short term – roughly equivalent to the aerobic granulation and sludge accumulation stages – and in the long term – equivalent to the final period of sludge instability.

Aerobic granulation and bioreactor accumulation phases

In the short-term horizon, Ag NPs seemed to exert no significant negative impact over the process of aerobic granulation proper despite the high influent concentration (10 mg L^{-1}), with both bioreactors recording significant improvements in sludge settleability over the first 50 days and going on to form granules unhindered. As stated above, previous studies conducted on our lab have demonstrated that silver nanoparticle loadings as high as 5 mg L^{-1} similarly bear no influence on the dynamics of aerobic granulation (Annex A; Bento, 2016; Rodrigues, 2017), which indicates AG formation is – at least along the tested loading range – relatively impervious to the antimicrobial action of Ag NPs. This sort of behaviour suggests that all relevant microbial functions involved in granulation could be maintained inside the bioreactors even after exposure to Ag NPs and points either to a high level of community resilience working among the microorganisms in the CAS sample or to some sort of environmental transformation that limited the antimicrobial potential of silver nanoparticles.

Results from a recent study conducted with activated sludge have demonstrated that, contrary to expectations, relatively low doses of Ag NPs (1 mg L^{-1}) – especially freshly prepared Ag NPs – can actually help maintain or even increase the diversity and functional richness of the microbial community

and thus contribute to increase its resistance in the event of further toxic shocks. The same study also documented an improvement in sludge settleability and a consequent increase in biomass concentrations after exposure, revealing a range of possible positive effects that could actually improve bioreactor operation (Sheng *et al.*, 2018). This sort of constructive spur in response to low concentrations of a toxicant is called a hormetic effect and has been reported in a number of other studies investigating the impacts of Ag NP dosing in both defined planktonic and biofilm cultures (Yang & Alvarez, 2012; Xiu *et al.*, 2012). In light of these results, the presence of Ag NPs in SBR1 in SBR2 during the initial stages of the operation might actually have contributed productively for some of the developments in AG formation, settleability and biomass accumulation, helping in the establishment of the AGS system.

In addition to community resilience, some of the operating specifics in SBR1 and SBR2 might also have acted to curb, however partially, the antimicrobial activity of Ag NPs. As previously stated, silver nanoparticle toxicity is mainly mediated by the release of free Ag⁺ ions through oxidative dissolution reactions at the NP's surface (Le Ouay & Stellacci, 2015). When in the environment, Ag NPs are known to interact with sulphides, chlorides and organic matter to form a number of poorly soluble derivatives that can significantly limit Ag⁺ bioavailability and thus result in reduced activity (Levard *et al.*, 2012; Kaegi *et al.*, 2013; Kroll *et al.*, 2014). Furthermore, high silver concentrations are known to promote Ag NP aggregation, increasing NP surface area and tortuosity and once again contributing for reduced silver ion releases (Chen & Zhang, 2012). All these phenomena can be expected to play a role in SBR1 and SBR2 – whether owing to the imposition of an anaerobic phase (prone to H₂S releases), to the chemical composition of the synthetic textile wastewater (rich in Cl⁻), to the presence of significant EPS concentrations in association with the sludge or even to the use of a concentrated Ag NP suspension (100 mg Ag L⁻¹) to feed the bioreactors – and likely proved important in determining effective Ag⁺ exposure levels in the bioreactors.

Sludge instability phase

In spite of the successful formation of AGs, sludge property developments recorded from day 70 onwards appeared to reveal a destabilizing effect lurking behind the constant addition of Ag NPs. As described above, right after the bioreactors reached their respective sludge retention thresholds, dramatic washout events on day 85 resulted in the removal of nearly half the resident biomass and initiated a period of cyclical sludge accumulation and sludge removal periods – accompanied by improvements and decays in settleability (Figures 3.4 and 3.5A). These patterns are at least partly in line with SVI and MLTSS profiles plotted for SBR1 in a previous operation carried out with a nominal Ag NP load of 5 mg L⁻¹ by Bento (2016), where a sharp drop in biomass concentrations could be detected few weeks after sludge accumulation ceased. The bioreactor was operated against an identical, Ag NP-free control that displayed no similar washout event, indicating a direct association between biomass removal and silver dosing (Annex A). The combination of these results seems to suggest that Ag NP accumulation in the bioreactors can occur with minor harm to the operation up to a given limit before negative impacts emerge. Biomass washout resulting from the violation of this limit results in a reduction

of accumulated nanoparticle contents and effectively initiates a new stage of the cycle where sludge properties improve continuously until the threshold is exceeded again. Similar conclusions were advanced by Sheng *et al.* (2018), who noted a decay in sludge settleability and biomass retention capacity 40 days into the operation of a CAS SBR exposed to fresh Ag NP suspensions despite initially positive developments. The bioreactor was stopped before severe washout events could be recorded and the cycle could be repeated, but Ag NP accumulation was equally suggested as the main causative factor.

This behaviour emerges as a consequence of the prime retention capacity of AGS reactors, seeing as sludge particles are allowed to remain in the system over extremely long periods of time, continually interacting with and amassing inbound nanoparticles. Control strategies aiming to limit Ag NP accumulation in these systems (or any other bioreactor designs characterized by high retention) should therefore be devised whenever consistently high NP loadings are expected. Periodical biomass removal for SRT control is one possible solution with a long track record in the context of wastewater treatment and should prove sufficient to avoid operational instability.

Interestingly, iterations of the accumulation/washout cycle seemed to take place according to similar timings in SBR1 and SBR2 despite all the other operational differences. While effective silver loads were exactly the same in both bioreactors, biochemical sludge properties and microbial communities in each system can be expected to vary significantly in response to specific parameters, in turn affecting the extent to which Ag NPs can interact with flocs and granules. In one example, carbohydrate-to-protein balances in the EPS matrix – an important factor determining Ag NP adsorption in the biomass (Kroll *et al.*, 2014) – have been shown to respond differently to different external shear stresses (Liu & Tay, 2002; Adav *et al.*, 2007b) and should therefore motivate some difference in the amount of accumulated silver. These observations raise some questions regarding the mechanisms by which Ag NPs lead to sludge instability and should form the subject of future research.

3.1.6 Long-term impacts of anaerobic feeding strategy on sludge properties

As previously mentioned, despite the evidence for granule reformation recorded in both bioreactors towards the end of the experimental run, sludge settleability in the two systems was seen to follow, after day 148, two inconsistent trends that hint at the accumulation of dense structures with high settling velocities in SBR2 and at the presence of low-density granules with poor sedimentation ability in SBR1 (Figure 3.3 and 3.4). These results contrast significantly with settleability trends identified throughout the remaining operation time and signal the influence of some factor other than hydrodynamic shear in defining the balance of macroscopic sludge properties. While no independent measurement performed throughout the experiment can be used to clearly establish what this factor was, the particularities of each system's anaerobic feeding strategy could be advanced as likely contenders. Causation links between feeding and these observations emerge in association with each system's characteristic fluid circulation patterns across the sludge bed and could result from different biomass concentrations inside the granules – as previously suggested by Franca *et al.* (2017a) in a different operation with the same bioreactors.

The use of a plug-flow hydrodynamic regime (as applied in SBR2) rising through the settled sludge bed, with a high substrate concentration, allows soluble, easily biodegradable substrates to penetrate the entire AG depth and be converted to storage polymers by relevant PAO and GAO populations. These storage polymers can subsequently be used as carbon and energy sources over the course of the aerobic phase, sustaining slow microbial growth down to the granule core and ensuring the development of a stable, dense structure. Conversely, by limiting the contact of the influent feed solution with the settled biomass, the fast, static filling arrangement imposed in SBR1 leaves the bulk of substrate consumption for the subsequent anaerobic mixed phase and forces AGs to contact with a diluted effluent – mixed in with the leftover effluent from the previous cycle (Franca *et al.*, 2017a). As a result, storage polymer reserves accumulated under anaerobiosis might prove insufficient to secure basic maintenance functions during the aerobic phase, leading to cell death and to the creation of empty pockets inside the granular volume that contribute for a light structure. Granules grown in SBR1 by Franca *et al.* (2017a) were indeed shown to display sparse storage polymer reserves towards the end of the reaction cycle and could serve as models for the AGs obtained during this work. To back the reasoning above, the following section will deal with the specifics of COD removal and particularly with the differences between the contribution posted by each system's feeding phase to the overall organic load remediation yield.

3.2 Treatment performance

3.2.1 COD removal performance and pH profiles

The influence of feeding strategy over carbon removal and the calculation of COD conversion yields

The carbon load removal performance of the SBR systems was evaluated through measurements of COD removal levels during several treatment cycles along the experimental period. COD concentrations were assayed (i) on the feed solution introduced into SBR2, (ii) on the effluent collected from SBR2 before the chosen representative cycle, and (iii) at 6 distinct time coordinates throughout the reaction stage, starting at the onset of the mixed anaerobic phase and ending immediately before aeration ceased. In order to evaluate treatment efficiency at each of these coordinates, the recorded COD levels were converted into removal yields by comparison with a reference initial concentration, defined in each bioreactor in accordance with the expected levels of substrate consumption during filling. In the case of SBR1, organic load removal was deemed negligible throughout this stage and the boundary condition was assumed as the COD level assayed immediately after the onset of mixing (MixSBR1). As stated above, this model regards the initial contact between the influent solution and the settled sludge blanket as inconsequential from the perspective of wastewater treatment and is based on experimental observations compiled for the same bioreactor in previous investigations (Franca *et al.*, 2017a). In the absence of any equivalent knowledge on the filling behaviour of SBR2, initial concentrations in the system were predicted theoretically assuming a perfect-mixing, null-conversion computation model that weighed the volumetric fractions and individual carbon loads of the feed solution, the Ag NP suspension and the leftover effluent from the previous cycle (ThSBR2). Unlike the case of SBR1, this strategy was

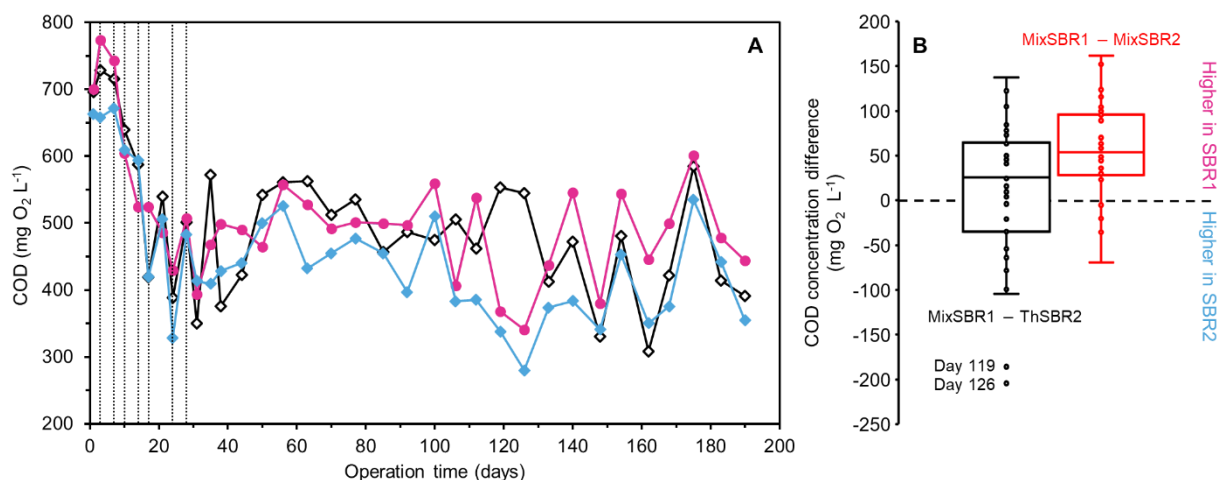


Figure 3.6 | Reference initial COD levels in the bioreactors. (A) Theoretical initial COD concentrations in SBR2 (ThSBR2, \diamond) and COD contents at the onset of the mixed anaerobic stage in SBR1 (MixSBR1, \bullet) and SBR2 (MixSBR2, \blacklozenge). Vertical dotted lines on the left-hand side denote the days where step reductions in settling time were applied. (B) Box plots of relative differences between the reference COD concentrations assumed in each bioreactor (MixSBR1 – ThSBR2, $-$) and between COD contents measured at the same process coordinate (MixSBR1 – MixSBR2, $-$). Whisker ends were defined in accordance with Tukey's test, *i.e.*, capped at the lowest and highest observations within 1.5 interquartile ranges of the 1st and 3rd quartiles, respectively; all data points lying beyond the whiskers were regarded as outliers and tagged with the corresponding operation day.

employed with the explicit aims of characterizing the contribution of the filling phase for the final remediation yield and avoiding any underestimated performance metrics that would dismiss it as insignificant. Figure 3.6 offers a breakdown of the reference concentrations recorded in SBR1 and SBR2 over the course of the experimental window, as well as the COD contents assayed on samples collected from SBR2 at the onset of anaerobic mixing (MixSBR2) – provided as a way of quantifying the relative COD remediation yield achieved during filling. For comparative purposes, two box plots charting the relative differences between the concentrations in each of the two systems (SBR1 – SBR2) are also provided.

As depicted, COD concentrations measured at the onset of mixing were consistently lower in SBR2 than in SBR1 (according to a median absolute difference of 54 mg O₂ L⁻¹), hinting at a measure of substrate consumption during plug-flow filling that could not take place under the fast, static filling arrangement of the latter system and lending some support to the use of a non-biased reference initial concentration derived from a fictitious null consumption scenario in SBR2. Conversely, differences between the values of ThSBR2 and MixSBR1 appeared to cut a much less defined trend, shifting arbitrarily in sign across the experimental window (most likely owing to local differences in feed preparation or to variations in volumetric loading; Figure 3.6A, B) and pointing more to a meaningful impact of random error than to a systematic difference between the two reference states. These results suggest a greater measure of comparability between the theoretical estimate derived for SBR2 and the COD content measured at the onset of mixing in SBR1 than between concentrations assayed at the same process coordinate and constitute, for the most part, a binding validation of the reference models assumed in each bioreactor.

However, they are not without exception. As represented in Figure 3.6, initial COD concentrations registered in SBR1 during days 119 and 126 fell markedly below the corresponding ThSBR2 values (by as much as 204 mg O₂ L⁻¹), suggesting some momentous change in the dynamics of organic loading was taking place in the former bioreactor. This hypothesis is supported by the close alignment between the MixSBR1 and MixSBR2 values recorded during the same days, which seems to hint at an abnormally large contribution to carbon removal coming both from plug-flow filling and from fast, static filling. These observations place a heavy weight on the basic assumption that pre-mixing conversion yields in SBR1 can be neglected and generates some anxiety regarding the validity of the remaining data. The deviation is, however, localized enough that it might be ignored when looking into the results of other representative cycles and dealt with by applying an extra measure of caution when examining the results from days 119 and 126 in relative terms (*i.e.*, when using conversion yields reported to the reference concentrations). Considering these restrictions, the main traits of the carbon removal profiles plotted for each reactor and the overall descriptors of COD removal performance will be listed over the following pages by shifting between absolute measurements of COD concentrations and conversion yields.

COD removal performance and pH profiles

The overall COD removal yields obtained along the experimental run are represented in Figure 3.7B together with the fraction of the overall yield that was removed (*i*) during plug-flow filling in SBR2 and (*ii*) by the end of the anaerobic mixing phase in both reactors. The corresponding COD concentrations in the mixed liquor are plotted in Figure 3.7A to aid in the discussion of the COD removal performance of the bioreactors. Finally, a breakdown of feed pH and COD levels registered throughout the operation is displayed in Figure 3.8 in conjunction with a number of COD depletion and pH variation curves selected for several representative cycles on the basis of their relevance in explaining the observed carbon removal behaviour. pH monitoring data will be used to track the production, accumulation and assimilation of volatile fatty acids (VFA; *e.g.*, acetate) and thus track the relevance of anaerobic fermentative metabolism (involved in the degradation of the primary substrate) and GAO-/PAO-related activities (involved in VFA uptake) at different operational coordinates.

As depicted, overall COD removal levels remained below the 50% mark during the first week of operation, likely due to the change in the main carbon substrate from domestic wastewater to the synthetic textile effluent with hydrolysed hydroxypropyl starch as carbon source. However, the microbial communities in the bioreactors efficiently adapted to the new carbon source, reaching COD removal yields of 70 and 75% on day 14 (in SBR1 and SBR2, respectively), and subsequently stabilizing in the 80–90% range (with occasional drops) from day 38 on – despite the continuous loading of Ag NPs and the observed shifts in granulation grade, biomass concentration, and sludge settleability. The absolute COD removal capacity of the bioreactors reached a steady state on day 17, limiting the consumption of organic matter up to residual levels in the 50–110 mg O₂ L⁻¹ range. Conversely, carbon load removal yields during the anaerobic stage saw significant variations throughout the operational run. Relative conversion during plug-flow filling in SBR2 varied between –14% (days 38 and 162) and 49% (day 126)

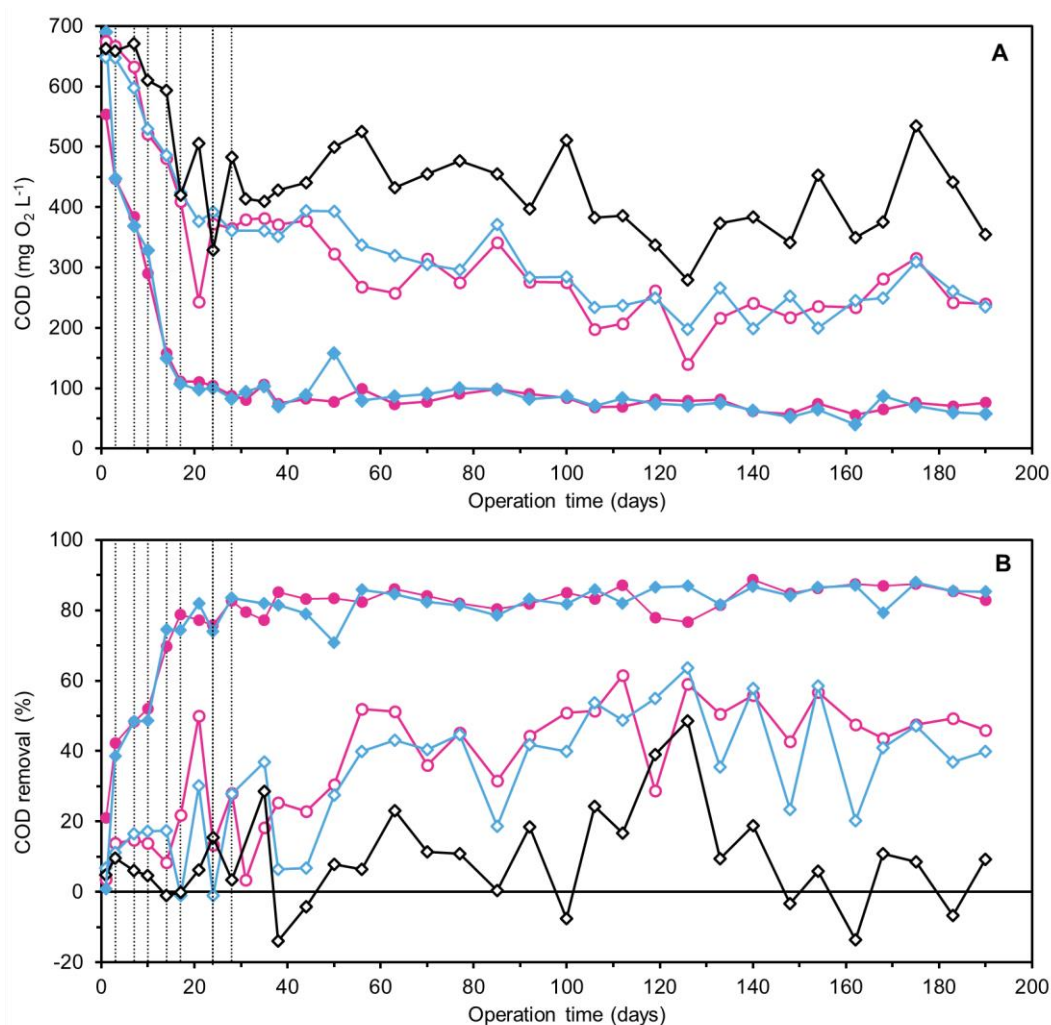


Figure 3.7 | COD removal performance along the experimental run. (A) Residual COD concentrations in SBR1 (●,○) and SBR2 (◆,◇) at the onset (open symbols) and at the end of aeration (full symbols), plus the COD contents measured immediately after plug-flow filling in SBR2 (◇). The same variables and graphic features are used in (B) to define relative filling, anaerobic and overall removal yields by comparison with the reference COD levels represented in Figure 3.6. Vertical dotted lines on the left-hand side denote the days where step reductions in settling time were applied.

according to a mostly random pattern, a result that could be ascribed to the non-tubular geometry of the bioreactor. As previously stated, low H/D ratios have previously been shown to hinder proper influent distribution across the settled sludge bed during plug-flow feeding by promoting random channelling routes. The random nature of these channels induces marked variations on the effective contact time between the biomass and the influent solution, steering the fluid through longer or shorter paths from cycle to cycle and thus causing COD conversion yields to oscillate profusely (Rocktaschel *et al.*, 2013).

Inconstant yields were, however, not limited to the feeding phase. After an initial increase over the first two weeks, total anaerobic COD removal (A_{nCOD}) dropped slightly on day 14 in SBR1 and sharply – to null levels – on day 17 in SBR2. The recorded reduction in SBR2 is in keeping with an abrupt decrease in sludge age (Figure 3.5B) and suggests that relevant bacterial species bolstering anaerobic carbon removal were washed out of the bioreactor; similar unrecorded sludge removal events are likely to have caused the drop in A_{nCOD} observed in SBR1 on day 14. After these two occurrences, anaerobic COD

removal yields in both bioreactors significantly surged, reaching 50 and 30% in SBR1 and SBR2 (respectively) on day 21, but subsequently fell to lower levels following another sludge washout episode on day 24. Parallel interpretation of the COD removal and pH profiles collected for the representative cycle of day 24 (Figure 3.8B) suggests that primary substrate fermentation took place during the mixed anaerobic stage and resulted in the production of VFA with a concomitant decrease in pH (from 6.38 to 6.16 in SBR1 and from 6.32 to 6.15 in SBR2). COD concentrations were marginally reduced in SBR1 along the same period, and slightly increased in SBR2, suggesting the accumulation of volatile fatty acids in the presence of a deficient anaerobic VFA-processing activity. The accumulated oxygen demand in the form of VFA (and possibly residual saccharides from Emsize E1 hydrolysis) was rapidly consumed by aerobic microorganisms on the surface of the sludge flocs and aerobic granules within the first 30 minutes of aeration and stabilized around $100 \text{ mg O}_2 \text{ L}^{-1}$ during the final two hours of the reaction stage. These results concur with the establishment of a famine period where substrate consumption and oxygen uptake drop to a minimum. The oxidation of the VFA produced during the anaerobic stage resulted in an increase in pH to levels around 6.6 in both bioreactors which reflect the equilibrium between the buffering action of all buffer salts in the mixed liquor, provided in the feed. As depicted in Figure 3.8, the same general trends could be identified in the COD and pH profiles obtained for the aerobic stages of all representative cycles.

Following the initial stepwise reductions in settling time, anaerobic COD removal yields progressively increased in both bioreactors, reaching local maxima of 52% in SBR1 (on day 56) and 45% in SBR2 (on day 77). These results are once again in keeping with a progressive maturation of the microbial population after the hydraulic selection pressure was set to constant levels, and follow a decrease in the residual mixed liquor COD concentration at the onset of aeration between days 28 and 77 (Figure 3.7A). In agreement with the reduction of active biomass concentrations observed in SBR1 on day 70 and in both systems on day 85 (Figure 3.5A), COD conversion during the mixed anaerobic stage fell by as much as 26% and resulted in increased organic loads going into the aerobic stage. COD removal profiles obtained for SBR2 on day 85 (Figure 3.8C) reflect a negligible difference between the computed reference values and the measurements performed right after the start of the mixed anaerobic reaction, and suggest that minimal carbon consumption occurred during the plug-flow feeding stage. These results starkly contrast with those from previous weeks, where COD removal yields as high as 23% (on day 63) could be obtained during filling (Figure 3.7B), and further signal that important species of the resident bacterial community were washed out of the bioreactor during this stage. Interestingly, despite the minor COD conversion during anaerobic feeding and mixing, the pH variation curves plotted during the same cycle for both bioreactors show a plateau centred around 6.4 and 6.3 in SBR1 and SBR2 (respectively) that falls significantly below the buffered pH levels of the subsequent aeration phase and thus suggests the presence of VFA in large amounts. These results might be attributed to the anaerobic degradation of organic matter in the feed solution, either in the feed containers or in the piping of the bioreactor system due to colonization by bacterial species from the sludge community. In keeping with this hypothesis, pH levels registered on feed samples collected on day 85 fell considerably short of the typical measurements from previous and subsequent weeks (5.67 as compared to values in the 6.5–6.9 range – Figure 3.8A), reflecting the possible accumulation of VFA. Similar drops in feed pH, which

resulted in comparable pH profiles during the anaerobic stage (as depicted in Figure 3.8E), could be identified near the end of the operation on days 148 and 162. In general, as suggested by Figure 3.8A, the pH of the feed changed on par with sharp declines in the influent COD load ($r = 0.7424$) throughout the entire run, further backing the thesis of an intimate relation between the two variables.

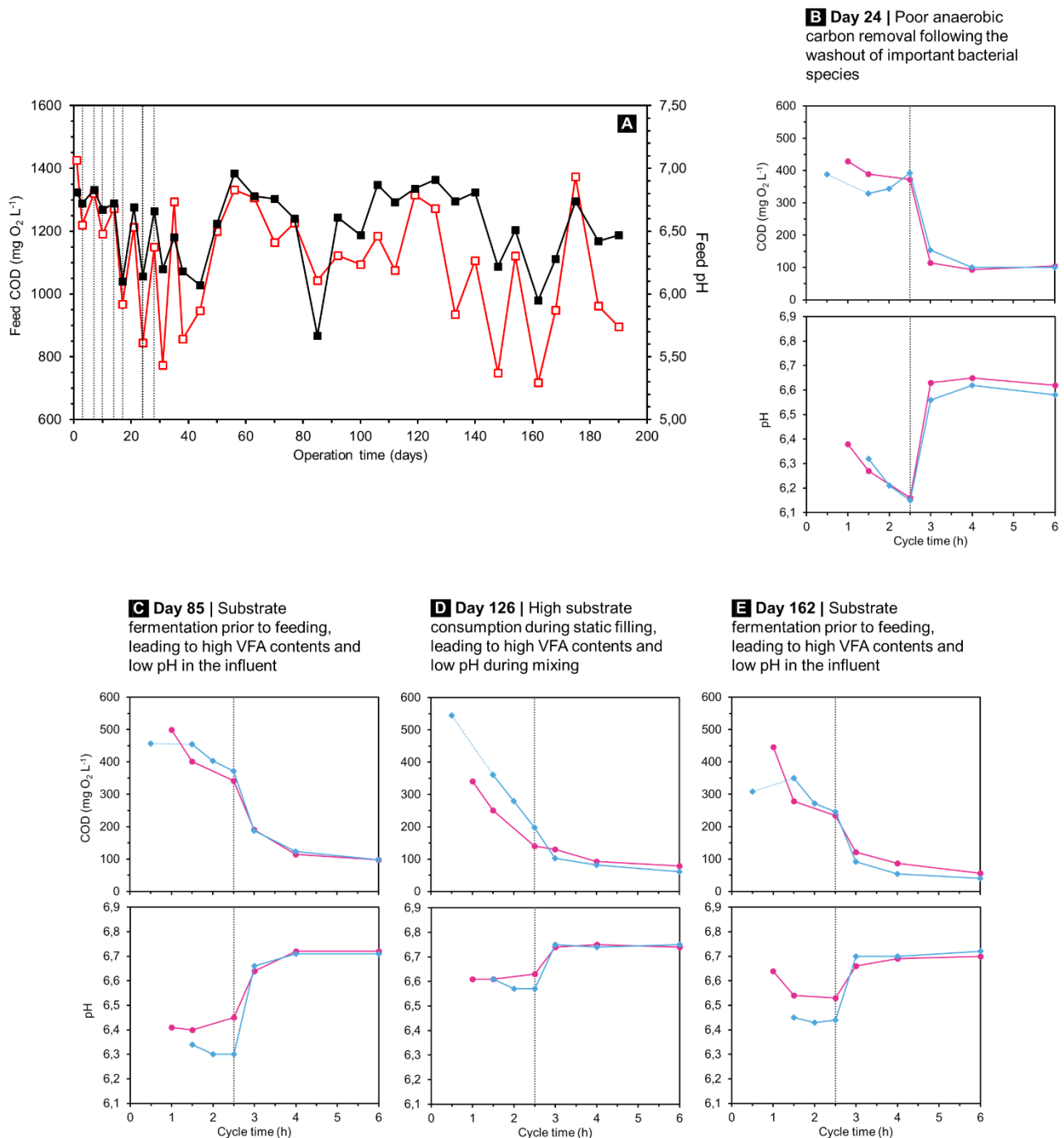


Figure 3.8 | Physicochemical feed characteristics along the operational run and COD conversion and pH variation curves along the reaction phase of selected representative cycles. (A) COD concentrations (\square) and pH levels (\blacksquare) of the feed solution. (B–E) Profiles for SBR1 (\bullet) and SBR2 (\blacklozenge) on (B) day 24, (C) day 85, (D) day 126, and (E) day 162. The zero coordinate of the cycle time axis is regarded as the end of the reaction stage of the previous cycle; theoretical initial COD concentrations for SBR2 are plotted on the time coordinate where bioreactor filling was initiated and connected to the first direct measurement by a blue dotted line. Vertical dotted lines denote the onset of aeration.

Following the washout event of day 85, anaerobic COD removal in the bioreactors further improved, providing for minimal residual concentrations at the onset of aeration on day 126 (140 and 198 mg O₂ L⁻¹ in SBR1 and SBR2, respectively). Unlike the previously registered increases in An_{COD}, these observations follow a period of high EVSS concentration and low sludge retention times (Figure 3.5), indicating that the relevant microbial activities could be maintained in the SBR systems in association with fast-settling granular structures. As previously mentioned, the initial COD concentrations in SBR1 fell significantly short of the predicted reference values in SBR2 between days 119 and 126, suggesting that relevant levels of carbon removal took place under anaerobic conditions during the contact of the feed solution with the sludge bed over the 30-minute feeding period. In agreement with these results, pH profiles plotted for SBR1 during this cycle (Figure 3.8D) are characterized by an initial plateau that advocates the presence of VFA from the onset of the anaerobic reaction. Unlike the previous cases, these observations are not obviously related to any meaningful drop in the pH level of the feed solution (Figure 3.8A) and therefore refute the influence of organic matter degradation before treatment. Interestingly, a slight drop in pH – which could be associated to the fermentation of residual saccharides in the feed solution – was observed on the same day during the first half hour of mixing in SBR2. This feature was present, however slightly, in the vast majority of the pH curves plotted throughout the operational run regardless of the characteristics of the influent wastewater, and could indicate that the VFA produced during the plug-flow rise were largely assimilated by the biomass, providing a margin for further acidification as soon as stirring was initiated and increased substrate mass transport could ensure faster production and accumulation of VFA in the mixed liquor. During this particular cycle, however, the range of sampled pH values – demonstrably narrower than those of other batches – might be regarded as evidence of a tight equilibrium between the production and consumption of VFA not just in SBR2 but also in SBR1.

From day 126 on, the previously described reductions in the influent organic load resulted (especially in SBR2) in violently oscillating anaerobic removal yields that reflect the attendant changes in the initial COD concentration (Figure 3.7B). The COD levels assayed at the end of the mixed anaerobic stage remained generally constant throughout the first few weeks (up until day 162), responding only slightly to shifts in organic loading and suggesting that no significant changes in the limits of anaerobic conversion were produced. During the final four weeks (days 168–190), average An_{COD} reached 47 and 41% in SBR1 and SBR2 (respectively), falling slightly from the maxima registered on day 126 as a consequence of significant biomass washout in process effluents throughout the final two months of operation (Figure 3.5A).

3.2.2 Colour removal and aromatic amine conversion

The influence of feeding strategy over colour removal and the decolourisation performance of the bioreactors

The colour removal performance of the bioreactors was evaluated in terms of equivalent Acid Red 14 concentrations, AR14_{eq.}, throughout the reaction stage by assessing the absorbance of the collected mixed liquor samples at 515 nm (the wavelength of maximum absorption for the dye). Much to the

similarity of the analysis into COD removal, initial colour levels in SBR2 (ThSBR2) were estimated from individual $AR_{14eq.}$ values obtained for the feed solution and for the leftover effluent in the bioreactor, and are summarized in Figure 3.9A; equivalent AR_{14} contents assayed at the onset of the reaction stage in both systems (MixSBR1 and MixSBR2) and on the feed solution are also provided. To validate the best initial conditions to assume in each bioreactor, two box plots charting the differences between ThSBR2, MixSBR2 and MixSBR1 are additionally represented in Figure 3.9B.

In analysing these differences, two important conclusions arise. On the one hand, $AR_{14eq.}$ levels registered in SBR2 after feeding proved much lower than those recorded in SBR1, once again validating

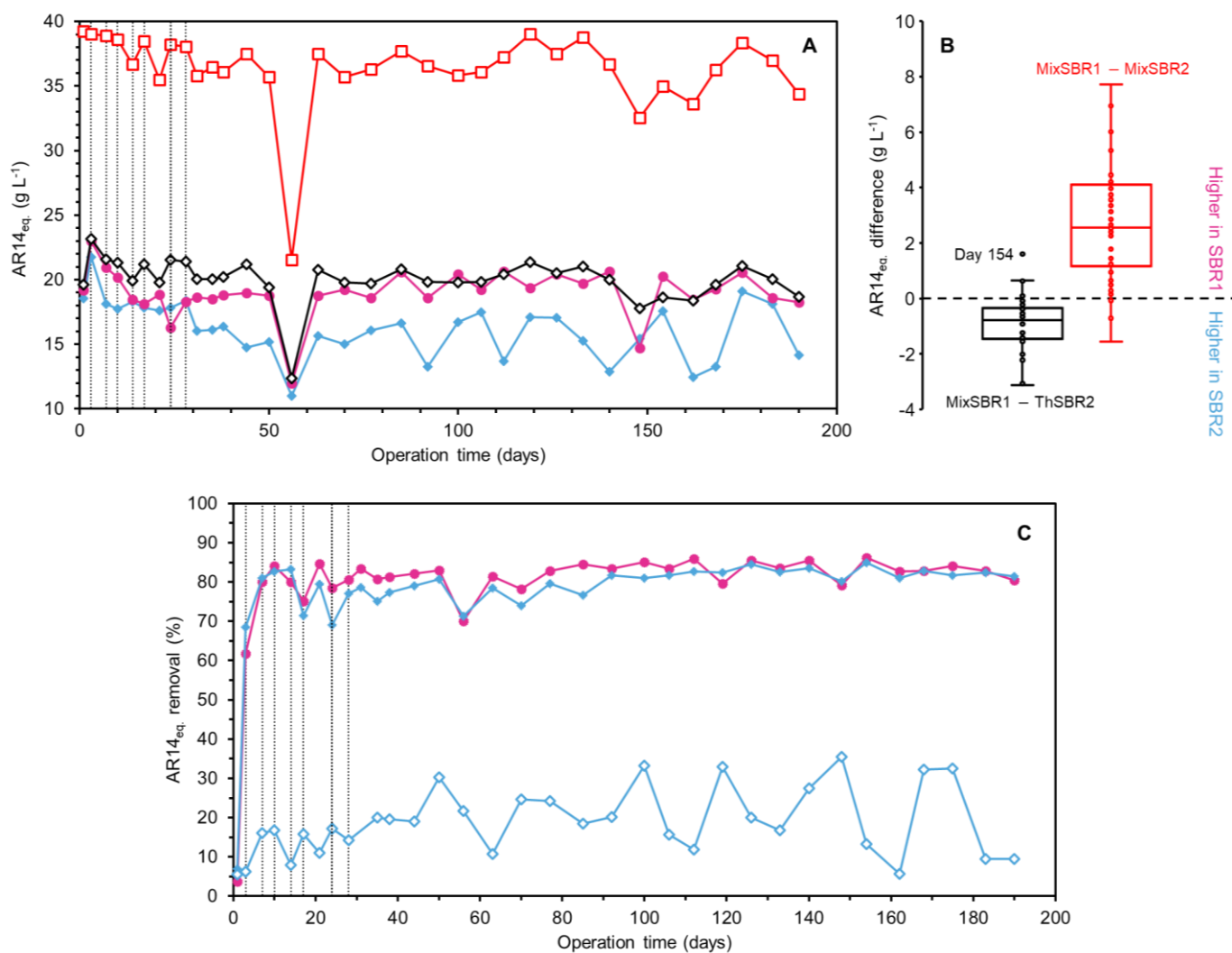


Figure 3.9 | Colour loading (measured as equivalent AR_{14} concentrations, $AR_{14eq.}$) and colour removal performance along the experimental run. (A) Influent colour loads (\square), theoretical initial $AR_{14eq.}$ in SBR2 (ThSBR2, \diamond), and $AR_{14eq.}$ contents at the onset of the mixed anaerobic stage in SBR1 (MixSBR1, \bullet) and SBR2 (MixSBR2, \blacklozenge). (B) Box plots of relative differences between the reference colour concentrations assumed in each bioreactor (MixSBR1 - ThSBR2, $-$) and between $AR_{14eq.}$ contents measured at the same process coordinate (MixSBR1 - MixSBR2, $-$). Whisker ends were defined in accordance with Tukey's test, i.e., capped at the lowest and highest observations within 1.5 interquartile ranges of the 1st and 3rd quartiles, respectively; all data points lying beyond the whiskers were regarded as outliers and tagged with the corresponding operation day. (C) Overall colour removal yields in SBR1 (\bullet) and SBR2 (\blacklozenge) and percent reduction in $AR_{14eq.}$ during the plug-flow feeding stage of SBR2 (\diamond). Vertical dotted lines on the left-hand side denote the days where step reductions in settling time were applied.

the superior position of the filling arrangement imposed in the former system when evaluating bioremediation efficiency. On the other hand, unlike the case described during COD removal analysis, local gaps between ThSBR2 and MixSBR1 seemed to give the upper hand to SBR2 on a consistent basis, striking a median absolute difference of 0.79 g L^{-1} and deviating in the opposite direction in less than 10% of all monitored cycles. This relative placement suggests that some residual AR14 removal took place during the static, 30-minute contact between the influent solution and the sludge blanket, and casts some doubt over the comparability of conversion yields measured against a reference point placed after the feeding phase. The extent of these differences can, however, be deemed negligible in the vast majority of cases – amounting to less than 10% of the nominal initial AR14_{eq} level in the bioreactors (20 g L^{-1}) – and should produce only slight underestimations. In light of these considerations, overall colour removal yields in SBR1 were computed against the AR14_{eq} levels assayed at the onset of mixing, whereas those of SBR2 were compared with the theoretical initial colour content. The obtained results are plotted on Figure 3.9C along with the fraction of the overall yield removed during the plug-flow feeding stage of SBR2.

As depicted, AR14 conversion during filling in SBR2 varied from a minimum of 5.6% on day 1 to a maximum of 35% on day 140 with significant oscillations along the experimental run that occurred randomly and according to no obvious relation with the remaining shifts in sludge properties. These results are once again easy to perceive as the direct consequence of an imperfect plug flow forming channels across the sludge bed and causing the effective sludge/influent contact time to vary from cycle to cycle.

Outside the filling phase, the resident sludge community in the bioreactors appeared to adapt rapidly to the synthetic textile effluent, providing AR14 removal levels of 80% after only 7 days of operation. During the initial step reductions in settling time, colour removal yields suffered isolated drops in SBR1 (days 14, 17 and 24) and SBR2 (days 17 and 24) following discrete washout episodes that likely resulted in the removal of bacterial species with an azoreductase activity. From day 28 onwards, however, removal yields stabilized in the 74–86% range. These levels are similar to those from previous studies conducted in silver-free AGS systems treating synthetic textile wastewaters with identical compositions (Franca *et al.*, 2015; Lourenço *et al.*, 2015) and suggest the continuous feeding of Ag NPs had no relevant impact over decolourisation performance. The multiple washout episodes registered throughout the operation also seemed to produce no meaningful changes in AR14 removal, signalling the upkeep of a high azo dye-degrading capacity independently from sludge age restrictions; this can be attributed to the prime sludge retention capacity of the AGS SBR systems, which was able to ensure sufficient biomass concentrations to tackle the influent colour loading.

The decrease in the overall colour removal yields observed on day 56 (to 75 and 72% in SBR1 and SBR2, respectively) – largely related to an error in the preparation of the feed solution that resulted in a reduced colour loading (Figure 3.19A) – represents the only significant deviation from the steady-state decolourisation conditions attained in the SBR systems and might be regarded as evidence of a direct correlation between colour removal efficiency and the initial dye concentration in the mixed liquor (*i.e.*, possibly first-order kinetics). This topic will be further explored in the following section.

Considerations on decolourisation kinetics

In order to analyse the kinetics of decolourisation during feeding and anaerobic mixing, colour removal profiles were plotted from the $AR_{14eq.}$ levels assayed along each cycle. Figure 3.10 depicts the progress of colour removal during the cycle of day 100 as a representative example of SBR performance throughout most of the experimental run. One relevant exception to the provided example was identified on day 1 during bioreactor start-up and will be briefly discussed further ahead.

As depicted in Figure 3.10, colour removal occurred mainly during the 1.5- or 1-hour mixed anaerobic stages (in SBR1 and SBR2, respectively) according to a dye concentration-dependent kinetics, with the highest percent reduction in $AR_{14eq.}$ levels registered during the first half hour of stirring. As previously stated, partial decolourisation yields during the plug-flow feeding stage of SBR2 varied sharply throughout the entire experimental run, but were invariably lower than those obtained after the onset of mixing. These results demonstrate a positive relation between the application of stirring and the decolourisation rate that might be attributed to increased fluid turbulence and to an attendant increment in dye mass transfer rates inside biomass flocs and aerobic granules. In light of these conclusions, the combination of a plug-flow feeding regime with a shorter anaerobic mixing period in SBR2 might be regarded as the main reason for the generally higher residual $AR_{14eq.}$ contents attained in the bioreactor when compared to those of SBR1 (as displayed in Figure 3.10) – even though relevant contributions to colour removal could be traced to the filling stage, the time period allotted to the mixed reaction phase was insufficient to ensure colour removal up to comparable levels in both SBRs. Interestingly, the use of a higher stirring speed in SBR2 seemed to have no power to rescue this situation. This detail suggests that the decolourisation process was under kinetic control in both bioreactors during the mixed anaerobic stage regardless of the governing hydrodynamic conditions and restricts the possible occurrence of diffusional control to the static setting of the feeding stage.

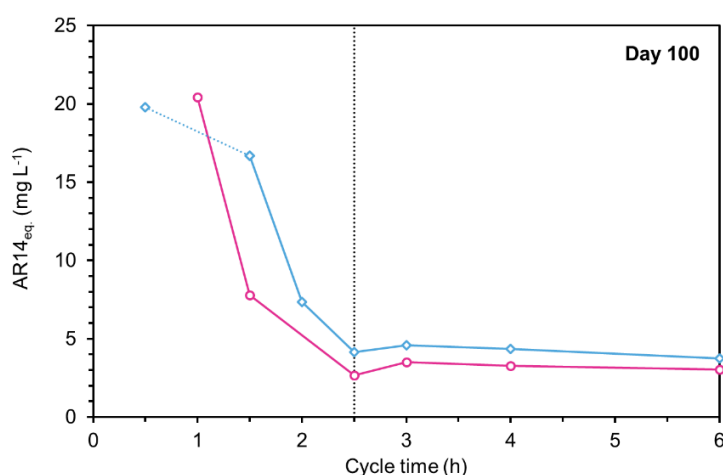


Figure 3.10 | Colour removal profiles along the reaction phase of a selected representative cycle. Profiles for SBR1 (○) and SBR2 (◇) on day 100. The zero coordinate of the cycle time axis is regarded as the end of the reaction stage of the previous cycle; theoretical initial $AR_{14eq.}$ levels for SBR2 are plotted on the time coordinate where bioreactor filling was initiated and connected to the first direct measurement by a blue dotted line. The vertical dotted line denotes the onset of aeration.

The formation and conversion of aromatic amines

Validation of the mechanism of colour removal was based on UV-visible absorption spectra plotted for collected mixed liquor samples and confronted with reference curves obtained for standard solutions of AR14 and of its aromatic amine moiety 4-amino-naphthalene-1-sulphonic acid (4A1NS; Figure 3.11). The second arylamine molecule produced during the reductive cleavage of Acid Red 14 – 1-naphthol-2-amino-4-sulphonic acid (1N2A4S; Figure 3.11) – is unavailable in standard form and could therefore not be used for independent spectrophotometric measurements. Figure 3.12 provides a comparison between the spectra of the existing standard solutions and that of the synthetic textile wastewater, together with a collection of spectral data gathered in selected cycles (*i*) at the onset of mixing, (*ii*) at the onset of aeration, and (*iii*) at the end of the reaction stage. All spectra were arbitrarily chosen to characterise the behaviour of SBR1 and are provided merely by way of illustrative example. Conclusions about the progress of colour removal and aromatic amine degradation drawn hereinafter are applicable to both bioreactors even when associated with specific periods of the operational run.

As depicted, besides the sharp peak around 515 nm, the absorption spectrum of aqueous Acid Red 14 solutions displays one discreet peak at 215 nm and a region of complex structuration between 260 and 350 nm that are conserved without any relevant changes in the spectrum of the feed solution. These data suggest that the presence of other components in the synthetic textile effluent contributes in a negligible manner to its optical properties in the UV-visible range and validates the analysis of spectral information as a practical method for tracking dye degradation during treatment.

Given the structural similarity with the intact dye molecule, the aromatic moiety 4A1NS retains one narrow absorption band centred around 218 nm (Figure 3.12A) that largely overlaps with the features of AR14 in the same region, but additionally displays a number of distinctive structures of its own – including a small peak at 238 nm, matched by a narrow shoulder in the spectrum of aqueous dye standards, and a defined, broad band with a maximum at 318 nm (Figure 3.12A), as opposed to a wide range of mixed absorption modes. The combination of these three features can thus be used to provide invaluable information regarding the accumulation of 4A1NS in the mixed liquor. Seeing as the amine molecule does not absorb visible light (Figure 3.12A), qualitative comparisons of absorbance measurements collected around these wavelengths can be backchecked against the patterns of light absorption by mixed liquor samples in the visible range to validate the process of dye reduction as the main decolourisation mechanism.

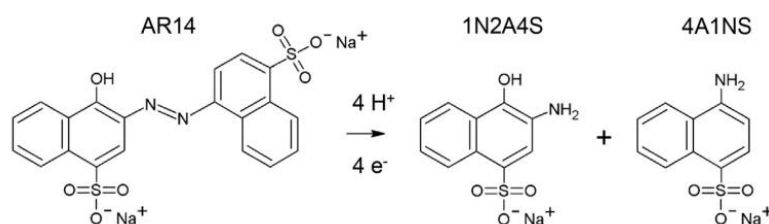


Figure 3.11 | Chemical structures of the azo dye Acid Red 14 and of the two aromatic amines formed during the azo bond reduction reaction. AR14 – Acid Red 14; 1N2A4S – 1-naphthol-2-amino-4-sulfonic acid; 4A1NS – 4-amino-naphthalene-1-sulfonic acid (after Franca *et al.*, 2015)

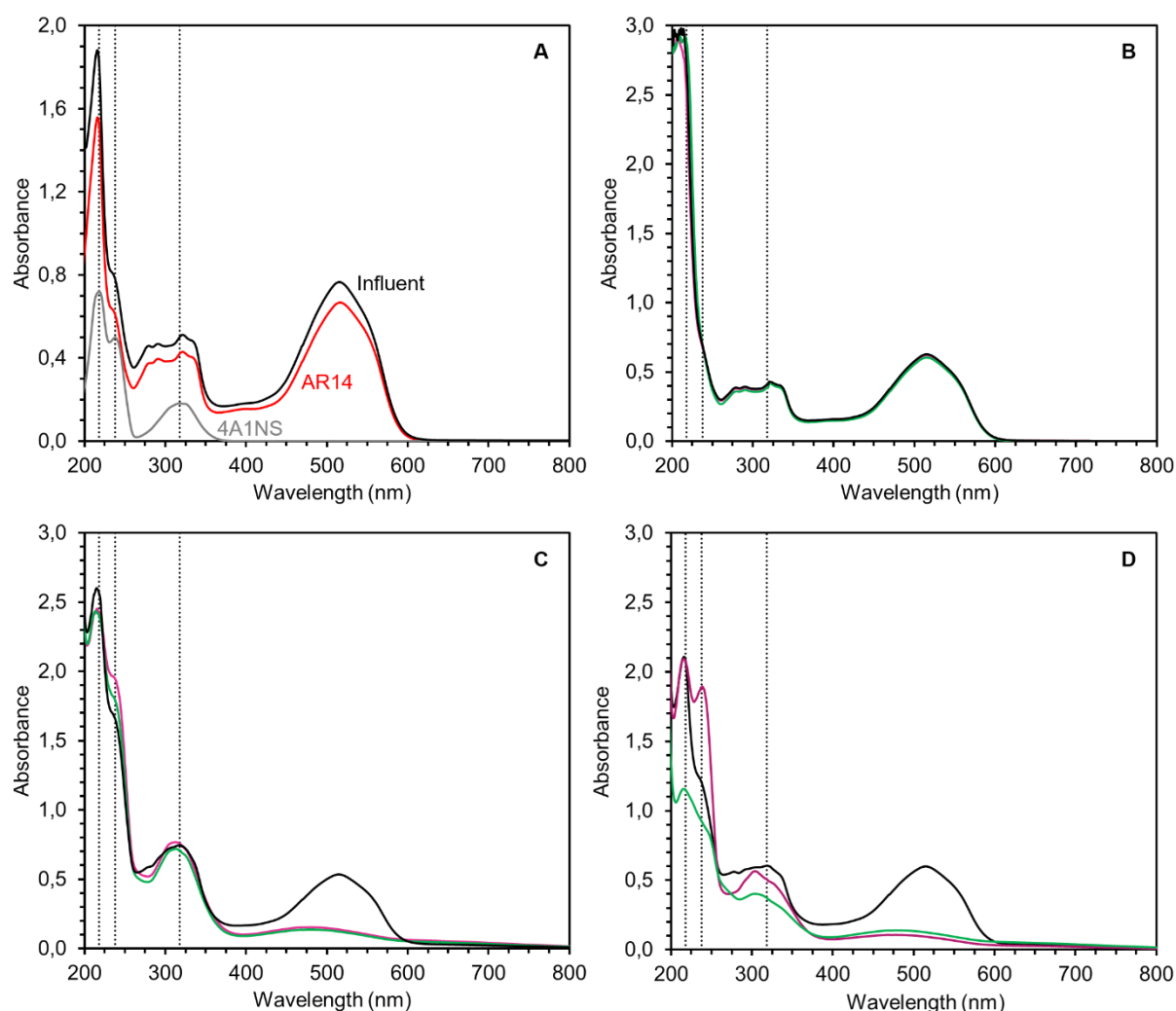


Figure 3.12 | UV-visible spectra for the analysis of colour removal and aromatic amine conversion. (A) UV-visible spectra of the influent feed solution used on day 63 (diluted 1:1) and of AR14 (15 mg L⁻¹) and 4A1NS (7.3 mg L⁻¹) standard solutions. (B)–(D) UV-visible spectra of mixed liquor samples collected from SBR1 at the onset of mixing (—), at the onset of aeration (—), and at the end of the reaction stage (—) during the representative cycles of (B) day 1, (C) day 24, and (D) day 190. Vertical dotted lines on the left-hand side represent the wavelengths of peak absorption of the aromatic amine 4A1NS, namely 218, 238, and 318 nm.

As illustrated in Figure 3.12C,D, colour removal on days 24 and 190 – as well as throughout most of the operation time – occurred primarily during the mixed anaerobic stage, resulting in increased absorbances at 238 nm and in the definition of a clear peak between 300 and 318 nm that points to the production and accumulation of 4A1NS. Conversely, UV-visible spectra collected during day 1 retained their main features unchanged throughout the entire reaction stage (Figure 3.12B), suggesting that whatever residual colour removal could be achieved during this cycle (3.7 and 7.0% in SBR1 and SBR2, respectively) was most likely mediated by adsorption of dye molecules onto the biomass.

In those batches where reductive decolourisation took place, the wavelength of maximum absorption in the visible range suffered a violet shift from 515 nm to 486 nm that was noticeable by the end of the anaerobic reaction and was maintained throughout the entire aeration period. This shift signals the accumulation of secondary coloured substances produced during treatment in the mixed liquor and might be related to the auto-oxidation of the unstable amine 1N2A4S in aerobic conditions (whether in

the bioreactor or, in those cases where samples from the anaerobic stage are concerned, during sample handling) – especially likely owing to the presence of a hydroxyl function in the *ortho*- position relative to the amino group (Kudlich *et al.*, 1999; Franca *et al.*, 2015). In keeping with this hypothesis, absorbances around 486 nm suffered slight increments in most sampled cycles following the transition from anaerobic to aerobic conditions (as represented in Figure 3.12D). In most cases, these increments resulted in increased equivalent AR14 contents (*i.e.*, increased colour) in the mixed liquor that subsisted with only marginal recoveries throughout the entire aeration period, suggesting that the accumulated coloured substances are difficult to degrade in aerobic conditions.

In spite of these setbacks, samples collected at the end of aeration generally displayed reduced absorption around the characteristic wavelengths of 4A1NS (218, 238, and 318 nm) when compared to the results obtained at the end of the anaerobic mixing stage (Figure 3.12C,D). Seeing as light absorption in the visible range – and thus the concentration of coloured substances – remained fairly constant along the aerated period, these results suggest a decrease in the concentration of the aromatic amine in the mixed liquor under aerobic conditions and could signal the establishment of a population with a 4A1NS-degrading activity. The difference in absorption between the onset and the end of aeration varied, however, from slight (Figure 3.12C) to large gaps (Figure 3.12D) that advocate the occurrence of dynamic shifts in the capacity for aromatic amine degradation throughout the experimental run. In order to aid in the identification of these shifts, percent reductions in mixed liquor absorbance (Abs) – as measured at 218, 238, and 318 nm – registered during the aerated phase were calculated along the experimental run and defined as reporter variables for the quantification of amine removal. The obtained results are represented in Figure 3.13.

As depicted, even though the observed trends for Abs₂₁₈ and Abs₂₃₈ suggest a progressive improvement in the capacity for aromatic amine removal throughout the first 50 days of operation, little changes in the absorption of the relevant wavelengths could be detected during the aerated reaction phase in either bioreactor along the same period. In a clear demonstration of the heterogeneous chemical composition and light absorption properties of the mixed liquor, significant divergences in the calculated percent reductions could be detected among the chosen reporter wavelengths, not only along this initial period but throughout the entire operation time. Light absorption in the near UV range during the aerated phase should reflect the additive contributions of both the accumulated products of dye reduction and whatever uncharacterised coloured substances are present in the bioreactor at the time. Seeing as no individual spectral features or quantitative compensations can be obtained for the latter, the defined percent reductions can be interpreted only as semi-quantitative devices that allow for the comparison between amine removal in different stages of the experimental run and not as definitive performance metrics. Even though different structuration at different incident wavelengths will invariably result in divergent values for each reporter variable, temporal trends should reflect the general variations in the capacity for arylamine degradation and remain conserved in all cases.

In agreement with these observations, aerobic percent reductions in the absorbances at 218, 238, and 318 nm underwent sharp simultaneous increases in both SBR1 (by 26, 26, and 21% respectively) and SBR2 (by 31, 31, and 17% respectively) between days 50 and 56, signalling the proliferation of bacterial

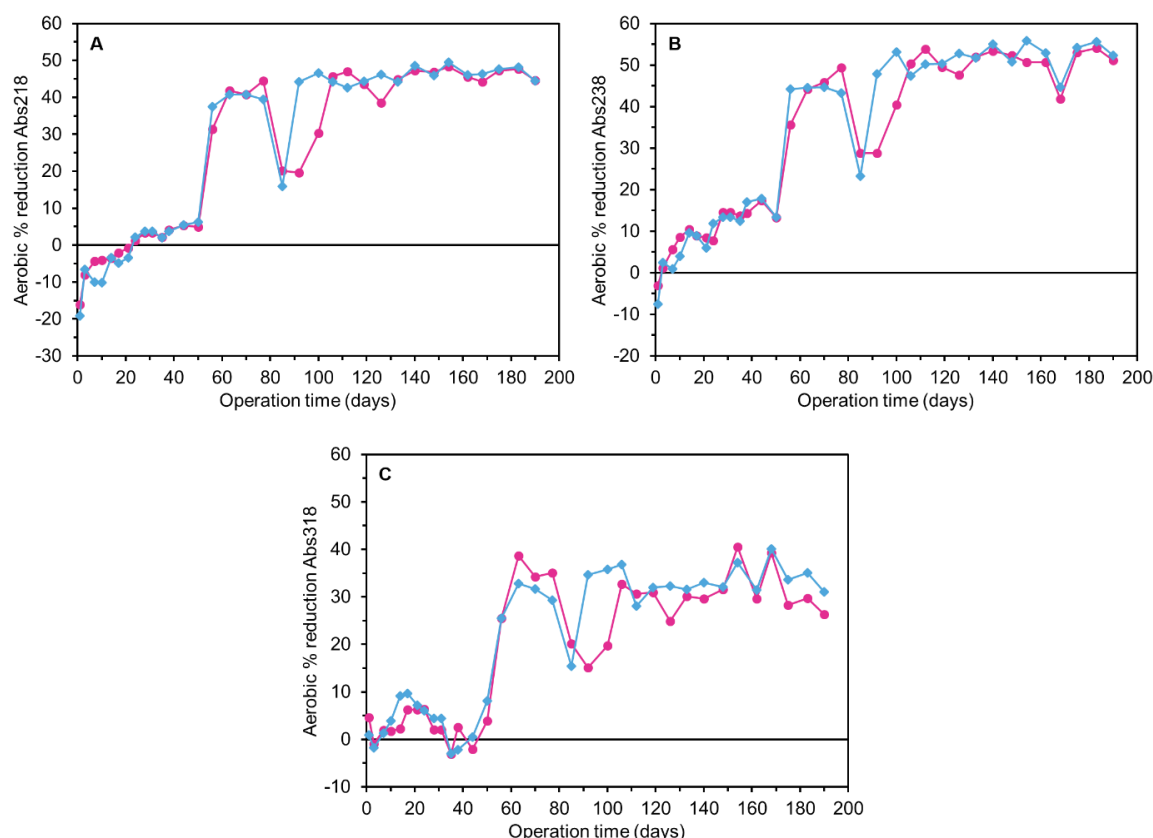


Figure 3.13 | Probing the aerobic degradation of aromatic amines along the experimental run in terms of near UV absorbance. Percent reduction in mixed liquor absorbance at (A) 218 nm, (B) 238 nm, and (C) 318 nm during the aerobic reaction period of SBR1 (●) and SBR2 (◆)

species with a capacity to metabolise 4A1NS. This result can be correlated with the progressive increase in sludge age observed along the first 70 days of operation (Clara *et al.*, 2005; Franca *et al.*, 2015; Lourenço *et al.*, 2015) and might suggest that the development of an arylamine-degrading activity in the sludge community is intimately associated with slow-growing bacterial strains or with a selective effect brought about by the prolonged exposure to aromatic amines. While positive, in endorsing the benefits of high sludge ages these results emerge as a problematic blow to previous considerations on the use of short SRTs to abate the destabilizing effects of Ag NP accumulation in the sludge. Further studies investigating whether an adequate balance between structural stability and aromatic amine degradation can be reached in Ag NP-fed systems are therefore required.

Following the marked decrease in biomass concentration registered between days 77 and 85, aerobic percent reductions in UV absorption once again dropped to lower levels in both systems, signalling a loss of bacterial species with relevant activities for the conversion of 4A1NS and further backing the hypothesis of SRT mediation. Interestingly, despite this localized episode, all three reporter variables maintained – even at their lowest (between days 85 and 92; Figure 3.13) – levels above those of the initial 50 days. Moreover, a previous washout event registered in SBR1 on day 70 (Figure 3.5A) did not seem to produce any discernible impact on the relative efficiency of amine removal. These results suggest that amine-degrading activities were established – at least partially – in association with fast-settling sludge particles (e.g., AGs) that were easily retained in the bioreactor – even when VSS concentrations in the effluent reached excessive levels – and could thus be maintained in the long run.

From this point on, all three reporter variables rapidly climbed back to the levels attained before the washout event and remained approximately constant throughout the remaining operation time – showing an ability to maintain the aerobic aromatic amine degrading activity even in the long term. Measurements from all three wavelengths seem to point to a slight drop in the amine removal performance of SBR1 on day 126 that could once more be interpreted as a result of the high EVSS concentrations registered around the same period (Figure 3.5). Besides this finding, however, no other consensual conclusions can be drawn for the final 80 days of operation.

3.3 AHL-based quorum sensing analysis

3.3.1 Development of the AHL bioassay and reference calibration curve

As previously described in 2.5.4, the applied AHL bioassay relied on the *N*-acyl-L-homoserine lactone (AHL)-mediated induction of β -galactosidase (β -gal) synthesis in cells of biosensor *Agrobacterium tumefaciens* NTL4(pZLR4) and on the subsequent assay of β -gal activities with the chromogenic substrate X-gal. Enzyme activity assays were based on spectrophotometric measurements performed at two different wavelengths on late exponential growth bacterial cultures containing whole biosensor cells and the insoluble blue pigment 5,5'-dibromo-4,4'-dichloro-indigo (produced as a result of X-gal hydrolysis) (Tang *et al.*, 2013). Working wavelengths were selected from the absorption spectrum of a pure indigo suspension in spent AT minimal medium (as depicted in Figure 3.14) to represent the regions of maximum and minimum absorption in the visible range. The final choice fell on spectral zones of low local first derivatives represented by two minima at 504 and 629 nm (Figure 3.14).

Optical densities of biosensor cultures were determined for each of the chosen wavelengths so as to isolate the absorptive contributions of indigo and biosensor cells and allow for the definition of cell density-normalized β -gal activities – equation (2.10). Calculations of normalized β -gal activities were performed using two correction factors, α and γ , defined as the ratio of absorbances at 504 and 629 nm in aqueous suspensions containing only one of the two absorbers. The values of the correction factors were obtained via linear regression of the optical densities of indigo and biosensor cells at different concentrations as depicted in Figure 3.15 (Tang *et al.*, 2013). When plotting OD504 against OD629 for indigo suspensions, or OD629 against OD504 for *A. tumefaciens* NTL4(pZLR4) suspensions, clear linear relations explained by coefficients of determination in excess of 0.99 were obtained. Using the slopes of the final regression lines, α and γ were defined at 0.679 and 0.161, respectively, and the formula for the calculation of normalized β -gal activities was rewritten as:

$$\text{Normalized } \beta\text{-gal activity} = \frac{0.679 \cdot \text{OD}_{504} - \text{OD}_{629}}{0.679 \cdot (0.161 \cdot \text{OD}_{629} - \text{OD}_{504})}, \quad (3.1)$$

where the listed optical densities represent the spectrophotometric measurements obtained after the bioassay.

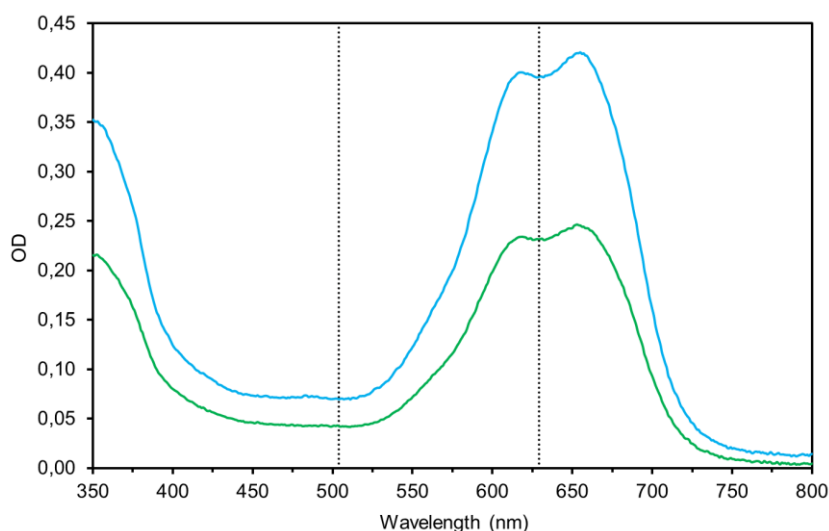


Figure 3.14 | UV-visible absorption spectrum of indigo in spent AT minimal medium. Spectral data are provided for two different (unknown) concentrations of 5,5'-dibromo-4,4'-dichloro-indigo (in blue and green); optical densities were measured against a distilled water blank. Vertical dotted lines denote the representative wavelengths chosen for the regions of maximum and minimum absorption, namely 504 and 629 nm.

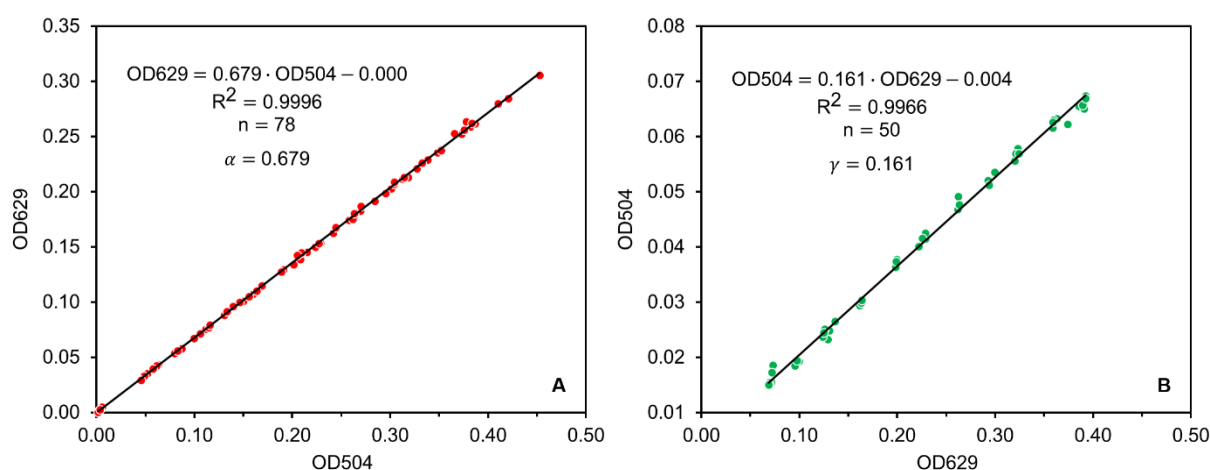


Figure 3.15 | Correction factors α and γ . OD504 and OD629 were measured in serially diluted suspensions of (A) biosensor cells and (B) 5,5'-dibromo-4,4'-dichloro-indigo against a distilled water blank. The slopes of the regression lines are the values of the correction factors (A) α and (B) γ of equation (2.10). The number of independent measurements (n) is displayed in each of the scatter plots.

The calculated activity levels were subsequently converted to equivalent 3OC12-HSL concentrations using a pre-established calibration curve so as to clearly document the AHL contents of the tested samples. The calibration curve was plotted by calculating the normalized β -gal activities elicited in response to increasing concentrations (in the 0–10 nM range) of the long-chain AHL *N*-3-oxo-dodecanoyl-homoserine lactone and is represented in Figure 3.16. As depicted, under the applied bacterial growth and enzyme assay conditions, the normalized β -gal activities increased in direct proportion to 3OC12-HSL concentration up to around 2 nM and saturated quickly between 2 and 5 nM. The reference calibration curve was derived using second-degree polynomial regression analysis in the 0–3 nM interval in order to capture as wide a range of β -gal activity levels as possible without significantly compromising the accuracy of equivalent 3OC12-HSL content estimates. Whenever the

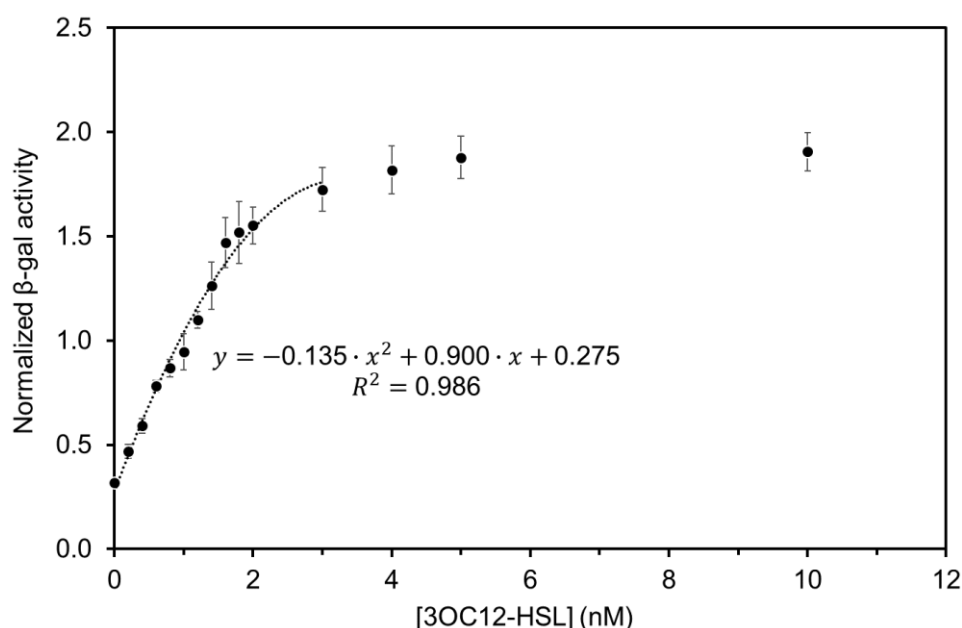


Figure 3.16 | Calibration curve for the conversion of normalized β -gal activities into equivalent 3OC12-HSL concentrations. Variation of normalized β -gal activities obtained after exposure to 0–10 nM of 3OC12-HSL. Overnight seed cultures of biosensor *A. tumefaciens* NTL4(pZLR4) were diluted to an OD600 of 0.02, supplemented with $250 \mu\text{g mL}^{-1}$ of X-gal, and mixed with $15 \mu\text{L}$ of the reference AHL solution to produce a final culture volume of $250 \mu\text{L}$. Biosensor cells were grown for 16–18 hours at 28°C before optical density measurements were performed at 504 and 629 nm to compute normalized β -gal activities. Data are presented as the mean \pm SEM of four independent replicates. 2nd-degree polynomial regression analysis was performed in the 0–3 nM range to obtain the reference calibration curve (dotted line); y – normalized β -gal activity; x – [3OC12-HSL].

normalized β -gal activities of the tested samples exceeded this range, the bioassay was repeated with sequential dilutions until a serviceable result was obtained. The final value was subsequently translated into an equivalent 3OC12-HSL concentration by factoring in the dilution ratio.

3.3.2 Equivalent 3OC12-HSL concentration profiles

In order to assess the influence of AHL-mediated quorum sensing in the formation and maintenance of aerobic granules in SBR1 and SBR2, *N*-acyl-L-homoserine lactone levels were assayed in sludge extracts collected along the experimental run using the procedure described above. AHL contents were evaluated in terms of the equivalent 3OC12-HSL concentration required to produce an equal normalized β -gal activity and subsequently corrected for sample biomass. The final results are expressed as 3OC12-HSL nmol-equivalents per milligram of volatile suspended solids, 3OC12-HSL_{eq.}, in Figure 3.17; significant differences between the levels examined in each bioreactor, as inspected by multiple unpaired *t*-tests, are marked with an asterisk. In the interest of clarity, adjusted *p*-values obtained for direct comparisons between the two SBR systems will hereinafter be represented by the symbol p_t . Results of the ANOVA performed individually for each bioreactor to track the evolution of AHL concentrations along the operation will similarly be backed, whenever relevant, by the corresponding *p*-values using the symbol p_A .

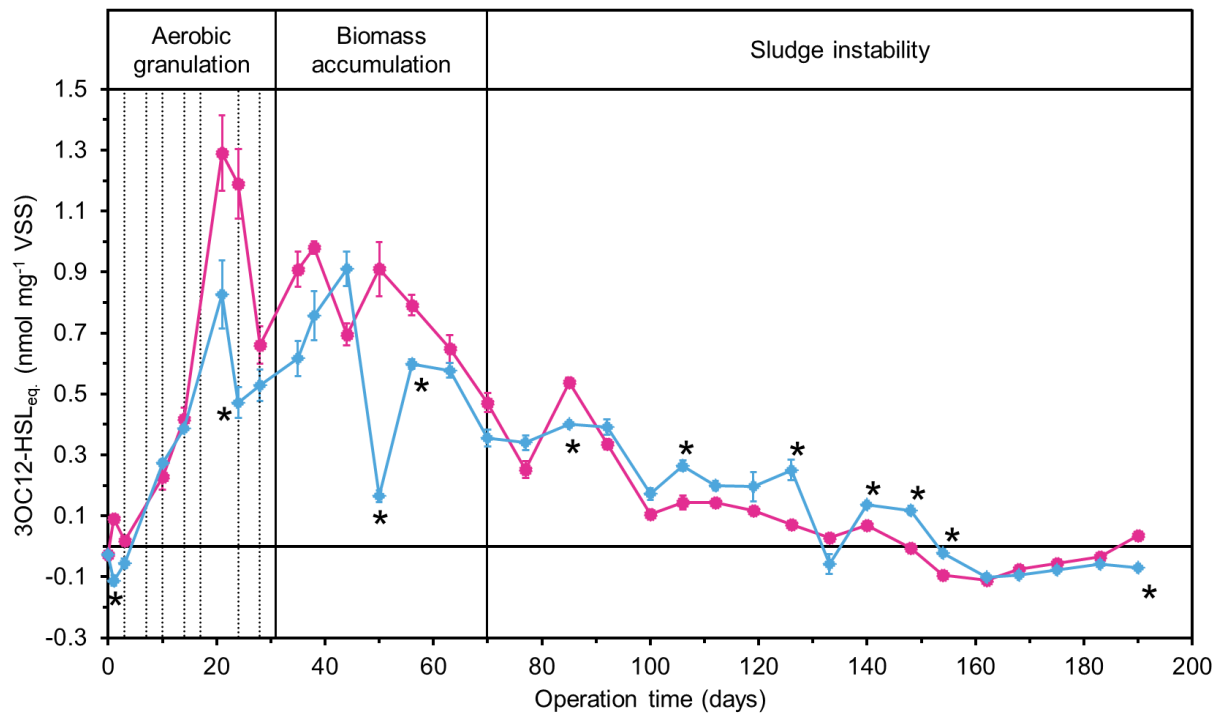


Figure 3.17 | Equivalent 3OC12-HSL concentrations, 3OC12-HSL_{eq}, in cell-free AGS extracts collected along the experimental run. Variations in AHL levels – expressed in terms of the reference 3OC12-HSL – in SBR1 (●) and SBR2 (◆). The data were normalized to the respective sample biomass and are presented as the mean \pm SEM of five or six independent replicates (cf. 2.5.4). Unpaired *t*-tests were conducted individually for every sampled day in order to compare the 3OC12-HSL_{eq} levels in each bioreactor. Significant differences ($p < 0.05$) are indicated by an asterisk next to the corresponding point in the profile of SBR2. Vertical dotted lines on the left-hand side denote the days when step reductions in settling time were applied.

Before drawing any conclusions, it should be stressed that the documented 3OC12-HSL_{eq} profiles were used more as a reference to describe the relative differences in the AHL levels assayed at different time points than as absolute representations of bioreactor behaviour. In fact, significant limitations to the quantitative power of the AHL bioassay were imposed by the physiological state of the biosensor culture when direct analyses on sludge extracts were initiated. Such limitations are best illustrated by the negative 3OC12-HSL_{eq} values assayed in samples collected towards the end of the operation (from day 156 on) as a consequence of a sub-blank synthesis of β -galactosidase. These results reflect fundamental differences in the metabolic activity of biosensor cells between the moment the reference calibration curve was obtained and the moment normalized β -gal activity levels were determined for the sludge extracts, which could derive from a lengthy storage period (roughly 4 weeks) during which the cells were not re-plated. In order to avoid similar discrepancies, future studies employing the AHL bioassay described herein should ensure continuous renovation of the storage medium and provide periodic confirmations of normalized β -gal activities for blank solutions and selected 3OC12-HSL concentrations as a means of validation for the reference calibration curve. Due to time constraints, repetition of the entire experimental routine was not possible. By way of remedial resolution, all collected sludge extracts were analysed in the bioassay setting over the course of two days in order to ensure that no further storage time-related effects were reproduced in the final 3OC12-HSL_{eq} profiles.

Aerobic granulation and bioreactor accumulation phases

Values of 3OC12-HSL_{eq.} were observed to increase rapidly and steeply in the first 21 days of operation from inoculum levels of -0.03 ± 0.02 (SEM) nmol mg⁻¹ VSS to 1.2 ± 0.1 (SEM) and 0.8 ± 0.1 (SEM) nmol mg⁻¹ VSS in SBR1 and SBR2, respectively ($p_A < 0.0001$ for both bioreactors). The observed evolution is consistent with the rapid development of aerobic granules recorded along the same period – as deduced from the size distribution and biomass morphology analyses – and suggests the existence of a direct association between granulation and AHL-based cell-to-cell signalling. These conclusions are consistent with those of previous studies demonstrating clear rises in sludge AHL contents during the early stages of granule development (Jiang & Liu, 2012; Li & Zhu, 2014; Tan *et al.*, 2014) and positive correlations between QS activity and microbial attachment potential (Lv *et al.*, 2014). Interestingly, the rise in 3OC12-HSL_{eq.} values seemed to follow the program of progressively decreasing sedimentation times quite closely, jolting upwards after every reduction. Similar results have been advanced by Tan *et al.* (2014), who found a significant increase in mixed-liquor AHL concentrations after settling times were reduced from 60 to 5 minutes, and by Xiong & Liu (2012) in a comparative study that found shorter settling periods to produce sharper increases in autoinducer-2 (AI-2) contents. The combination of these results suggests a strong positive correlation between sedimentation time and QS signal concentrations and once again underscores the importance of the settling phase in steering aerobic granulation.

The gap registered on day 21 between the 3OC12-HSL_{eq.} levels of the SBR systems ($p_t = 0.3260$) suggests that the high hydrodynamic shear promoted during the mixed anaerobic stage of SBR2 exerted a deleterious effect over AHL quorum sensing during the initial granulation stage and is largely consistent with previous observations regarding the presence of smaller granular fractions and the proliferation of small granules in SBR2. Significant differences between the two bioreactors were additionally found on day 1 ($p_t < 0.0001$) following a slight increase in the 3OC12-HSL_{eq.} levels of SBR1 and a slight decrease in SBR2, which could further support the theory of a shear-related impact over the synthesis of AHLs. Even though these results were not backed by relevant differences in an analysis of variance context (day 0 vs. day 1: $p_A = 0.9842$ and > 0.9999 for SBR1 and SBR2, respectively), the described trend is consistent with the variations in SVI₅ registered during the first day of operation (Figure 3.4) and provides complementary evidence for a relation between AHL-based quorum sensing mechanisms and the evolution of biomass properties during the granulation stage.

After the peak levels of day 21, 3OC12-HSL_{eq.} values dropped by 0.35 nmol mg⁻¹ VSS in SBR2 on day 24 and by 0.63 nmol mg⁻¹ VSS in SBR1 on day 28 ($p_A < 0.0001$ in both cases). These decreases follow two progressive reductions in settling time that could have resulted in the washout of AHL-producing bacterial populations and thus limited the concentration of signal molecules in sludge samples. Conceptual backing for this hypothesis can be found in the work by Tan *et al.* (2014), who reported concurrent variations in AHL content and the abundance of common AG community members with known QS activity. As previously discussed, MLVSS and EVSS measurements performed throughout the final week of settling time reductions (Figure 3.5A) seem to reflect a halt in the accumulation of biomass caused by the discharge of significant sludge volumes, and could thus offer some additional support to this hypothesis.

Despite the localized reduction, however, AHL contents in SBR2 described a rising trend following the definition of settling periods lower than 7 minutes, reaching peak levels of 0.91 ± 0.06 (SEM) nmol mg⁻¹ VSS on day 44 (1.9 times higher than the minimum of day 24; $p_A < 0.0001$). Similar developments were registered in SBR1, with 3OC12-HSL_{eq.} levels increasing by 0.32 nmol mg⁻¹ VSS between days 28 and 38 ($p_A < 0.0001$) to reach a local maximum of 0.98 ± 0.02 (SEM) nmol mg⁻¹ VSS. This evolution coincides with the detection of EPS-rich, light-coloured, round bacterial aggregates in the sludge systems of both bioreactors, and could effectively point to an intimate relationship between AHL-based quorum sensing signalling and the production of high levels of bound extracellular polymeric substances.

Correlations similar to this one have been established in previous studies by numerous authors (Jiang & Liu, 2012; Li & Zhu, 2014; Tan *et al.*, 2014) and suggested to act as one of the effective QS regulation mechanisms behind the process of aerobic granulation (Chen *et al.*, 2018). Bacteria are thought to deploy QS signalling to produce more EPS and improve the embedding matrix for cell attachment, endorsing aggregate growth and consolidation. Rising microbial densities within the aggregate cause signal molecule contents to rise significantly further and generate a snowball effect that simultaneously increases EPS content, attachment potential, cell surface hydrophobicity, granule size and – ultimately, from a system-wide perspective – the granulation grade (Chen *et al.*, 2018). In analysing the results from this work, however, one important fault seems to emerge in this model. While AHL levels and EPS contents could indeed be seen to peak simultaneously between days 21 and 44 (approximately), sludge granularity along the same period seemed to follow the opposite trend, with AG disruption events – likely caused, as previously stated, by the runaway levels of EPS secretion themselves – recorded in both bioreactors. In analysing the full picture, the concept of excessive AHL production – and consequent runaway EPS production – emerges more as a problem than as a positive aspect in the developmental cycle of AGs and could suggest the balance between the three processes – QS regulation, EPS secretion and granulation – is more delicate than thought. Similar conclusions were recently advanced by Liu *et al.* (2017) in a study comparing the progress of granulation in three SBRs augmented with either AHL-producing bacteria, AHL-quenching bacteria or none of the two (control). Despite boasting the highest sludge AHL levels and hosting mostly comparable EPS concentrations to those found in the control, mean granule sizes in the reactor dosed with AHL producers proved the smallest out of the three, hinting once again at some sort of break in the mechanics of QS-regulated granulation. These results endorse further studies that can place a limit on the linearity of this correlation and elaborate on the ways it might hinder granule growth.

In order to clearly differentiate the influence of AHL-based QS on AGS properties during the granulation/ start-up stage and later periods, Pearson correlation coefficients were computed independently for the biomass accumulation phase proper (up to days 38 and 44 in SBR1 and SBR2, respectively) by pairing four different variables (MLTSS, MLVSS, SVI₅, and SVI₃₀) with the observed 3OC12-HSL_{eq.} profiles. Throughout this stage, AHL levels were found to correlate strongly and positively with biomass concentrations in SBR1 ($r > 0.88$, $p = 0.0007$ for pairings with both MLTSS and MLVSS) and SBR2 ($r > 0.96$, $p < 0.0001$ for MLTSS and MLVSS both), and more modestly with sludge volume indexes. In the latter case, correlations between AHL levels and SVI₅ were found to be slightly more meaningful

than those evaluated with the SVI_{30} profiles (r values; SBR1: -0.6475 vs. -0.6071 ; SBR2: -0.8704 vs. -0.8311), suggesting a closer association between the concentration of signal molecules and the development of fast-settling biomass structures (reproduced in smaller SVI_5 values). These findings offer additional support to the theory of a meaningful impact of AHL-based bacterial quorum sensing in the granulation process.

Long-term granule maintenance

The local maximum $3OC12-HSL_{eq.}$ levels recorded around day 40 were observed as a prelude to a period of approximately constant biomass concentrations in the bioreactors (starting on days 44 and 50 in SBR1 and SBR2, respectively; Figure 3.5A) – consistent, as described above, with the respective maximum sludge accumulation thresholds. Throughout this period, AHL levels described a sharp descending drift, falling to below half their peak levels by day 70 ($p_A < 0.0001$ for both SBRs) and effectively reversing the rising trend of previous weeks. While several possible motivations for this evolution can be invoked, regular biomass washout events along the MLVSS plateaus – with significant reductions in AHL-producing bacterial populations – are perhaps the most plausible candidates, backed in principle by the high EVSS levels recorded throughout (especially in SBR1; Figure 3.5A). In its most basic terms, this theory agrees with the idea of a sludge accumulation limit being pushed over the course of several weeks, forcing the bioreactors to level biomass growth and retention capacity with occasional instances of sludge removal. Judging by the steep drop in AHL levels between days 38 and 44 in SBR1 and between days 44 and 50 in SBR2, particularly intense episodes during unmonitored cycles (and thus not reflected by effluent solids measurements) can be specifically expected during these same intervals.

After day 70, $3OC12-HSL_{eq.}$ levels in SBR1 and SBR2 carried on decreasing from their initially high reaches, dropping to absolute minimum values on day 162 ($p_A < 0.0001$ in both systems for comparisons between the two dates). This evolution fared simultaneously with two surges in the proportion of granules in each sludge system (Figure 3.3) and seems to point to a substantive divergence between granule reformation and AHL synthesis during the final leg of the operation. Several common features among the SVI , $MLVSS$, and $3OC12-HSL_{eq.}$ profiles obtained in each bioreactor could, however, be distinguished even along this stage, suggesting that some level of correlation between the two processes was maintained. First, the progressive improvements in sludge settleability recorded in both systems between days 100 and 119 (Figure 3.4) seem to hold some association with two coextensive and relatively stable $3OC12-HSL_{eq.}$ plateaus maintained until some point between days 119 and 126. The subsequent rise in SVI values and decrease in $MLVSS$ concentrations (Figures 3.4 and 3.5A) are, in turn, concurrent with a gradual drop in AHL levels that progressed more or less swiftly in each reactor until past day 156. Finally, simultaneous increases in the granular fractions (Figure 3.3) and $3OC12-HSL_{eq.}$ levels of both SBRs observed during the last 30 days of the experimental run seem to definitely restore the validity of a correlation between the two variables regardless of the operational stage. Given previous considerations on the influence of Ag NP accumulation in driving most of the instability recorded throughout this final leg of the operation, some

association between the antimicrobial action of silver and the recorded drops in AHL during periods of sludge washout could exist. To confirm it, however, further investigations are required.

The main difference between the initial granulation and final instability periods seems, therefore, to reflect almost exclusively in terms of higher or lower average 3OC12-HSL_{eq.} levels that do not significantly impact granule (re)development. In a recent investigation, Ma *et al.* (2018) noted a similar pattern during the maturation stages of anaerobic granular sludge, and suggested that the effective AHL level required for granule maintenance might not be as high as that mandated by the granulation process – as indicated by a decline in signal molecule contents after granule formation. Likewise, comprehensive mixed liquor concentration profiles plotted by Tan *et al.* (2014) for a number of AHLs with different chain lengths revealed severe drops in the levels of most signal molecules after the granulation phase was over. In trying to explain this trend, a look into the mechanisms of QS regulation working within the AG volume at different stages of the normal granule life cycle (preliminary aggregation → aerobic granulation → maturation → maintenance → decay) might prove an insightful source of information. Recent studies on the issue have established that microbial communities in AGs include both signal producers and microorganisms with quorum quenching abilities whose activities equilibrate to regulate environmental signal concentrations. The balance between the two communities is responsible for tuning interspecific and intraspecific communication inside the granule and can affect the sludge's structure and properties by controlling the expression of QS-based phenotypes related to granulation (such as EPS production) (Song *et al.*, 2012; Tan *et al.*, 2015; Li *et al.*, 2016). In analysing QS regulation during aerobic granulation, Tan *et al.* (2015) found a significant shift in the dominant species from potential signal quenchers to signal producers, underlining the role of species composition and associated signalling activities in coordinating community level behaviours. In agreement with these findings, AHL with four to eight acyl chain carbons were shown to accumulate at the granular stage, reaching concentrations at least three times higher than those of the floccular stage. Reframing the discussion within the context of the current work, an opposite shift in the QQ-to-QS balance of the microbial community to that reported by Tan *et al.* (2015) during long-term operation – promoting an increase in quenching activities and causing AHL levels to drop – might serve to justify the different 3OC12-HSL_{eq.} values recorded in earlier and later stages of the experimental run. In agreement with this observation, Li *et al.* (2016) suggested that the proliferation of AHL quenchers and AHL producers in AGs is likely not synchronous, reporting a drop in AHL activity and diversity as granules matured and grew in size and finding consistent increases in the sludge's *N*-octanoyl-homoserine lactone-degrading activity over time.

Aside from these shared trends, direct comparisons between the equivalent AHL concentrations recorded in SBR1 and SBR2 between days 70 and 192 seem to reflect an initial stage of relatively higher levels in SBR2 that were gradually surpassed by those of SBR1 during the final month (significant differences recorded on days 85, 106, 126, 140, 148, 154, and 190; $p_t < 0.002$ in all cases). The described evolution clearly illustrates the influence of factors other than hydrodynamic shear – previously inferred as the prevalent driver of comparative differences between SBR1 and SBR2 during the aerobic granulation stage – over AHL synthesis and is similar to that of SVI values recorded in each system along the final leg of the operation.

4 Conclusions and future work

4.1 The impacts of Ag NPs over AGS properties, stability and treatment performance

Effects of silver nanoparticles on AGS stability were shown to be concentration-dependent, showing no apparent noxious action in the low concentration range but causing significant settleability decays and biomass washout when accumulated over long periods of time. In order to check whether these effects are avoidable, future studies could be designed to include periodic biomass withdrawals as a way of removing some of the accumulated silver and verifying sludge property evolutions. Any such strategy should, however, strive to achieve an optimum periodicity for sludge removal in such a way that SRTs are kept simultaneously low enough to stop the noxious action of Ag NPs from unfolding and high enough to secure the development of aromatic amine-degrading activities (achievable only at reasonably high sludge ages, as also demonstrated here).

Despite its impact on stability, Ag NP addition appeared to have no significant effect on the overall COD removal and decolourization abilities of either bioreactor, with relatively stable performance levels sustained at over 75% throughout the entire operation. Some secondary effects emerging in association with Ag NP-mediated destabilization could, nonetheless, be identified, specifically in terms of anaerobic COD removal (seen to drop on many an occasion as a result of sludge washout) and, in one occasion around day 85, in terms of the apparent amine-degrading activity. These results suggest important bacterial activities can be eliminated if Ag NP toxicity is not curbed and further advocate containment strategies that can limit silver accumulation in the biomass.

4.2 The effects of hydrodynamic shear and anaerobic feeding strategy over AGS properties and stability

Hydrodynamic shear proved important in defining the main macro- and microscopic properties of the sludge in the short-term horizon, with lower stresses promoting the development of AGS with better sludge settleability and facilitating granule growth. However, no apparent shear-associated effect could help steer biomass properties over the long run, with multiple incoherent variations in granulation grade and settleability taking place according to no set timing in either bioreactor. Conversely, positive effects conceivably associated with the use of a plug-flow filling strategy seemed to emerge towards the end of the operation, promoting the establishment of aerobic granules with high densities that caused a late rise in SVI in SBR2 concurrent with a continued decay in the settleability of the statically-fed SBR1. Even though some erratic COD and colour removal behaviours could be associated with the faulty nature of the plug flow, this configuration could prove helpful even in non-tubular bioreactors to secure stable aerobic granule structures.

4.3 AHL-based QS signalling as a reporter variable for sludge properties

AHL-based quorum sensing signalling proved an important feature of the aerobic granulation process, correlating positively with biomass accumulation and negatively with SVI values. Like most other properties evaluated during this work, signal molecule levels proved higher in the lower shear environments of SBR1 during the initial stages of the AG life cycle. In the long run, however, detected AHL concentrations dropped significantly, which might suggest a lesser importance for QS mechanisms in AG maintenance. In aiming to explain the drivers behind this reduction, future studies should strive to analyze the importance of both QS and QQ in order to paint an integrated picture of quorum sensing regulation networks at all developmental AG stages and understand how the two processes balance each other. Combining a strategy to characterize the quorum quenching activity of aerobic granules with some method of QS molecule analysis and the community-level identification of signal producers and quenchers should provide relevant information. Finally, some alignment between the falling AHL concentrations and the cyclical, Ag NP-related instability events recorded in the long run seemed to emerge from the data. Characterizing the effects of Ag NPs over QS signalling networks should also form a priority of future studies as a way of integrating all the available information.

References

- Adav, S. S., & Lee, D. J. (2008b). Single-culture aerobic granules with *Acinetobacter calcoaceticus*. *Applied microbiology and biotechnology*, 78(3), 551-557.
- Adav, S. S., & Lee, D. J. (2008c). Extraction of extracellular polymeric substances from aerobic granule with compact interior structure. *Journal of hazardous materials*, 154(1-3), 1120-1126.
- Adav, S. S., Chen, M. Y., Lee, D. J., & Ren, N. Q. (2007a). Degradation of phenol by aerobic granules and isolated yeast *Candida tropicalis*. *Biotechnology and bioengineering*, 96(5), 844-852.
- Adav, S. S., Lee, D. J., & Lai, J. Y. (2007b). Effects of aeration intensity on formation of phenol-fed aerobic granules and extracellular polymeric substances. *Applied microbiology and biotechnology*, 77(1), 175-182.
- Adav, S. S., Lee, D. J., & Lai, J. Y. (2009). Biological nitrification–denitrification with alternating oxic and anoxic operations using aerobic granules. *Applied microbiology and biotechnology*, 84(6), 1181-1189.
- Adav, S. S., Lee, D. J., Show, K. Y., & Tay, J. H. (2008a). Aerobic granular sludge: recent advances. *Biotechnology advances*, 26(5), 411-423.
- Agrawal, P. (2005). *The performance of pectinase and cutinase in cotton scouring* (Doctor). University of Twente.
- American Public Health Association (APHA), 1995. Standard Methods for the Examination of Water and Wastewater. In: Eaton, A.D., Clesceri, L.S., Greenberg, A.E. (Eds.), 19th ed. American Public Health Association, Washington, DC, USA.
- Apel, K., & Hirt, H. (2004). Reactive oxygen species: metabolism, oxidative stress, and signal transduction. *Annu. Rev. Plant Biol.*, 55, 373-399.
- Arrojo, B., Mosquera-Corral, A., Garrido, J. M., & Méndez, R. (2004). Aerobic granulation with industrial wastewater in sequencing batch reactors. *Water Research*, 38(14-15), 3389-3399.
- Arslan, S., Eyvaz, M., Gürbulak, E., & Yüksel, E. (2016). A Review of State-of-the-Art Technologies in Dye-Containing Wastewater Treatment–The Textile Industry Case. In *Textile Wastewater Treatment*. InTech.
- Barsing, P., Tiwari, A., Joshi, T., & Garg, S. (2011). Application of a novel bacterial consortium for mineralization of sulphonated aromatic amines. *Bioresource technology*, 102(2), 765-771.
- Bassin, J. P. (2018). Aerobic granular sludge technology. In *Advanced Biological Processes for Wastewater Treatment* (pp. 75-142). Springer, Cham.
- Bassin, J. P., Kleerebezem, R., Dezotti, M., & Van Loosdrecht, M. C. M. (2012). Simultaneous nitrogen and phosphate removal in aerobic granular sludge reactors operated at different temperatures. *Water Research*, 46(12), 3805-3816.
- Benn, T. M., & Westerhoff, P. (2008). Nanoparticle silver released into water from commercially available sock fabrics. *Environmental science & technology*, 42(11), 4133-4139.
- Bento, J. (2016). Interaction of silver nanoparticles with aerobic granular sludge in textile wastewater treatment bioreactors (MSc). Instituto Superior Técnico, Universidade de Lisboa.
- Beun, J. J., Hendriks, A., Van Loosdrecht, M. C. M., Morgenroth, E., Wilderer, P. A., & Heijnen, J. J. (1999). Aerobic granulation in a sequencing batch reactor. *Water Research*, 33(10), 2283-2290.
- Beun, J. J., Van Loosdrecht, M. C. M., & Heijnen, J. J. (2002). Aerobic granulation in a sequencing batch airlift reactor. *Water Research*, 36(3), 702-712.
- Bisschops, I., & Spanjers, H. (2003). Literature review on textile wastewater characterisation. *Environmental Technology*, 24(11), 1399-1411.
- Blaser, S. A., Scheringer, M., MacLeod, M., & Hungerbühler, K. (2008). Estimation of cumulative aquatic exposure and risk due to silver: contribution of nano-functionalized plastics and textiles. *Science of the total environment*, 390(2), 396-409.
- Butirón, G., Razo-Flores, E., Meruz, M., & Alatríste-Mondragon, F. (2006). Biological wastewater treatment systems. In F. Cervantes, S. Pavlostathis & V. Adrianus, *Advanced Biological Treatment Processes for Industrial Wastewaters: Principles and Applications* (1st ed., pp. 141-187). London, UK: IWA Publishing.
- Cabral Gonçalves, I., Penha, S., Matos, M., Franco, F., & Pinheiro, H. M. (2005). Evaluation of an integrated anaerobic/aerobic SBR system for the treatment of wool dyeing effluents. *Biodegradation*, 16(1), 81-89.
- Carmen, Z., & Daniela, S. (2012). Textile organic dyes–characteristics, polluting effects and separation/elimination procedures from industrial effluents—a critical overview. In *Organic Pollutants Ten Years After the Stockholm Convention-Environmental and Analytical Update* (pp. 55-86). InTech.
- Chan, Y. J., Chong, M. F., Law, C. L., & Hassell, D. G. (2009). A review on anaerobic–aerobic treatment of industrial and municipal wastewater. *Chemical Engineering Journal*, 155(1), 1-18.

- Chen, H., Li, A., Cui, D., Wang, Q., Wu, D., Cui, C., & Ma, F. (2018). N-Acyl-homoserine lactones and autoinducer-2-mediated quorum sensing during wastewater treatment. *Applied microbiology and biotechnology*, 102(3), 1119-1130.
- Chen, S. F., & Zhang, H. (2012). Aggregation kinetics of nanosilver in different water conditions. *Advances in natural sciences: nanoscience and nanotechnology*, 3(3), 035006.
- Chen, Y., Jiang, W., Liang, D. T., & Tay, J. H. (2007). Structure and stability of aerobic granules cultivated under different shear force in sequencing batch reactors. *Applied microbiology and biotechnology*, 76(5), 1199-1208.
- Chequer, F. M. D., de Oliveira, G. A. R., Ferraz, E. R. A., Cardoso, J. C., Zanon, M. V. B., & de Oliveira, D. P. (2013). Textile dyes: dyeing process and environmental impact. In *Eco-friendly textile dyeing and finishing*. InTech.
- Çinar, Ö., & Demiröz, K. (2010). Biodegradation of azo dyes in anaerobic-aerobic sequencing batch reactors. In *Biodegradation of Azo Dyes* (pp. 59-72). Springer Berlin Heidelberg.
- Clara, M., Kreuzinger, N., Strenn, B., Gans, O., & Kroiss, H. (2005). The solids retention time—a suitable design parameter to evaluate the capacity of wastewater treatment plants to remove micropollutants. *Water research*, 39(1), 97-106.
- Correia, V., Stephenson, T., & Judd, S. (1994). Characterisation of textile wastewaters - a review. *Environmental Technology*, 15(10), 917-929.
- Corsino, S. F., Capodici, M., Torregrossa, M., & Viviani, G. (2016). Fate of aerobic granular sludge in the long-term: the role of EPSs on the clogging of granular sludge porosity. *Journal of environmental management*, 183, 541-550.
- Coughlin, M. F., Kinkle, B. K., & Bishop, P. L. (2002). Degradation of acid orange 7 in an aerobic biofilm. *Chemosphere*, 46(1), 11-19.
- Dangcong, P., Bernet, N., Delgenes, J. P., & Moletta, R. (1999). Aerobic granular sludge—a case report. *Water Research*, 33(3), 890-893.
- De Bruin, L. M. M., De Kreuk, M. K., Van Der Roest, H. F. R., Uijterlinde, C., & Van Loosdrecht, M. C. M. (2004). Aerobic granular sludge technology: an alternative to activated sludge?. *Water Science and Technology*, 49(11-12), 1-7.
- De Kreuk, M. K., Heijnen, J. J., & Van Loosdrecht, M. C. M. (2005b). Simultaneous COD, nitrogen, and phosphate removal by aerobic granular sludge. *Biotechnology and bioengineering*, 90(6), 761-769.
- De Kreuk, M. K., McSwain, B. S., Bathe, S., Tay, S. T. L., Schwarzenbeck, N., & Wilderer, P. A. (2005a). Discussion outcomes. *Aerobic granular sludge*, 153-169.
- De Kreuk, M. V., & Van Loosdrecht, M. C. M. (2004). Selection of slow growing organisms as a means for improving aerobic granular sludge stability. *Water Science and Technology*, 49(11-12), 9-17.
- Demirel, B. (2016). The impacts of engineered nanomaterials (ENMs) on anaerobic digestion processes. *Process Biochemistry*, 51(2), 308-313.
- Derlon, N., Wagner, J., da Costa, R. H. R., & Morgenroth, E. (2016). Formation of aerobic granules for the treatment of real and low-strength municipal wastewater using a sequencing batch reactor operated at constant volume. *Water research*, 105, 341-350.
- Deycard, V. N., Schäfer, J., Petit, J. C., Coynel, A., Lancelot, L., Dutruch, L., ... & Blanc, G. (2017). Inputs, dynamics and potential impacts of silver (Ag) from urban wastewater to a highly turbid estuary (SW France). *Chemosphere*, 167, 501-511.
- Dos Santos, A. B., Cervantes, F. J., & van Lier, J. B. (2007). Review paper on current technologies for decolourisation of textile wastewaters: perspectives for anaerobic biotechnology. *Bioresource technology*, 98(12), 2369-2385.
- Doshi, R., & Shelke, V. (2001). Enzymes in textile industry—An environment-friendly approach. *Indian Journal of Fibre & Textile Research*, 26, 202-205.
- Dutta, A., & Sarkar, S. (2015). Sequencing batch reactor for wastewater treatment: recent advances. *Current Pollution Reports*, 1(3), 177-190.
- Environmental Protection Agency (EPA) Office of Compliance (1997). *Profile of the Textile Industry* (pp. 3-71). Washington, DC.
- Environmental Protection Agency (EPA). (1996). *Best Management Practices for Pollution Prevention in the Textile Industry* (pp. 1-30). Cincinnati, OH.
- European Commission. (2017). *Textiles and clothing in the EU*. Retrieved 8 July 2017, from https://ec.europa.eu/growth/sectors/fashion/textiles-clothing/eu_en
- European Integrated Pollution Prevention and Control Bureau (EIPPCB) (2003). *Reference Document on Best Available Techniques for the Textiles Industry* (pp. i-xx). Seville.
- Feng, Q., Xiao, Y., Wang, X., Li, J., Wu, Y., Xue, Z., ... & Oleyiblo, J. O. (2016). The influences of shear stress on Extracellular Polymeric Substances of activated sludge. *Desalination and Water Treatment*, 57(34), 15835-15842.
- Franca, R. D. G., Ortigueira, J., Pinheiro, H. M., & Lourenço, N. D. (2017a). Effect of SBR feeding strategy and feed composition on the stability of aerobic granular sludge in the treatment of a simulated textile wastewater. *Water Science and Technology*, wst2017300.

- Franca, R. D., Pinheiro, H. M., van Loosdrecht, M. C., & Lourenço, N. D. (2017b). Stability of aerobic granules during long-term bioreactor operation. *Biotechnology advances*.
- Franca, R. D., Vieira, A., Mata, A. M., Carvalho, G. S., Pinheiro, H. M., & Lourenço, N. D. (2015). Effect of an azo dye on the performance of an aerobic granular sludge sequencing batch reactor treating a simulated textile wastewater. *Water research*, 85, 327-336.
- Gao, D., Liu, L., & Wu, W. M. (2011b). Comparison of four enhancement strategies for aerobic granulation in sequencing batch reactors. *Journal of hazardous materials*, 186(1), 320-327.
- Gao, D., Liu, L., Liang, H., & Wu, W. M. (2011a). Aerobic granular sludge: characterization, mechanism of granulation and application to wastewater treatment. *Critical reviews in biotechnology*, 31(2), 137-152.
- Gao, Y., & Cranston, R. (2008). Recent advances in antimicrobial treatments of textiles. *Textile research journal*, 78(1), 60-72.
- Gerber, L. C., Mohn, D., Fortunato, G., Astasov-Frauenhoffer, M., Imfeld, T., Waltimo, T., ... & Stark, W. J. (2011). Incorporation of reactive silver-tricalcium phosphate nanoparticles into polyamide 6 allows preparation of self-disinfecting fibers. *Polymer Engineering & Science*, 51(1), 71-77.
- Gereffi, G., & Frederick, S. (2010). The global apparel value chain, trade and the crisis: challenges and opportunities for developing countries.
- Ghaly, A.E., Ananthashankar, R., Alhattab, M., & Ramakrishnan, V.V. (2014). Production, Characterization and Treatment of Textile Effluents: A Critical Review. *J Chem Eng Process Technol*, 5(182).
- Giesen, A., De Bruin, L. M. M., Niermans, R. P., & Van der Roest, H. F. (2013). Advancements in the application of aerobic granular biomass technology for sustainable treatment of wastewater. *Water Practice and Technology*, 8(1), wpt-2013007.
- Gonzalez-Gil, G., & Holliger, C. (2011). Dynamics of microbial community structure and enhanced biological phosphorus removal of propionate-and acetate-cultivated aerobic granules. *Applied and environmental microbiology*, AEM-05738.
- Gottschalk, F., Sonderer, T., Scholz, R. W., & Nowack, B. (2009). Modeled environmental concentrations of engineered nanomaterials (TiO₂, ZnO, Ag, CNT, fullerenes) for different regions. *Environmental science & technology*, 43(24), 9216-9222.
- Gouveia, I. C., Fiadeiro, J. M., & Queiroz, J. A. (2008). Enzymatic removal of plant residues from wool: Application of experimental design techniques for optimization parameters. *Biochemical Engineering Journal*, 41(2), 157-165.
- Grau, P. (1991). Textile Industry Wastewater Treatment. *Wat Sci Tech*, 24(1), 97-103.
- Gu, L., Li, Q., Quan, X., Cen, Y., & Jiang, X. (2014). Comparison of nanosilver removal by flocculent and granular sludge and short-and long-term inhibition impacts. *Water research*, 58, 62-70.
- Hailei, W., Guangli, Y., Guosheng, L., & Feng, P. (2006). A new way to cultivate aerobic granules in the process of papermaking wastewater treatment. *Biochemical Engineering Journal*, 28(1), 99-103.
- Henriet, O., Meunier, C., Henry, P., & Mahillon, J. (2016). Improving phosphorus removal in aerobic granular sludge processes through selective microbial management. *Bioresource technology*, 211, 298-306.
- Holkar, C., Jadhav, A., Pinjari, D., Mahamuni, N., & Pandit, A. (2016). A critical review on textile wastewater treatments: Possible approaches. *Journal Of Environmental Management*, 182, 351-366.
- Hou, L., Li, K., Ding, Y., Li, Y., Chen, J., Wu, X., & Li, X. (2012). Removal of silver nanoparticles in simulated wastewater treatment processes and its impact on COD and NH₄ reduction. *Chemosphere*, 87(3), 248-252.
- Inocencio, P., Coelho, F., van Loosdrecht, M. C. M., & Giesen, A. (2013). The future of sewage treatment: Nereda technology exceeds high expectations. *Water* 21, 15, 28-29.
- Isanta, E., Suárez-Ojeda, M. E., del Río, Á. V., Morales, N., Pérez, J., & Carrera, J. (2012). Long term operation of a granular sequencing batch reactor at pilot scale treating a low-strength wastewater. *Chemical engineering journal*, 198, 163-170.
- Jiang, B., & Liu, Y. (2012). Roles of ATP-dependent N-acylhomoserine lactones (AHLs) and extracellular polymeric substances (EPSs) in aerobic granulation. *Chemosphere*, 88(9), 1058-1064.
- Jiang, H. L., Tay, J. H., Liu, Y., & Tay, S. T. L. (2003). Ca²⁺ augmentation for enhancement of aerobically grown microbial granules in sludge blanket reactors. *Biotechnology letters*, 25(2), 95-99.
- Kaegi, R., Voegelin, A., Ort, C., Sinnet, B., Thalmann, B., Krismer, J., ... & Mueller, E. (2013). Fate and transformation of silver nanoparticles in urban wastewater systems. *Water research*, 47(12), 3866-3877.
- Kaegi, R., Voegelin, A., Sinnet, B., Zuleeg, S., Hagendorfer, H., Burkhardt, M., & Siegrist, H. (2011). Behavior of metallic silver nanoparticles in a pilot wastewater treatment plant. *Environmental Science and Technology-Columbus*, 45(9), 3902.
- Kamal, A. K. I., Ahmed, F., Hassan, M., Uddin, M., & Hossain, S. M. (2016). Characterization of Textile Effluents from Dhaka Export Processing Zone (DEPZ) Area in Dhaka, Bangladesh. *Pollution*, 2(2), 153-161.

- Kant, R. (2012). Textile dyeing industry an environmental hazard. *Natural Science*, 04(01), 22-26.
- Kanu, I., & Achi, O. K. (2011). Industrial effluents and their impact on water quality of receiving rivers in Nigeria. *Journal of applied technology in environmental sanitation*, 1(1), 75-86.
- Khan, S., & Malik, A. (2014). Environmental and health effects of textile industry wastewater. In *Environmental Deterioration and Human Health* (pp. 55-71). Springer Netherlands.
- Kong, Y., Liu, Y. Q., Tay, J. H., Wong, F. S., & Zhu, J. (2009). Aerobic granulation in sequencing batch reactors with different reactor height/diameter ratios. *Enzyme and Microbial Technology*, 45(5), 379-383.
- Kroll, A., Behra, R., Kaegi, R., & Sigg, L. (2014). Extracellular polymeric substances (EPS) of freshwater biofilms stabilize and modify CeO₂ and Ag nanoparticles. *PLoS One*, 9(10), e110709.
- Kudlich, M., Hetheridge, M. J., Knackmuss, H. J., & Stolz, A. (1999). Autoxidation reactions of different aromatic o-aminohydroxynaphthalenes that are formed during the anaerobic reduction of sulfonated azo dyes. *Environmental science & technology*, 33(6), 896-901.
- Lacasse, K. & Baumann, W. (2004). The textile chain (from raw materials to finished goods). In: K. Lacasse & W. Baumann, ed., *Textile chemicals*, 1st ed (pp. 70-83). New York, NY: Springer-Verlag Berlin Heidelberg.
- Ladchumananandasivam, R. (2011). *Processos Químicos Têxteis: Acabamento Têxtil - Volume V* (5th ed., pp. 30-32) [Portuguese in the original]. Natal, RN: Universidade Federal do Rio Grande do Norte.
- Le Ouay, B., & Stellacci, F. (2015). Antibacterial activity of silver nanoparticles: a surface science insight. *Nano today*, 10(3), 339-354.
- Lee, D. J., Chen, Y. Y., Show, K. Y., Whiteley, C. G., & Tay, J. H. (2010). Advances in aerobic granule formation and granule stability in the course of storage and reactor operation. *Biotechnology advances*, 28(6), 919-934.
- Lemaire, R., Webb, R. I., & Yuan, Z. (2008b). Micro-scale observations of the structure of aerobic microbial granules used for the treatment of nutrient-rich industrial wastewater. *The ISME Journal*, 2(5), 528.
- Lemaire, R., Yuan, Z., Blackall, L. L., & Crocetti, G. R. (2008a). Microbial distribution of *Accumulibacter* spp. and *Competibacter* spp. in aerobic granules from a lab-scale biological nutrient removal system. *Environmental Microbiology*, 10(2), 354-363.
- Levard, C., Hotze, E. M., Lowry, G. V., & Brown Jr, G. E. (2012). Environmental transformations of silver nanoparticles: impact on stability and toxicity. *Environmental science & technology*, 46(13), 6900-6914.
- Levard, C., Mitra, S., Yang, T., Jew, A. D., Badireddy, A. R., Lowry, G. V., & Brown Jr, G. E. (2013). Effect of chloride on the dissolution rate of silver nanoparticles and toxicity to *E. coli*. *Environmental science & technology*, 47(11), 5738-5745.
- Levard, C., Reinsch, B. C., Michel, F. M., Oumahi, C., Lowry, G. V., & Brown Jr, G. E. (2011). Sulfidation processes of PVP-coated silver nanoparticles in aqueous solution: impact on dissolution rate. *Environmental science & technology*, 45(12), 5260-5266.
- Li, A. J., Yang, S. F., Li, X. Y., & Gu, J. D. (2008). Microbial population dynamics during aerobic sludge granulation at different organic loading rates. *Water Research*, 42(13), 3552-3560.
- Li, J., Garmy, K., Neu, T., He, M., Lindenblatt, C., & Horn, H. (2007). Comparison of some characteristics of aerobic granules and sludge flocs from sequencing batch reactors. *Water science and technology*, 55(8-9), 403-411.
- Li, X. M., Liu, Q. Q., Yang, Q., Guo, L., Zeng, G. M., Hu, J. M., & Zheng, W. (2009). Enhanced aerobic sludge granulation in sequencing batch reactor by Mg²⁺ augmentation. *Bioresource technology*, 100(1), 64-67.
- Li, Y. C., & Zhu, J. R. (2014). Role of N-acyl homoserine lactone (AHL)-based quorum sensing (QS) in aerobic sludge granulation. *Applied microbiology and biotechnology*, 98(17), 7623-7632.
- Li, Y. S., Cao, J. S., Li, B. B., Li, W. W., Fang, F., Tong, Z. H., & Yu, H. Q. (2016). Outcompeting presence of Acyl-Homoserine-Lactone (AHL)-quenching bacteria over AHL-producing bacteria in aerobic granules. *Environmental Science & Technology Letters*, 3(1), 36-40.
- Li, Y. S., Pan, X. R., Cao, J. S., Song, X. N., Fang, F., Tong, Z. H., ... & Yu, H. Q. (2017). Augmentation of acyl homoserine lactones-producing and-quenching bacterium into activated sludge for its granulation. *Water research*, 125, 309-317.
- Li, Y., Lv, J., Zhong, C., Hao, W., Wang, Y., & Zhu, J. (2014). Performance and role of N-acyl-homoserine lactone (AHL)-based quorum sensing (QS) in aerobic granules. *Journal of Environmental Sciences*, 26(8), 1615-1621.
- Li, Z. H., Kuba, T., & Kusuda, T. (2006). The influence of starvation phase on the properties and the development of aerobic granules. *Enzyme and Microbial Technology*, 38(5), 670-674.
- Libra, J. A., Borchert, M., Vigelahn, L., & Storm, T. (2004). Two stage biological treatment of a diazo reactive textile dye and the fate of the dye metabolites. *Chemosphere*, 56(2), 167-180.

- Liu, X., Sun, S., Ma, B., Zhang, C., Wan, C., & Lee, D. J. (2016). Understanding of aerobic granulation enhanced by starvation in the perspective of quorum sensing. *Applied microbiology and biotechnology*, 100(8), 3747-3755.
- Liu, Y. Q., & Tay, J. H. (2008). Influence of starvation time on formation and stability of aerobic granules in sequencing batch reactors. *Bioresource technology*, 99(5), 980-985.
- Liu, Y. Q., Moy, B., Kong, Y. H., & Tay, J. H. (2010). Formation, physical characteristics and microbial community structure of aerobic granules in a pilot-scale sequencing batch reactor for real wastewater treatment. *Enzyme and Microbial Technology*, 46(6), 520-525.
- Liu, Y., & Tay, J. H. (2002). The essential role of hydrodynamic shear force in the formation of biofilm and granular sludge. *Water research*, 36(7), 1653-1665.
- Liu, Y., Wang, Z. W., Qin, L., Liu, Y. Q., & Tay, J. H. (2005). Selection pressure-driven aerobic granulation in a sequencing batch reactor. *Applied microbiology and biotechnology*, 67(1), 26-32.
- Liu, Y., Yang, S. F., & Tay, J. H. (2004). Improved stability of aerobic granules by selecting slow-growing nitrifying bacteria. *Journal of Biotechnology*, 108(2), 161-169.
- Lourenço, N. D., Franca, R. D. G., Moreira, M. A., Gil, F. N., Viegas, C. A., & Pinheiro, H. M. (2015). Comparing aerobic granular sludge and flocculent sequencing batch reactor technologies for textile wastewater treatment. *Biochemical Engineering Journal*, 104, 57-63.
- Lourenco, N. D., Novais, J. M., & Pinheiro, H. M. (2000). Reactive textile dye colour removal in a sequencing batch reactor. *Water Science and Technology*, 42(5-6), 321-328.
- Lourenco, N. D., Novais, J. M., & Pinheiro, H. M. (2001). Effect of some operational parameters on textile dye biodegradation in a sequential batch reactor. *Journal of Biotechnology*, 89(2), 163-174.
- Loza, K., Diendorf, J., Sengstock, C., Ruiz-Gonzalez, L., Gonzalez-Calbet, J. M., Vallet-Regi, M., ... & Eppe, M. (2014). The dissolution and biological effects of silver nanoparticles in biological media. *Journal of Materials Chemistry B*, 2(12), 1634-1643.
- Luo, Z. Q., Clemente, T. E., & Farrand, S. K. (2001). Construction of a derivative of *Agrobacterium tumefaciens* C58 that does not mutate to tetracycline resistance. *Molecular plant-microbe interactions*, 14(1), 98-103.
- Lv, J., Wang, Y., Zhong, C., Li, Y., Hao, W., & Zhu, J. (2014). The effect of quorum sensing and extracellular proteins on the microbial attachment of aerobic granular activated sludge. *Bioresource technology*, 152, 53-58.
- Lv, Y., Wan, C., Lee, D. J., Liu, X., & Tay, J. H. (2014). Microbial communities of aerobic granules: granulation mechanisms. *Bioresource technology*, 169, 344-351.
- Ma, H., Ma, S., Hu, H., Ding, L., & Ren, H. (2018). The biological role of N-acyl-homoserine lactone-based quorum sensing (QS) in EPS production and microbial community assembly during anaerobic granulation process. *Scientific reports*, 8(1), 15793.
- Madoni, P. (2011). Protozoa in wastewater treatment processes: a minireview. *Italian Journal of Zoology*, 78(1), 3-11.
- Marambio-Jones, C., & Hoek, E. M. (2010). A review of the antibacterial effects of silver nanomaterials and potential implications for human health and the environment. *Journal of Nanoparticle Research*, 12(5), 1531-1551.
- Maxwell, D., McAndrew, L., Ryan, J. (2015), The State of the Apparel Sector Report – Water. 11-21.
- McSwain, B. S., Irvine, R. L., Hausner, M., & Wilderer, P. A. (2005). Composition and distribution of extracellular polymeric substances in aerobic flocs and granular sludge. *Applied and Environmental Microbiology*, 71(2), 1051-1057.
- Metcalf & Eddy, I., Tchobanoglous, G., Burton, F., & Stensel, H. (2014). *Wastewater Engineering: Treatment and Resource Recovery* (5th ed., pp. 555-561, 700-707). New York: McGraw-Hill Education.
- Mizell, L. R., Davis, A. E., & Oliva, E. C. (1962). A Critical Study of Wool Carbonizing 1. *Textile Research Journal*, 32(6), 497-505.
- Morgenroth, E., Sherden, T., Van Loosdrecht, M. C. M., Heijnen, J. J., & Wilderer, P. A. (1997). Aerobic granular sludge in a sequencing batch reactor. *Water Research*, 31(12), 3191-3194.
- Morones, J. R., Elechiguerra, J. L., Camacho, A., Holt, K., Kouri, J. B., Ramirez, J. T., & Yacaman, M. J. (2005). The bactericidal effect of silver nanoparticles. *Nanotechnology* 16(10), 2346.
- Muda, K., Aris, A., Salim, M. R., Ibrahim, Z., Yahya, A., van Loosdrecht, M. C., ... & Nawahwi, M. Z. (2010). Development of granular sludge for textile wastewater treatment. *Water research*, 44(15), 4341-4350.
- Mullai, P., Yogeswari, M. K., Vishali, S., Namboodiri, M. T., Gebrewold, B. D., Rene, E. R., & Pakshirajan, K. (2016). Aerobic Treatment of Effluents From Textile Industry. *Current Developments in Biotechnology and Bioengineering: Biological Treatment of Industrial Effluents*, 3-34.
- Nancharaiyah, Y. V., & Reddy, G. K. K. (2018). Aerobic granular sludge technology: mechanisms of granulation and biotechnological applications. *Bioresource technology*, 247, 1128-1143.

- Ni, B. J., Hu, B. L., Fang, F., Xie, W. M., Kartal, B., Liu, X. W., ... & Yu, H. Q. (2010). Microbial and physicochemical characteristics of compact anaerobic ammonium-oxidizing granules in an upflow anaerobic sludge blanket reactor. *Applied and environmental microbiology*, 76(8), 2652-2656.
- Ni, B. J., Xie, W. M., Liu, S. G., Yu, H. Q., Wang, Y. Z., Wang, G., & Dai, X. L. (2009). Granulation of activated sludge in a pilot-scale sequencing batch reactor for the treatment of low-strength municipal wastewater. *Water Research*, 43(3), 751-761.
- O'Neill, C., Hawkes, F. R., Hawkes, D. L., Lourenço, N. D., Pinheiro, H. M., & Delée, W. (1999). Colour in textile effluents—sources, measurement, discharge consents and simulation: a review. *Journal of Chemical Technology and Biotechnology*, 74(11), 1009-1018.
- Oehmen, A., Lemos, P. C., Carvalho, G., Yuan, Z., Keller, J., Blackall, L. L., & Reis, M. A. (2007). Advances in enhanced biological phosphorus removal: from micro to macro scale. *Water research*, 41(11), 2271-2300.
- Organisation for Economic Cooperation and Development (OECD). (2004). *Environmental Exposure Assessment: Draft Emission Scenario on Textile Manufacturing Woven Mills* (pp. 7-18). Canada.
- Pan, S., Tay, J. H., He, Y. X., & Tay, S. L. (2004). The effect of hydraulic retention time on the stability of aerobically grown microbial granules. *Letters in Applied Microbiology*, 38(2), 158-163.
- Pang, Y. L., & Abdullah, A. Z. (2013). Current status of textile industry wastewater management and research progress in Malaysia: a review. *Clean—Soil, Air, Water*, 41(8), 751-764.
- Pareek, V., Gupta, R., & Panwar, J. (2018). Do physico-chemical properties of silver nanoparticles decide their interaction with biological media and bactericidal action? A review. *Materials Science and Engineering: C*.
- Park, H. J., Kim, J. Y., Kim, J., Lee, J. H., Hahn, J. S., Gu, M. B., & Yoon, J. (2009). Silver-ion-mediated reactive oxygen species generation affecting bactericidal activity. *Water research*, 43(4), 1027-1032.
- Patel, H., & Vashi, R. T. (2015). *Characterization and treatment of textile wastewater* (pp. 2-18). Elsevier.
- Pearce, C. I., Lloyd, J. R., & Guthrie, J. T. (2003). The removal of colour from textile wastewater using whole bacterial cells: a review. *Dyes and pigments*, 58(3), 179-196.
- Pereira, L., & Alves, M. (2012). Dyes—environmental impact and remediation. In *Environmental protection strategies for sustainable development* (pp. 111-162). Springer Netherlands.
- Pereira, L., Mondal, P. K., & Alves, M. (2015). Aromatic amines sources, environmental impact and remediation. In *Pollutants in buildings, water and living organisms* (pp. 297-346). Springer International Publishing.
- Picioreanu, C., Van Loosdrecht, M. C., & Heijnen, J. J. (1998). Mathematical modeling of biofilm structure with a hybrid differential-discrete cellular automaton approach. *Biotechnology and bioengineering*, 58(1), 101-116.
- Pinheiro, H. M., Touraud, E., & Thomas, O. (2004). Aromatic amines from azo dye reduction: status review with emphasis on direct UV spectrophotometric detection in textile industry wastewaters. *Dyes and pigments*, 61(2), 121-139.
- Popli, S., & Patel, U. D. (2015). Destruction of azo dyes by anaerobic–aerobic sequential biological treatment: a review. *International Journal of Environmental Science and Technology*, 12(1), 405-420.
- Prabhu, S., & Poulouse, E. K. (2012). Silver nanoparticles: mechanism of antimicrobial action, synthesis, medical applications, and toxicity effects. *International Nano Letters*, 2(1), 32.
- Pronk, M., Abbas, B., Al-Zuhairy, S. H. K., Kraan, R., Kleerebezem, R., & Van Loosdrecht, M. C. M. (2015b). Effect and behaviour of different substrates in relation to the formation of aerobic granular sludge. *Applied microbiology and biotechnology*, 99(12), 5257-5268.
- Pronk, M., De Kreuk, M. K., De Bruin, B., Kamminga, P., Kleerebezem, R. V., & Van Loosdrecht, M. C. M. (2015a). Full scale performance of the aerobic granular sludge process for sewage treatment. *Water research*, 84, 207-217.
- Qin, L., Liu, Y., & Tay, J. H. (2004a). Effect of settling time on aerobic granulation in sequencing batch reactor. *Biochemical Engineering Journal*, 21(1), 47-52.
- Qin, L., Tay, J. H., & Liu, Y. (2004b). Selection pressure is a driving force of aerobic granulation in sequencing batch reactors. *Process Biochemistry*, 39(5), 579-584.
- Quan, X., Cen, Y., Lu, F., Gu, L., & Ma, J. (2015). Response of aerobic granular sludge to the long-term presence of nanosilver in sequencing batch reactors: reactor performance, sludge property, microbial activity and community. *Science of the Total Environment*, 506, 226-233.
- Radetić, M. (2013). Functionalization of textile materials with silver nanoparticles. *Journal of Materials Science*, 48(1), 95-107.
- Rawat, D., Mishra, V., & Sharma, R. S. (2016). Detoxification of azo dyes in the context of environmental processes. *Chemosphere*, 155, 591-605.

- Ren, T. T., Yu, H. Q., & Li, X. Y. (2010). The quorum-sensing effect of aerobic granules on bacterial adhesion, biofilm formation, and sludge granulation. *Applied microbiology and biotechnology*, 88(3), 789-797.
- Rico-Martínez, R., Arzate-Cárdenas, M. A., Robles-Vargas, D., Pérez-Legaspi, I. A., Jesús, A. F., & Santos-Medrano, G. E. (2016). Rotifers as Models in Toxicity Screening of Chemicals and Environmental Samples. In *Invertebrates-Experimental Models in Toxicity Screening*. InTech.
- Rivero, P. J., Urrutia, A., Goicoechea, J., & Arregui, F. J. (2015). Nanomaterials for functional textiles and fibers. *Nanoscale research letters*, 10(1), 501.
- Rocktäschel, T., Klarmann, C., Helmreich, B., Ochoa, J., Boisson, P., Sørensen, K. H., & Horn, H. (2013). Comparison of two different anaerobic feeding strategies to establish a stable aerobic granulated sludge bed. *Water research*, 47(17), 6423-6431.
- Rodrigues, A. (2017). Impact of engineered nanoparticles on the performance of aerobic granular sludge sequencing batch reactors treating textile wastewater (MSc). Instituto Superior Técnico, Universidade de Lisboa.
- Royal HaskoningDHV (2018). About the Nereda Wastewater Treatment Process. Retrieved from <https://www.royalhaskoningdhv.com/en-gb/nereda/about-nereda-technology>
- Russ, R., Rau, J., & Stolz, A. (2000). The function of cytoplasmic flavin reductases in the reduction of azo dyes by bacteria. *Applied and Environmental Microbiology*, 66(4), 1429-1434.
- Saratale, R. G., Saratale, G. D., Chang, J. S., & Govindwar, S. P. (2011). Bacterial decolorization and degradation of azo dyes: a review. *Journal of the Taiwan Institute of Chemical Engineers*, 42(1), 138-157.
- Sarayu, K., & Sandhya, S. (2012). Current Technologies for Biological Treatment of Textile Wastewater—A Review. *Applied Biochemistry And Biotechnology*, 167(3), 645-661.
- Sarma, S. J., Tay, J. H., & Chu, A. (2017). Finding knowledge gaps in aerobic granulation technology. *Trends in biotechnology*, 35(1), 66-78.
- Savin, I. I., & Butnaru, R. (2008). WASTEWATER CHARACTERISTICS IN TEXTILE FINISHING MILLS. *Environmental Engineering & Management Journal (EEMJ)*, 7(6).
- Schindler, W., & Hauser, P. (2004). Antimicrobial finishes. In W. Schindler & P. Hauser, *Chemical finishing of textiles* (pp. 165-174). Cambridge: Woodhead Publishing Ltd and CRC Press LLC.
- Schwarzenbeck, N., Borges, J. M., & Wilderer, P. A. (2005). Treatment of dairy effluents in an aerobic granular sludge sequencing batch reactor. *Applied Microbiology and Biotechnology*, 66(6), 711-718.
- Seviour, T., Pijuan, M., Nicholson, T., Keller, J., & Yuan, Z. (2009). Gel-forming exopolysaccharides explain basic differences between structures of aerobic sludge granules and floccular sludges. *Water research*, 43(18), 4469-4478.
- Sheng, Z., Van Nostrand, J. D., Zhou, J., & Liu, Y. (2018). Contradictory effects of silver nanoparticles on activated sludge wastewater treatment. *Journal of hazardous materials*, 341, 448-456.
- Simoncic, B., & Tomsic, B. (2010). Structures of novel antimicrobial agents for textiles-a review. *Textile Research Journal*, 80(16), 1721-1737.
- Singh, M., & Srivastava, R. K. (2011). Sequencing batch reactor technology for biological wastewater treatment: a review. *Asia-Pacific Journal of Chemical Engineering*, 6(1), 3-13.
- Society of Dyers and Colourists, & AATCC. (2017). *Welcome to the Colour Index | Colour Index*. *Colour-index.com*. Retrieved 10 August 2017, from <https://colour-index.com/>
- Solís, M., Solís, A., Pérez, H. I., Manjarrez, N., & Flores, M. (2012). Microbial decolouration of azo dyes: a review. *Process Biochemistry*, 47(12), 1723-1748.
- Song, X. N., Cheng, Y. Y., Li, W. W., Li, B. B., Sheng, G. P., Fang, C. Y., ... & Yu, H. Q. (2014). Quorum quenching is responsible for the underestimated quorum sensing effects in biological wastewater treatment reactors. *Bioresource technology*, 171, 472-476.
- Spartan Environmental Technologies. (2017). *Color Measurement in Water - Spartan Environmental Technologies*. *Spartanwatertreatment.com*. Retrieved 28 October 2017, from <http://www.spartanwatertreatment.com/color-measurement-water.html>
- Stolz, A. (2001). Basic and applied aspects in the microbial degradation of azo dyes. *Applied microbiology and biotechnology*, 56(1), 69-80.
- Su, K. Z., & Yu, H. Q. (2005). Formation and characterization of aerobic granules in a sequencing batch reactor treating soybean-processing wastewater. *Environmental Science & Technology*, 39(8), 2818-2827.
- Tan, C. H., Koh, K. S., Xie, C., Tay, M., Zhou, Y., Williams, R., ... & Kjelleberg, S. (2014). The role of quorum sensing signalling in EPS production and the assembly of a sludge community into aerobic granules. *The ISME journal*, 8(6), 1186.
- Tan, C. H., Koh, K. S., Xie, C., Zhang, J., Tan, X. H., Lee, G. P., ... & Kjelleberg, S. (2015). Community quorum sensing signalling and quenching: microbial granular biofilm assembly. *npj Biofilms and Microbiomes*, 1, 15006.

- Tan, N. C., Van Leeuwen, A., Van Voorthuizen, E. M., Slenders, P., Prenafeta-Boldu, F. X., Temmink, H., ... & Field, J. A. (2005). Fate and biodegradability of sulfonated aromatic amines. *Biodegradation*, 16(6), 527-537.
- Tang, J., Wu, Y., Esquivel-Elizondo, S., Sørensen, S. J., & Rittmann, B. E. (2018). How Microbial Aggregates Protect against Nanoparticle Toxicity. *Trends in biotechnology*.
- Tang, K., Zhang, Y., Yu, M., Shi, X., Coenye, T., Bossier, P., & Zhang, X. H. (2013). Evaluation of a new high-throughput method for identifying quorum quenching bacteria. *Scientific reports*, 3.
- Tay, J. H., Ivanov, V., Pan, S., & Tay, S. L. (2002). Specific layers in aerobically grown microbial granules. *Letters in Applied Microbiology*, 34(4), 254-257.
- Tay, J. H., Liu, Q. S., & Liu, Y. (2001a). Microscopic observation of aerobic granulation in sequential aerobic sludge blanket reactor. *Journal of Applied Microbiology*, 91(1), 168-175.
- Tay, J. H., Liu, Q. S., & Liu, Y. (2001b). The effects of shear force on the formation, structure and metabolism of aerobic granules. *Applied microbiology and biotechnology*, 57(1-2), 227-233.
- Tay, J. H., Pan, S., He, Y., & Tay, S. T. L. (2004). Effect of organic loading rate on aerobic granulation. II: Characteristics of aerobic granules. *Journal of Environmental Engineering*, 130(10), 1102-1109.
- The Project on Emerging Nanotechnologies. (2017). *Silver. Nanotechproject.org*. Retrieved 26 October 2017, from <http://www.nanotechproject.org/cpi/browse/nanomaterials/silver-nanoparticle/?sort=title>
- Toh, S., Tay, J., Moy, B., Ivanov, V., & Tay, S. (2003). Size-effect on the physical characteristics of the aerobic granule in a SBR. *Applied Microbiology and Biotechnology*, 60(6), 687-695.
- Tran, Q. H., & Le, A. T. (2013). Silver nanoparticles: synthesis, properties, toxicology, applications and perspectives. *Advances in Natural Sciences: Nanoscience and Nanotechnology*, 4(3), 033001.
- Tsuneda, S., Nagano, T., Hoshino, T., Ejiri, Y., Noda, N., & Hirata, A. (2003). Characterization of nitrifying granules produced in an aerobic upflow fluidized bed reactor. *Water Research*, 37(20), 4965-4973.
- Van der Zee, F. P., & Villaverde, S. (2005). Combined anaerobic-aerobic treatment of azo dyes—a short review of bioreactor studies. *Water research*, 39(8), 1425-1440.
- Forgacs, E., Cserhati, T., & Oros, G. (2004). Removal of synthetic dyes from wastewaters: a review. *Environment international*, 30(7), 953-971.
- Van der Zee, F. P., Lettinga, G., & Field, J. A. (2001). Azo dye decolourisation by anaerobic granular sludge. *Chemosphere*, 44(5), 1169-1176.
- Verawaty, M., Pijuan, M., Yuan, Z., & Bond, P. L. (2012). Determining the mechanisms for aerobic granulation from mixed seed of floccular and crushed granules in activated sludge wastewater treatment. *Water research*, 46(3), 761-771.
- Verawaty, M., Tait, S., Pijuan, M., Yuan, Z., & Bond, P. L. (2013). Breakage and growth towards a stable aerobic granule size during the treatment of wastewater. *Water research*, 47(14), 5338-5349.
- Vigo, T. (1994). *Textile processing and properties* (pp. 1-108). Amsterdam: Elsevier.
- Volmajer Valh, J., Majcen Le Marechal, A., Vajnhandl, S., Jerič, T. and Šimon, E. (2011). Water in the Textile Industry. *Treatise on Water Science*, 4, 685-706.
- Wang, Z. W., Liu, Y., & Tay, J. H. (2005). Distribution of EPS and cell surface hydrophobicity in aerobic granules. *Applied microbiology and biotechnology*, 69(4), 469.
- Wanner, J. (1998). Process theory: biochemistry, microbiology, kinetics, and activated sludge quality control. *Activated Sludge Process Design and Control: Theory and Practice*. WW Eckenfelder, P. Grau (eds), Technomic Pub. Co., Lancaster, PA, 1-55.
- Weber, S. D., Ludwig, W., Schleifer, K. H., & Fried, J. (2007). Microbial composition and structure of aerobic granular sewage biofilms. *Applied and environmental microbiology*, 73(19), 6233-6240.
- Wilén, B. M., Liébana, R., Persson, F., Modin, O., & Hermansson, M. (2018). The mechanisms of granulation of activated sludge in wastewater treatment, its optimization, and impact on effluent quality. *Applied microbiology and biotechnology*, 102(12), 5005-5020.
- Winkler, M. H., Kleerebezem, R., Strous, M., Chandran, K., & Van Loosdrecht, M. C. M. (2013). Factors influencing the density of aerobic granular sludge. *Applied microbiology and biotechnology*, 97(16), 7459-7468.
- Winkler, M. K. H., Meunier, C., Henriot, O., Mahillon, J., Suárez-Ojeda, M. E., Del Moro, G., ... & Weissbrodt, D. G. (2017). An integrative review of granular sludge for the biological removal of nutrients and recalcitrant organic matter from wastewater. *Chemical Engineering Journal*.
- Winkler, M. K., Bassin, J. P., Kleerebezem, R., De Bruin, L. M. M., Van den Brand, T. P. H., & Van Loosdrecht, M. C. M. (2011b). Selective sludge removal in a segregated aerobic granular biomass system as a strategy to control PAO-GAO competition at high temperatures. *Water research*, 45(11), 3291-3299.
- Winkler, M. K., Kleerebezem, R., & Van Loosdrecht, M. C. M. (2012). Integration of anammox into the aerobic granular sludge process for main stream wastewater treatment at ambient temperatures. *Water research*, 46(1), 136-144.

- Winkler, M. K., Kleerebezem, R., Kuenen, J. G., Yang, J., & van Loosdrecht, M. C. (2011a). Segregation of biomass in cyclic anaerobic/aerobic granular sludge allows the enrichment of anaerobic ammonium oxidizing bacteria at low temperatures. *Environmental science & technology*, 45(17), 7330-7337.
- World Trade Organization. (2017). *WTO - Statistics - Trade and tariff maps*. Wto.org. Retrieved 16 October 2017, from https://www.wto.org/english/res_e/statis_e/statis_map_s_e.htm
- Xiong, Y., & Liu, Y. (2012). Essential roles of eDNA and AI-2 in aerobic granulation in sequencing batch reactors operated at different settling times. *Applied microbiology and biotechnology*, 93(6), 2645-2651.
- Xiu, Z. M., Zhang, Q. B., Puppala, H. L., Colvin, V. L., & Alvarez, P. J. (2012). Negligible particle-specific antibacterial activity of silver nanoparticles. *Nano letters*, 12(8), 4271-4275.
- Yang, Y., & Alvarez, P. J. (2015). Sublethal concentrations of silver nanoparticles stimulate biofilm development. *Environmental Science & Technology Letters*, 2(8), 221-226.
- Yin, W. F., Purmal, K., Chin, S., Chan, X. Y., Koh, C. L., Sam, C. K., & Chan, K. G. (2012). N-acyl homoserine lactone production by *Klebsiella pneumoniae* isolated from human tongue surface. *Sensors*, 12(3), 3472-3483.
- Zero Discharge of Hazardous Chemicals Programme (ZDHC). (2015). *Textile Industry Wastewater Discharge Quality Standards* (pp. 80-84). ZDHC.
- Zhang, B., Ji, M., Qiu, Z., Liu, H., Wang, J., & Li, J. (2011). Microbial population dynamics during sludge granulation in an anaerobic-aerobic biological phosphorus removal system. *Bioresource Technology*, 102(3), 2474-2480.
- Zhang, C., Hu, Z., Li, P., & Gajaraj, S. (2016). Governing factors affecting the impacts of silver nanoparticles on wastewater treatment. *Science of The Total Environment*, 572, 852-873.
- Zhang, F., Wu, X., Chen, Y., & Lin, H. (2009). Application of silver nanoparticles to cotton fabric as an antibacterial textile finish. *Fibers and Polymers*, 10(4), 496-501.
- Zhang, L., Feng, X., Zhu, N., & Chen, J. (2007). Role of extracellular protein in the formation and stability of aerobic granules. *Enzyme and Microbial Technology*, 41(5), 551-557.
- Zheng, Y. M., & Yu, H. Q. (2007). Determination of the pore size distribution and porosity of aerobic granules using size-exclusion chromatography. *Water Research*, 41(1), 39-46.
- Zheng, Y. M., Yu, H. Q., & Sheng, G. P. (2005). Physical and chemical characteristics of granular activated sludge from a sequencing batch airlift reactor. *Process Biochemistry*, 40(2), 645-650.
- Zheng, Y. M., Yu, H. Q., Liu, S. J., & Liu, X. Z. (2006). Formation and instability of aerobic granules under high organic loading conditions. *Chemosphere*, 63(10), 1791-1800.
- Zhou, D., Niu, S., Xiong, Y., Yang, Y., & Dong, S. (2014). Microbial selection pressure is not a prerequisite for granulation: dynamic granulation and microbial community study in a complete mixing bioreactor. *Bioresource technology*, 161, 102-108.
- Zhu, L., Xu, X., Luo, W., Cao, D., & Yang, Y. (2008). Formation and microbial community analysis of chloroanilines-degrading aerobic granules in the sequencing airlift bioreactor. *Journal of applied microbiology*, 104(1), 152-160.
- Zhu, L., Yu, Y., Dai, X., Xu, X., & Qi, H. (2013). Optimization of selective sludge discharge mode for enhancing the stability of aerobic granular sludge process. *Chemical engineering journal*, 217, 442-446.

Annex A | SVI and MLVSS profiles (from Bento, 2016)

Operational note. Bioreactors (SBR1 and SBR2) were configured in equivalent fashion to that applied in SBR1 during this work and fed with a synthetic textile wastewater entirely identical to that described in chapter 2 (albeit with a lower AR14 content – 20 mg L^{-1}). Ag NPs were fed to SBR1 at a concentration of 5 mg Ag L^{-1} along a 178-day operational period followed by a 60-day interval during which Ag NPs were absent from the feed. After this cleaning period, Ag NP feeding was resumed.

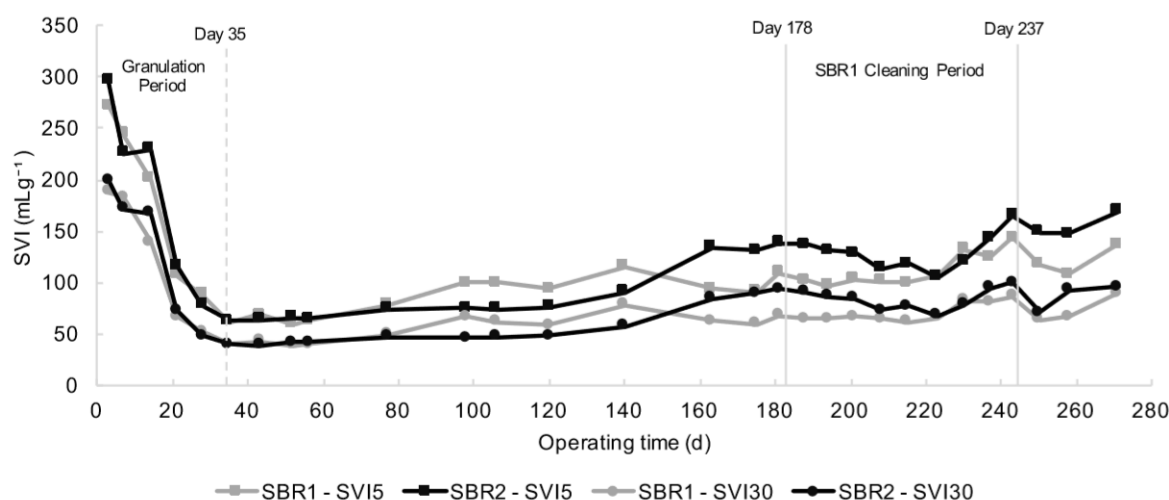


Figure A.1 | Sludge volume index profiles along the experimental run (from Bento, 2016). Sludge volume index (SVI) profiles along the experimental time of 271 days, including SVI values measured after 5 min settling (SVI5) and after 30 min settling (SVI30) for Ag NP-fed SBR1 and Ag NP-free control SBR2. As depicted, settleability in SBR1 decayed slowly after day 60, but was maintained relatively unaltered in SBR2. The vertical dashed line indicates the end of the granulation period (Day 35), while the vertical solid lines indicate the onset (Day 178) and the end (Day 237) of the cleaning period.

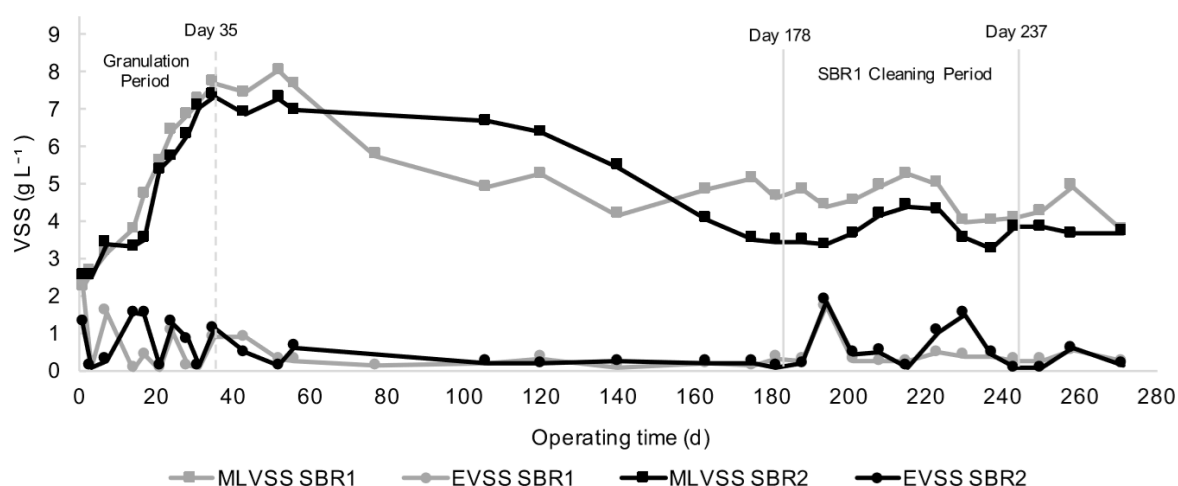


Figure A.2 | Biomass concentration profiles along the experimental run (from Bento, 2016). Volatile suspended solids profile obtained from the mixed liquor (MLVSS) and in the discharged effluent (EVSS) of Ag NP-fed SBR1 and Ag NP-free control SBR2 along the experimental period of 271 days. As depicted, MLVSS concentrations in the bioreactor with Ag NP loading dropped markedly between days 60 and 80, but were maintained relatively unaltered in SBR2. The vertical dashed line indicates the end of the granulation period (Day 35), while the vertical solid lines indicate the onset (Day 178) and the end (Day 237) of the cleaning period.